I. Exploration of Amphitropic Protein Interactions at the Membrane Interface; II. DNF2—A Plant Protein with Homology to Bacterial PI-PLC Enzymes

Author: Tao He

Boston College

The Graduate School of Arts and Sciences

Department of Chemistry

I. EXPLORATION of AMPHITROPIC PROTEIN INTERACTIONS AT THE MEMBRANE INTERFACE; II. DNF2—A PLANT PROTEIN WITH HOMOLOGY TO BACTERIAL PI-PLC ENZYMES.

A Dissertation

by

TAO HE

Submitted in partial fulfillment of the requirements

for the degree of

Doctor of Philosophy

December 2015

I. Exploration of amphitropic protein interactions at the membrane interface; II. DNF2—a plant protein with homology to bacterial PI-PLC enzymes.

Tao He

Under the direction of Dr. Mary F. Roberts

ABSTRACT

Amphitropic proteins, such as the virulence factor phosphatidylinositol-specific phospholipase C (PI-PLC) from *Bacillus thuringiensis*, often depend on lipid-specific recognition of target membranes. However, the recognition mechanisms for zwitterionic lipids such as phosphatidylcholine (PC), which is enriched in the outer leaflet of eukaryotic cell membranes, are not well understood. Molecular dynamics (MD) simulation and mutagenesis results strongly indicate that PI-PLC interacts with PC head groups via cation-π interactions with aromatic tyrosine residues, and suggest that cation-π interactions at the interface may be a mechanism for specific lipid recognition by amphitropic and membrane proteins.

Aromatic amino acids can not only form cation-π interactions at the interface but also insert into membranes and have hydrophobic interactions with lipid tails. Heretofore there has been no facile way to differentiate these two types of interactions. We show that specific incorporation of fluorinated amino acids into proteins can experimentally distinguish cation-π interactions from membrane insertion of the aromatic side-chains. Fluorinated aromatic amino acids destabilize the cation-π interactions by altering electrostatics of the aromatic ring while their enhanced hydrophobicity enhances

membrane insertion. Incorporation of pentafluorophenylalanine or difluorotyrosine into a *Staphylococcus aureus* phosphatidylinositol-specific phospholipase C (PI-PLC) variant engineered to contain a specific PC-binding site demonstrates the effectiveness of this methodology. Applying this methodology to the plethora of tyrosine residues in *Bacillus thuringiensis* PI-PLC identifies those involved in cation-π interactions with PC.

Cation-π interactions provide a likely molecular mechanism for *Bt*PI-PLC PC specificity but do not account for its preference for bilayers containing a small fraction of anionic lipids. MD simulations and fluorescence correlation spectroscopy (FCS) vesicle binding measurements of positively charged amino acids as well as surface tyrosine residues are used to formulate a complete model of *Bt*PI-PLC specific binding to mixed anionic phospholipid/PC membrane.

DNF2, a new plant protein with homology to bacterial PI-PLC, is confirmed to be the first plant small PI-PLC enzyme that can cleave both PI and glycosylphosphatidylinositol (GPI) anchored proteins. GPI-anchored protein cleavage also confirms that DNF2 plays an important role in symbiosome, the intracellular compartment formed by the plant that contains nitrogen fixing bacteria.

Acknowledgements

I would like to begin by thanking my advisor, Professor Mary Roberts. I can't thank her enough for her guidance, encouragement, patience, and support throughout my graduate study. I am so grateful to have her as my advisor and her great personality will influence my time to come.

I would like to thank all my collaborators: Prof. Anne Gershenson, Dr. Boqian Yang, Dr. Stephen Eyles, Prof. Nathalie Reuter, Dr. Cedric Gauffel, Prof. Jianmin Gao, Prof. Dong Wang and Onur Oztasfor. Thank you all for your help and advices during my thesis work. I also want to thank Prof. Evan Kantrowitz for teaching me X-ray crystallography.

I would like to thank all the members of Roberts group: Dr. Jiongjia Cheng, Dr. Yang Wei, Dr. Jingfei Cai, Dr. Rebecca Goldstein and Delilah Jewel. It's a pleasure to have them around to work with and learn from. I'll miss the fun time we shared together.

I would also like to thank Dr. John Boylan, Dr. Thusitha Jayasundera and Dr. Bo Li, for their support during my NMR and X-ray crystallography study. Thanks also go to all the supporting staff in Merkert. Without them, my research would not have been so successful.

Lastly, I want thank to my parents and sister for their unwavering love and care. I also want to thank my husband, Feilong, for his love and support, for all the happiness he brings to me I can't thank him enough.

Abbreviations

AF488-Cys	Alexa Fluor 488 C5 maleimide
AF488-N-term	Alexa Fluor 488 carboxylic acid, succinimidyl ester
APS	ammonium persulfate
B. cereus	*Bacillus cereus*
B. thuringiensis	*Bacillus thuringiensis*
BSA	bovine serum albumin
*Bt*PI-PLC	*Bacillus thuringiensis* phosphatidylinositol-specific phospholipase C
C2	protein kinase C conserved region 2
CD	circular dichroism
cIP	inositol 1,2-cyclic phosphate
CMC	critical micelle concentration
CSA	chemical shift anisotropy
D_2O	deuterium oxide
DAG	diacylglycerol
DC	detergent compatible
DNF	defective nitrogen fixation
diC_6PC	dihexanoyl-phosphatidylcholine
diC_7PC	diheptanoyl-phosphatidylcholine
DLS	dynamic light scattering
DMPC	1,2-dimyristoyl-phosphatidylcholine

DMSO	dimethyl sulfoxide
DOPA	1,2-dioleoyl-phosphatidic acid
DOPG	1,2-dioleoyl-phosphatidyglycerol
dsRNA	double-stranded RNA
DTNB	5,5'-dithiobis-(2-nitrobenzoic acid)
DTT	dithiothreitol
E. coli	*Escherichia coli*
EDTA	ethylenediaminetetraacetic acid
EF	elongation factor
fc-P-NMR	high resolution field cycling ^{31}P NMR
FCS	fluorescence correlation spectroscopy
f_{max}	apparent maximum fraction bound
FRET	fluorescence resonance energy transfer
GMML	glycerol minimal media with leucine
GPI	glycosylphosphatidylinositol
GST	glutathione S-transferase
HEPES	4-(2-hydroxyethyl)-1-piperazineethanesulfonic acid
His-tag	poly histidine tag
I-1-P	inositol 1-phosphate
IPTG	isopropyl β-D-1-thiogalactopyranoside
ITC	isothermal titration calorimetry
K_d	apparent dissociation constant
K_m	Michaelis constant

L. monocytogenes	*Listeria monocytogenes*
LUV	large unilamellar vesicle
MD	molecular dynamics
MES	2-(N-morpholino) ethane-sulfonic acid
MS	mass spectrometry
MSA	multiple sequence alignment
Ni-NTA	nickel-nitrilotriacetic acid
NMR	nuclear magnetic resonance
O.D.	optical density
PA	phosphatidic acid
PBS	phosphate buffered saline
PC	phosphatidylcholine
PCR	polymerase chain reaction
PE	phosphatidylethanolamine
PEG	polyethylene glycol
PG	phosphatidylglycerol
PH	pleckstrin homology
pI	isoelectric point
PI	phosphatidylinositol
PIA	phosphatidylinositol analog
PI-PLC	phosphatidylinositol-specific phospholipase C
PIP_n	phosphoinositide
PLA	phospholipase A

PLB	phospholipase B
PLC	phospholipase C
PLD	phospholipase D
PLP	pyridoxal 5'-phosphate
PMe	phosphatidylmethanol
POPC	1-palmitoyl-2-oleoyl-phosphatidylcholine
PS	phosphatidylserine
QFF	Q-Sepharose Fast Flow
S. aureus	*Staphylococcus aureus*
*Sa*PI-PLC	*Staphylococcus aureus* phosphatidylinositol-specific phospholipase C
SDS-PAGE	sodium dodecyl sulfate polyacrylamide gel electrophoresis
SH2	Src homology 2
SPR	surface plasmon resonance
SUV	small unilamellar vesicle
TEMED	N,N,N',N'-tetramethylethylenediamide
TIM	triosephosphate isomerase
T_m	thermal denaturation temperature
Tris	tris(hydroxymethyl)aminomethane
TX-100	Triton X-100
V_{max}	maximal rate in Michaelis–Menten kinetics
WT	wild type
X_{PC}	mole fraction of PC

Table of Contents

List of Figures

List of Tables

Chapter 1

Introduction

1.1 Amphitropic proteins

Peripheral membrane proteins refer to those that are water-soluble, and have reversible interactions with membrane [1]. They adhere only temporarily to the biological membrane either through direct interactions with the polar head group of phospholipid in the bilayer or through indirect interactions with an integral membrane protein. Amphitropic proteins have both lipophilic and hydrophilic characteristics and bind to lipids in the cell or organelle membrane in order to function.

Several structural motifs have been employed by amphitropic proteins to associate with membranes: lipid clamps, covalent lipid anchors and amphipathic helices. Lipid clamps contain motifs that associate specifically with the head groups of lipid monomers (Figure 1-1A). These motifs have been found in C1, C2 and PH (pleckstrin homology) domains. [2,3,4]. C1 domains bind diacylglycerol (DAG) and phorbol esters; C2 domains usually bind calcium, phosphatidylserine or phosphatidylcholine; The PH domains bind different phosphoinositides. Another class of amphitropic proteins contain lipid covalent anchors which can insert into the membrane (Figure 1-2A). At the cell surface, these lipid-anchored proteins can be covalently attached to the lipids glycosylphosphatidylinositol (GPI) and cholesterol [5]. Often this is a reversible process, as the acyl chain of the protein can be buried in the hydrophobic binding pocket after dissociation from the membrane. In addition, many proteins in this category combine a single lipid anchor with a polybasic site that interacts electrostatically with the negative polar head group region of a membrane. A third class of proteins contains an amphiphatic α-helix, which non-specifically binds to a membrane by partitioning into the membrane bilayer (Figure 1-3A). The hydrophobic face of the helix is sequestered from water, while

its polar face can still contact the aqueous phase. One example of this class of protein is DnaA [6].

Figure 1-1. Schematic reperesentations of membrane binding motifs of amphitropic proteins. (A) lipid clamp; (B) lipid covalent anchors; (C) amphipathic helix; (D) hydrophobic loops.

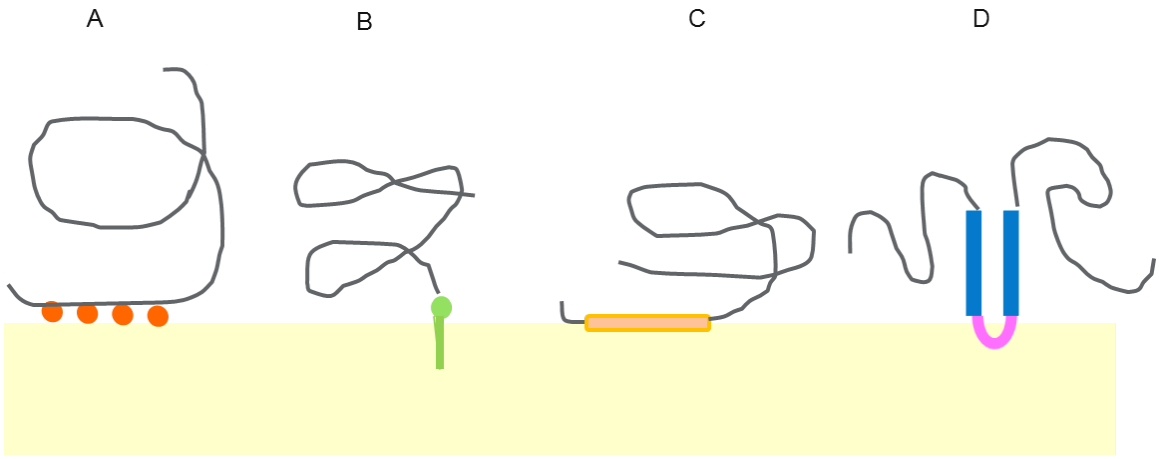

Besides these interactions, unstructured hydrophobic loops on the protein surface can also contribute to the protein interactions with membrane (Figure 1-1D). Cation-π interactions that happen between aromatic residues of protein surface and positive charged portions of the phospholipid head groups, also play an important role in lipid recognition and interactions. Examples where loops contain key membrane interacting residues include cytochrome P450, annexins as well as phospholipases [7].

Amphitropic proteins bind reversibly to lipid vesicles with equilibrium association constants typically between $10^3\ M^{-1}$ to $10^7\ M^{-1}$ [7]. For many of them it is thought that electrostatic interactions drive their positioning and orientation at the membrane surface thus facilitating the intercalation of a few hydrophobic groups. It is generally acknowledged that the association of amphitropic proteins with lipid bilayers is fast while the dissociation is slow; the dissociation rate constant is thus the main determinant of the binding strength. As a consequence, in simple systems where the protein does not

undergo conformational changes and does not interact with other proteins, the affinity for the membrane is mostly accounted for by interactions between the protein interfacial binding site and lipids. The energy and specificity of these interactions is generally estimated by including contributions from electrostatics, −1.4 kcal/mol for each positively charged amino acid interacting with the lipid headgroups [8], and hydrophobic interactions with the bilayer core, −0.8 kcal/mol per acyl chain CH_2 group interacting with the protein [9]. Recently we have reported approximately −2.5 kcal/mol for an aromatic amino acid binding to positive charged lipid head group [10].

1.2 Phospholipids

The biological membrane consists mainly of lipids and proteins. There are three major types of membrane lipids: steroids, glycolipids, and phospholipids. Phospholipids are the most abundant class of membrane, comprising 20-80% of the membrane mass [11,12]. In eukaryotic membranes, glycerophospholipids are the major components: phosphatidylcholine (PC), phosphatidylethanolamine (PE), phosphatidylserine (PS), phosphatidylinositol (PI), phosphatidylglycerol (PG) and phosphatidic acid (PA) (Fig. 1-2) [12]. Phospholipids are amphiphatic, composed of a hydrophilic headgroup (R-) and hydrophobic acyl chains. The different polar head groups linked by the glycerophosphate moiety generate phospholipids that are either zwitterionic (PC, PE) or anionic (PI, PS, PG, PA) (Fig. 1-2).

A phospholipid bilayer is also called bimolecular sheet. The hydrophilic head groups interacting with the aqueous medium on each side of the sheet, and hydrophobic tails of each individual sheet interact with one another.

Besides lipid bilayer, a variety of aggregates can be formed from phospholipids in

aqueous solution mainly through hydrophobic interactions of the acyl chains [13]. As shown in Figure 1-3, at the air-water interface, lipids always form monolayers with the polar headgroups in the aqueous solution and the acyl chains stick into the air. In aqueous solutions, phospholipids are present as monomers as well as different forms of aggregates depending on the concentration and length of the acyl chains [14]. Below critical micelle concentration (CMC), they exist as monomers. If acyl chain lengths are short (e.g., dihexanoyl-PC, diC_6PC) or the polar head groups are very large (e.g., ganglioside GM1) the lipid molecules aggregate to form micelles. Phospholipid mixed with a detergent at a proper ratio will form detergent mixed micelles. If the acyl chains are moderately long, the molecules aggregate and form bilayer vesicles, MLVs (multilamellar vesicles) if just hydrated with water, and SUVs (small unilamellar vesicles) and LUVs (large unilamellar vesicles) if one extrudes the MLVs through a small orifice or sonicates the MLVs. Both SUVs and LUVs are good models to study membrane protein function, folding and assembly. SUVs are highly curved with 20–50 nm diameters; these are easily prepared by sonication [15]. LUVs can be prepared that have a wide range of sizes, from 50 to 1000 nm. Both the micelle and vesicle systems are widely used as models to study protein-membrane interactions and other cell processes that have membrane bound constituents.

Figure 1-2. General phospholipid structure.

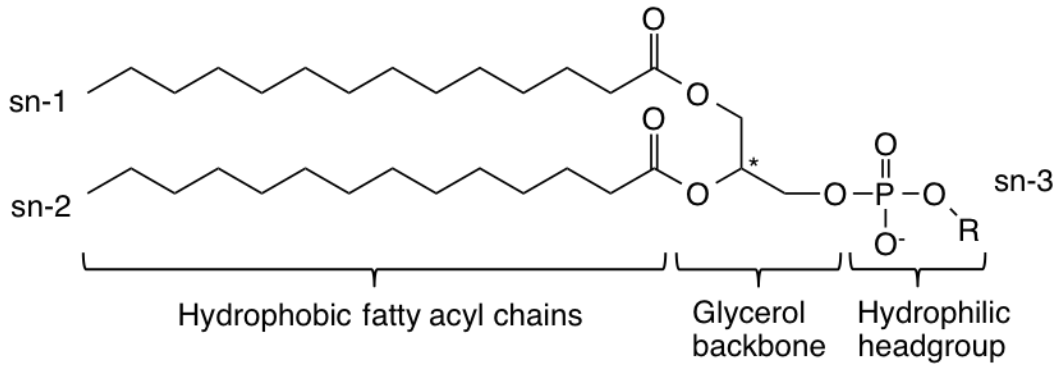

Lipid name	R	Net charge at physiological pH
Phosphatidic Acid (PA)	—H	-2
Phosphatidylmethanol (PMe)	—CH_3	-1
Phosphatidylserine (PS)	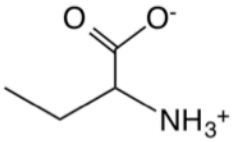	-1
Phosphatidylglycerol (PG)	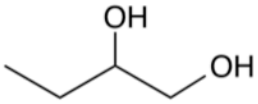	-1
Phosphatidylinositol (PI)	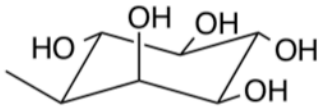	-1
Phosphatidylethanolamine (PE)	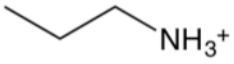	0
Phosphatidylcholine (PC)	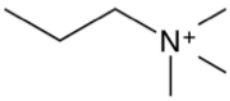	0

Figure 1-3. Physical states of phospholipids in aqueous solution.

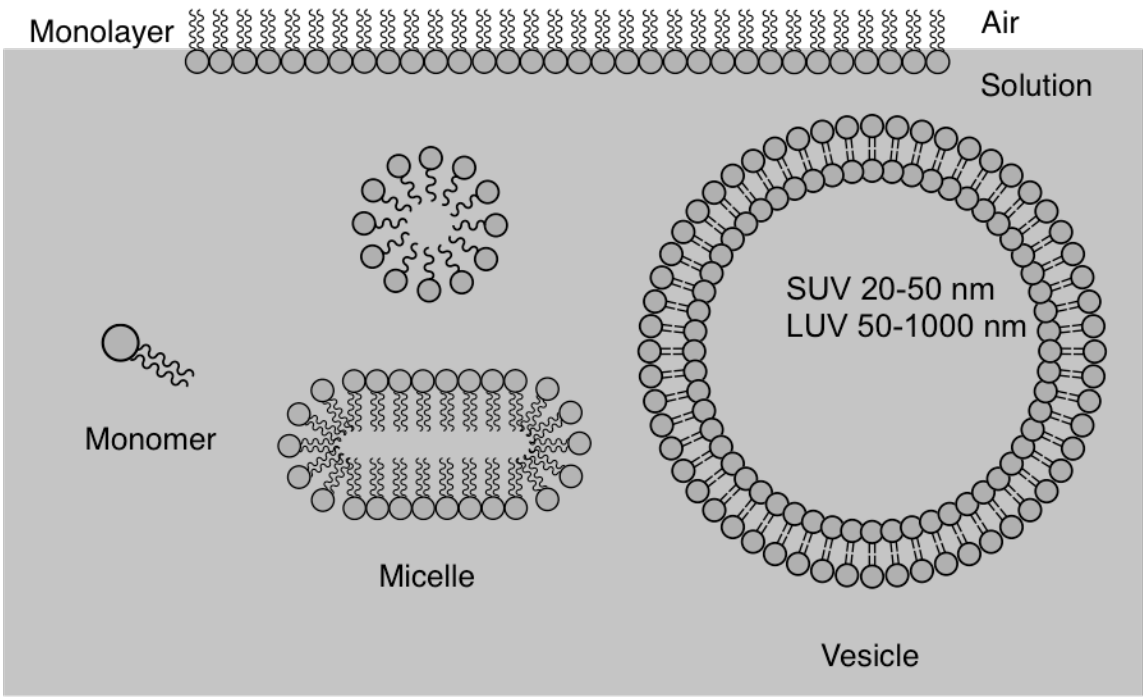

1.3 Phosphatidylinositol-specific phospholipase C (PI-PLC) enzymes

Phospholipase enzymes hydrolyze different ester linkages in a variety of phospholipids [16]. Phosphatidylinositol-specific phospholipase C (PI-PLC) enzymes are a large family of phospholipases that specifically catalyze the hydrolysis of polar head group of phosphoinositide substrates. The substrates of bacterial PI-PLC enzymes are PI and glycosylphosphatidylinositol (GPI), while most mammalian enzymes prefer PIP_n (PI molecules phosphorylated on C4 and C5 of the inositol ring), which are important in signaling pathways [17,18]. In our lab, a new plant protein DNF2 has been confirmed to be able to hydrolyze PI and is a first small plant PI-PLC enzyme resembling a bacterial PI-PLC.

Figure 1-4. The mechanism of the two sequentially reactions catalyzed by bacterial PI-PLC. (adapted from Jiongjia Cheng's thesis, Boston College, 2013).

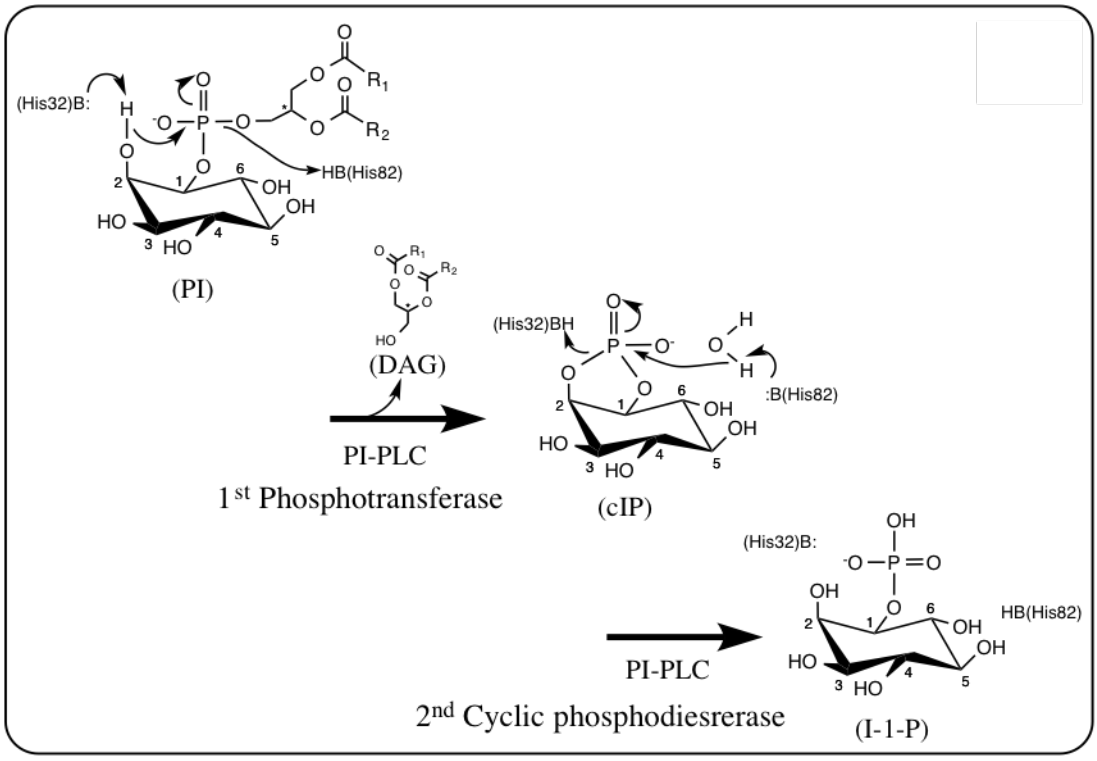

As shown in Figure 1-4, the bacterial PI-PLC cleaves its substrate via an intramolecular phosphotransferase reaction of the PI moiety to form a cyclic inositol phosphate molecule (inositol 1,2-cyclic phosphate, or cIP) and diacylglycerol (DAG) [19]. The enzyme further hydrolyzes the water-soluble intermediate cIP to inositol-1-phosphate (I-1-P) [20,21]. A similar mechanism is used by mammalian PI-PLCs, except that Ca^{2+} is used to stabilize the transition state.

Bacterial PI-PLC is a virulence factor produced and secreted by many Gram-positive bacteria, including the pathogens *Bacillus cereus, Bacillus thuringiensis, Listeria monocytogenes,* and *Staphylococcus aureus.* [22-28]. In addition to the cleavage of non-phosphorylated PI, PI-PLCs secreted by extracellular pathogens (e.g. *Bacillus* and *Staphylococcus* strains) can also cleave GPI anchors [22] to release proteins that are

tethered to the outer surface of mammalian cell membrane. One of the products, DAG, a second messenger, can translocate across the bilayer [29] to interfere with intracellular signaling processes [30].

The mammalian phospholipase C family has thirteen isozymes: PLC-$\beta_{(1-4)}$, PLC-$\gamma_{(1-2)}$, PLC-$\delta_{(1,3,4)}$, PLC-ε, PLC-ζ, and PLC-η (Figure 1-5) [31]. These PLC isoforms share four EF-hand motifs (usually associated with Ca^{2+} binding), the X and Y catalytic domains, a C-terminal C2 domain for calcium-dependent membrane targeting and a N-terminal PH domain (the one exception is PLC-ζ) to localize the enzymes to their substrate in the membrane and also to interact with other signaling components [32,33].

Figure1-5. The mammalian PLC family. (adapted from [31])

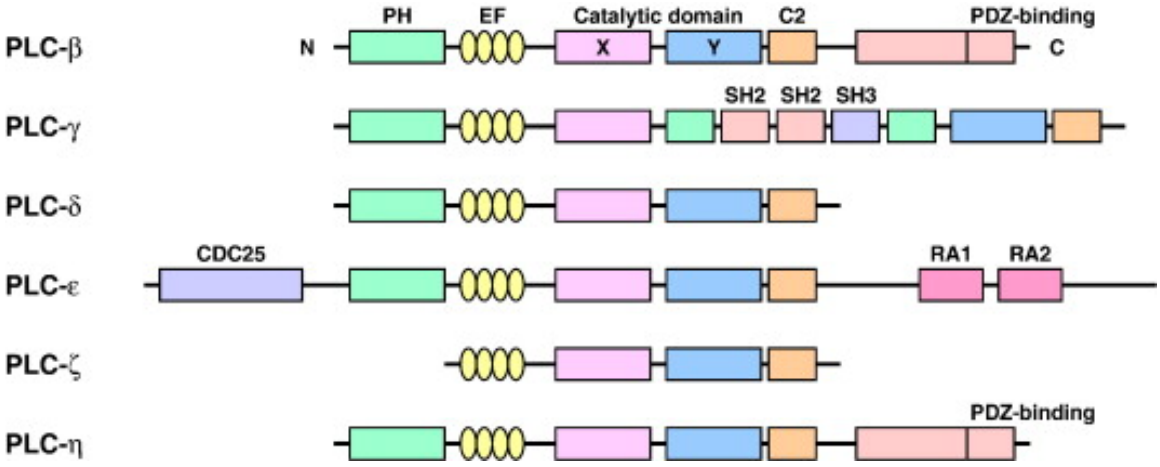

In contrast to their multi-domain eukaryotic relatives, the bacterial PI-PLCs have a single catalytic domain (homologous to the X-Y domains of mammalian PLC enzymes) for both catalysis and membrane binding.

There are two crystal structures of mammalian PI-PLC enzymes, PI-PLC δ1 (Figure 1-6A) and PI-PLC β2 (Figure 1-6B). Both the catalytic domains adopt a $(\beta\alpha)_8$-barrel (TIM barrel) structure. The structures of PI-PLCs from *B. cereus, B. thuringiensis, S. aureus*

and L. monocytogenes have been solved. They all fold as a single domain and are homologous to the catalytic domain in mammalian PI-PLCs. Secondary structures superimpose well with each other (Figure 1-6C). Sequence alignment of the three bacterial PI-PLCs shows 26−40% identity (Figure 1-7). Two key structural features of the bacterial enzymes have been implicated in membrane binding [34-37]. One is short helix B (containing Trp47 in *Bacillus* PI-PLC and Trp45 in *S. aureus* PI-PLC) and the other a mobile rim loop (containing Trp242 in *Bacillus* PI-PLC and Phe249 in *S. aureus* PI-PLC). In *S. aureus* PI-PLC, helix B is one residue longer than in the *B. cereus* structure and has two positive charged lysine residues. This can form an extended positively charged motif when combined with the other positively charged residues in the barrel rim. The key hydrophobic residue in the mobile rim loop can adopt different orientations. For example, under basic conditions, Phe249 in *S. aureus* PI-PLC [38] is pointed outward and toward the membrane interface compared with the homologous side chain (Trp242) in *Bacillus* enzymes. In the latter the tryptophan residues are pointed away from the membrane interface. This stresses the flexibility of the rim loop [38]. In *L. monocytogenes*, Trp 49 in helix B points inward where it may be involved in interacting with substrates. F247 in rim loop that is homologous to Trp242 in *Bacillus* enzymes points outward and can insert into the membrane through hydrophobic interactions [49].

Figure 1-6. Comparison of the overall structures of different PI-PLC enzymes: (A) PLC δ1 (1QAS); (B) PLC β2 (2FJU); (C) superposition of *B. cereus* PI-PLC (1PTG), *S. aureus* PI-PLC (3V16) and *L. monocytogenes* PI-PLC (1AOD). PH domain (green), EF hand (magenta), catalytic domain (cyan), C2 domain (yellow).

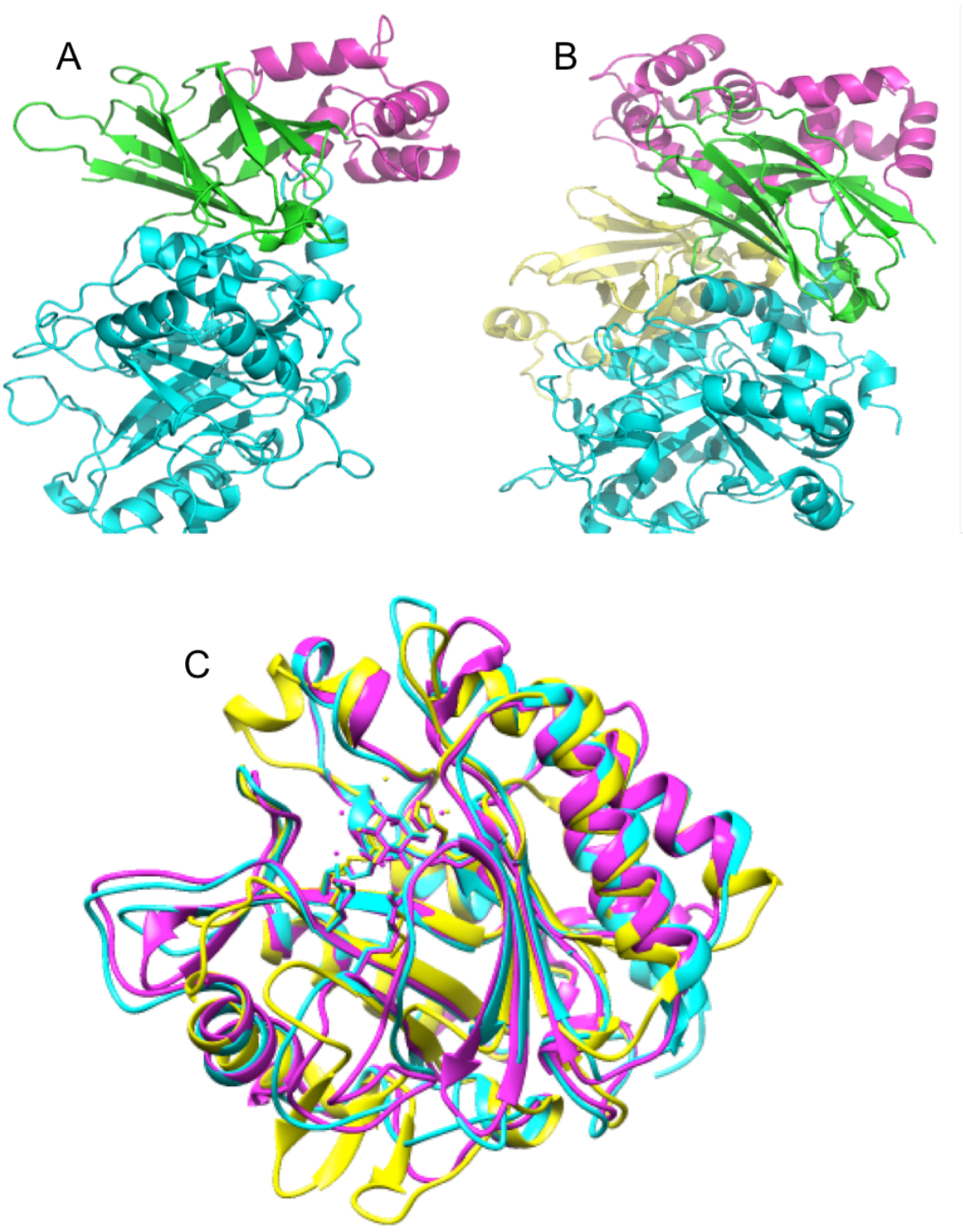

Figure 1-7. Sequence alignment of the three bacterial PI-PLCs.

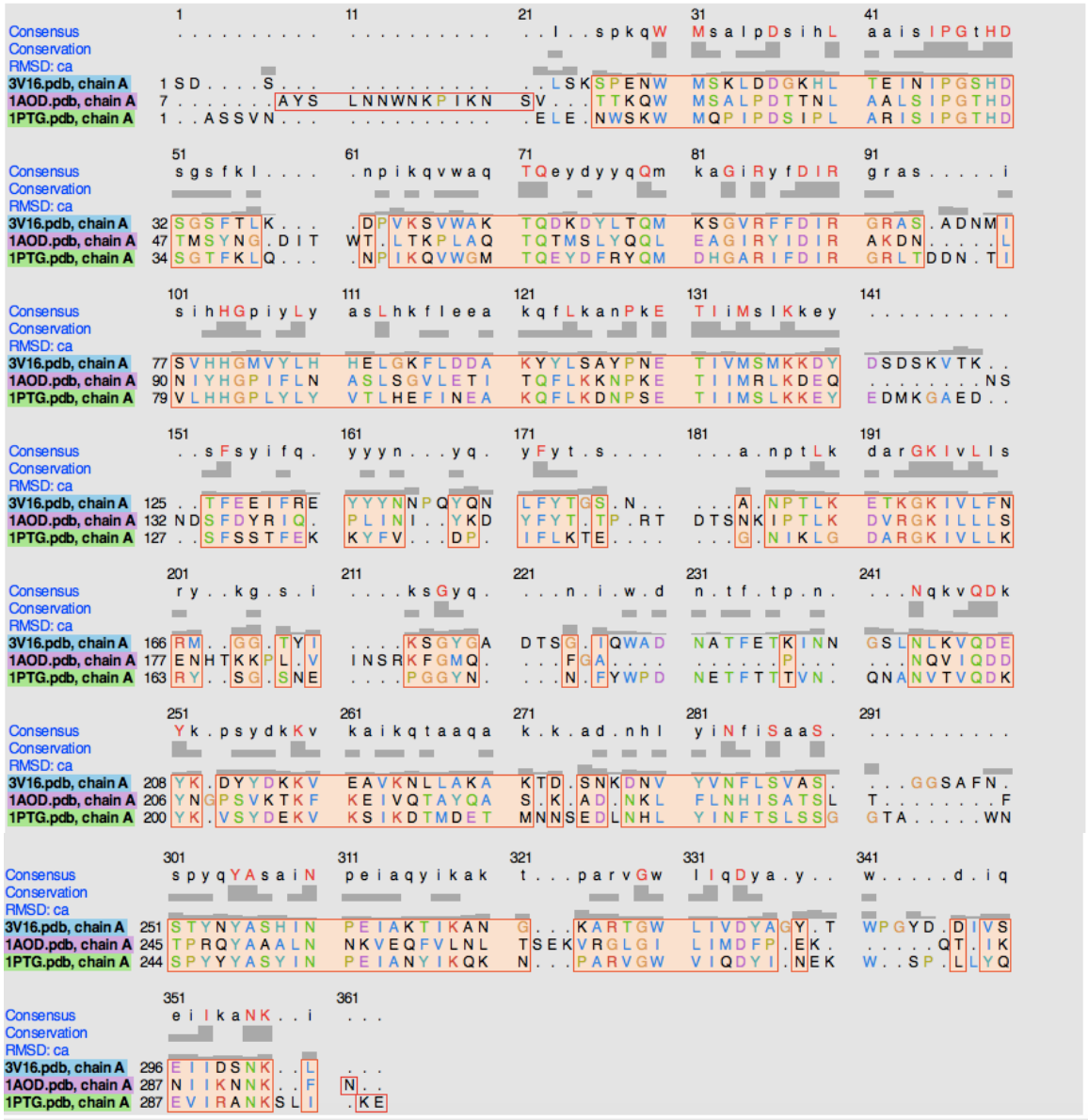

1.4 Interfacial activation and inhibition of PI-PLC

'Interfacial activation' is a sharp increase in enzyme activity when the substrate is presented at an interface as opposed to a monomer molecule [39] and this effect has been observed for many peripheral enzymes, including phospholipases. For hydrolysis reactions taking place at an aqueous-lipid interface, the enzyme in the solution must initially bind to the interface. The interface-associated enzyme likely undergoes some conformational changes to bind the substrate in the active site. When one hydrolysis cycle finishes, the enzyme releases the products to regenerate free enzyme and looks for the next substrate [40]. The overall rate of the catalytic turnover is thus affected not only by the kinetics of those interfacial catalytic steps but also by the kinetics of binding and desorption of the enzyme at the interface. *B. thuringiensis* PI-PLC exhibits a second type of 'interfacial activation'. In the presence of zwitterionic phospholipid PC, a large enhancement of the enzyme specific PI-PLC activity is observed. Much of the enhanced activity generated by this non-substrate phospholipid is thought to represent a specific binding interaction [41].

However, adding more non-substrate lipids dilutes the substrate concentration at the interface and this local concentration instead of bulk lipid concentration is important for the overall kinetic rate. This phenomenon is called "surface dilution inhibition" [42,43]. The bacterial PI-PLCs also exhibit "scooting mode catalysis", where enzyme completes several rounds of substrate catalysis at the substrate interface before dissociating from the particle [44]. Scooting mode catalysis becomes extremely important with the decreased interfacial substrate concentration.

The *Bacillus* PI-PLC enzymes are activated by strong binding to PC [20,37,47]. Recent

work on *B. thuringiensis* PI-PLC vesicle binding, combining high-resolution field-cycling ^{31}P NMR relaxation experiments [37] with mutagenesis studies [45] have shown that there is a discrete binding site for the activator PC. The specific PC binding site was suggested to be rich in tyrosines that could form choline cation/Tyr π boxes or sandwiches. It was suggested that a tyrosine strip (Tyr246-248 and Tyr251) near the membrane interface forms the PC recognition motif. However, all the evidence for the PC binding pocket was indirect and required further experiments to validate this hypothesis. Interestingly, a mutant of *S. aureus* PI-PLC, while the wildtype protein shows weak PC affinity, exhibited greatly enhance affinity for PC. The mutant enzyme was constructed to mimic the tyrosine strip of *B. thuringiensis* [46]. A specific PC binding site was identified in a crystal structure of the mutant N254Y/H258Y [46]. It suggested that the choline cation/ tyrosine π interactions contribute to the PC binding affinity. However, the crystal structure used a soluble PC and only the polar headgroup was visible. Further work was needed to confirm the importance of those tyrosine residues on *Bt*PI-PLC and to clarify if they interact through cation-π interactions.

Although it may be important for other amphitropic proteins, PC binding is not a universal mechanism of interfacial activation for bacterial PI-PLCs. *S. aureus* PI-PLC has weak affinity for PC and is sensitive to salt. Instead of binding, PC modulates the pH and salt dependence of *S. aureus* PI-PLC activity. The higher the PC content, the less sensitive the enzyme is to salt and the higher the specific activity [48]. The enzyme from *Listeria monocytogenes* is activated by many noncharged or zwitterionic amphiphiles in a nonspecific fashion [49]. Consistent with this mode of PC activation, *L. monocytogenes* PI-PLC has very low affinity for PC SUVs but very high affinity for anionic phospholipid

interfaces. Adding PC reduces the interfacial negative charge which in turn prevents aggregation of the protein to form nonproductive complexes [49].

1.5 Membrane binding assays for amphitropic proteins

Membrane binding is critical for amphitropic proteins to carry out their cellular function, a sensitive and quantitative method for measuring membrane affinity is essential.

Traditional binding methods include assays that involve physical separation of membrane bound proteins and free proteins such as centrifugation and gel filtration, or indirect assays that allow monitoring of membrane-protein binding, such as fluorescence and NMR line-width methods [50]. Centrifugation to separate free and vesicle-bound protein is the simplest assay. It is useful for a first estimation of binding affinity. However, the major drawback of this kind of assays is that the long centrifugation time may perturb the binding equilibrium. Thus the K_d measured may not be the true equilibrium constant [51,52]. Chromatographic gel filtration assays are less sensitive and require large amounts of both protein and lipids.

Fluorescence spectroscopy has been adopted for monitoring protein that contains one or more tryptophan (or tyrosine) residues in the vicinity of the membrane binding surface. The intrinsic fluorescence of the protein, dominated by tryptophan, is sensitive to the changes in polarity of the environment. When protein binds to the hydrophobic core of membranes, tryptophan fluorescence generally shifts to a shorter wavelength and exhibits an increase in intensity [53-55]. This method requires the presence of tryptophan residues at the membrane interface. However, multiple tryptophan residues at the interface might cancel each other out. Also, different changes can occur for different lipids and variable

sensitivity have greatly limited the application of this method. As an alternative, Förster resonance energy transfer (FRET) has been widely used [56-58]. In these experiments, fluorophore containing lipids (e.g., dansyl- or pyrene- lipids) are incorporated in the membranes; the absorption spectrum of the lipids strongly overlaps with tryptophan emission. Thus, association of the protein with the bilayer results in quenching of the tryptophan fluorescence due to FRET. Compared to intrinsic fluorescence, this assay has a higher sensitivity, yet it still requires the presence of tryptophan in the protein or an introduced extrinsic fluorophore whose absorption or emission spectrum overlaps with the lipid fluorophore.

Fluorescence correlation spectroscopy (FCS) can be used to replace intrinsic fluorescence or FRET. It has a much higher sensitivity and lower sample requirement (<10 nM protein and μL volumes) [59-61]. Tryptophan residues, which have only moderate quantum yields and are easily bleached, are not suitable for nM detection. By introducing on the protein an extrinsic fluorophore, the protein and lipid donor/acceptor pair can be chosen to optimize quantum yield and stability to bleaching. FCS uses the difference in Brownian motion of free and vesicle-bound protein. Vesicle bound protein has a retarded translational diffusion speed and this change can be easily measured by FCS. Also, the protein concentration used in FCS is comparable to what is used in kinetic assays. I have mainly used this assay to study PI-PLC interactions with SUVs composed of both zwitterionic and anionic lipids during my thesis work.

Surface plasmon resonance (SPR) methods have also been developed to measure binding affinity of different interacting species. Binding is monitored by measuring the refractive index change caused by the increased mass introduced onto the SPR chip

[62,63]. In a typical SPR assay, lipids are immobilized on the sensor chip surface that forms a wall of the sample cell and protein solution of different concentrations flows through the cell. When protein binds to the membrane, the refractive index near the surface will be changed and the signal can be recorded in real time. It is label free and the rate constants for association (k_a) and dissociation (k_d) steps can be extracted in real time. However, this assay also has its limitations. Nonspecific binding can complicate the interpretation of the binding result. Also, the determined $K_d = k_d/k_a$ is expressed in terms of molarity of protein binding sites instead of lipid concentration. Most importantly, lipid immobilization results in a planar surface without curvature, which is a potential problem in working with the bacterial PI-PLC enzymes that prefer high curvature for membrane binding.

Isothermal titration calorimetry has also been developed for characterizing the binding affinity of proteins with their ligands. It has high precision and sensitivity to exothermic and endothermic heat changes as well as the capacity to simultaneously determine the association and dissociation constant, the binding enthalpy and the binding stoichiometry [64]. One of the significant drawbacks of this technique is the complexity of data analysis for non-standard models. It also requires a large amount of protein, which might be a big problem for precious samples.

1.6 Thesis directions

The first aim of my dissertation is to define the overlooked cation-π interactions and formulate a complete model to understand the mechanism of *Bt*PI-PLC membrane binding. In order to investigate the cation-π interactions, we combined MD simulations, mutagenesis along with binding and activity assays, to study the role of tyrosine residues

at the protein membrane surface in regulating the binding and activity of *Bt*PI-PLC. Tyr86, Tyr88, Tyr204, Tyr246, Tyr247, Tyr248 and Tyr251 were associated with DMPC bilayer binding affinity in simulations. This observation in MD simulation led us to mutate these tyrosines to alanines. The variations in both enzymatic activity and vesicle binding affinity between mutant protein and WT were measured to identify the important tyrosine residues in cation-π interactions with membrane.

Aromatic amino acids can not only form cation-π interactions at the interface but also insert into membranes and have hydrophobic interactions with lipid tails. Heretofore there has been no facile way to differentiate these two types of interactions. To experimentally distinguish cation-π interactions from membrane insertion of the aromatic side chain, we introduced fluorinated amino acids into proteins. Fluorinated aromatic amino acids destabilize the cation-π interactions by altering electrostatics of the aromatic ring while their enhanced hydrophobicity enhances membrane insertion. *Sa*PI-PLC was used as a model system. Incorporation of pentafluorophenylalanine or difluorotyrosine into mutant N254Y/H258Y engineered to contain a specific PC-binding site would demonstrate the effectiveness of this methodology. And this methodology would be applied to the plethora of tyrosine residues in *Bt*PI-PLC to identify those involved in cation-π interactions with PC.

Cation-π interactions provide a likely molecular mechanism for *Bt*PI-PLC PC specificity but do not account for its preference for bilayers containing a small fraction of anionic lipids. MD dynamic simulation and FCS affinity measurement of positive charged amino acid as well as surface tyrosine residue mutants, we could formulate a complete model of *Bt*PI-PLC specific binding to anionic PC-containing lipid.

Finally, *dnf2*, a gene important for plant nitrogen fixation in the nodule organism, has a hypothetical homology protein structure to bacterial PI-PLC. To identify if it is a PI-PLC, the gene was cloned into tagged vectors and recombinant protein was expressed. The crude cell lysate could be subjected to activity assay towards PI to determine if it was a PI-PLC. Once confirmed, more assays could be performed using purified DNF2 protein.

Reference

1. Burn, P., (1988) Amphitropic proteins: a new class of membraneproteins. *Trends in Biochemical Science*, 13, 79 - 83.
2. Hurley, J. H., Newton, A. C., Parker, P. J., Blumberg, P. M., and Nishizuka, Y. (1997) Taxonomy and function of C1 protein kinase C homology domains. *Protein Science, 6*, 477-480.
3. Rebecci, M. J., and Scarlata, S. (1998), Pleckstrin homology domains: a common fold with diverse functions. *Annu. Rev. Biophys*, *27*, 503-528.
4. Rizo, J. and Sudhof, T. C. (1998) C2-domains: structure and function of a universal calcium binding domain. *J. Biol. Chem. 273*, 15879-15882.
5. Silvius, J. R. (2003) Lipidated peptides as tools for understanding the membrane interactions of lipid modified proteins. *Current Topics in membranes, 52*, 371-395.
6. Garner, J. and Crookie, E. (1996) Membrane regulation of the chromosomal replication acivity of E. coli DnaA requires a discrete site on the protein. *EMBO, 15*, 3477-3485.
7. Johnson, J. E. and Cornell, R. B. (1999) Amphitropic proteins: regulation by reversible membrane interactions. *Mol. Membr. Biol.16*, 217-235.
8. Kim, J. Y., Mosior, M., Chuang, L. A., Wu, H., and Mclaughlin, S. (1991) Binding of peptides with basic residues to membranes containing acidic phospholipids. *Biophys J*, 60, 135-148.
9. Luckey, M. (2008) *Membrane Structual Biology: with Biochemical and Biophysical Foundations, Cambridge University Press.*
10. Grauffel, C., Yang, B., He, T., Roberts, M. F., Gershenson, A., and Reuter, N. (2013) Cation-π interactions as lipid specific anchors for phosphatidylinositol-specific phospholipase-C. *J. Am. Chem. Soc. 135*, 5740-5750.
11. van Meer, G., Voelker, D. R., and Feigenson, G. W. (2008) Membrane lipids: where they are and how they behave. *Nat. Rev. Mol. Cell Biol.*, 9, 112–124.
12. Yeagle, P. L. (2005) The structure of biological membranes, CRC press.
13. Chandler, D. (2005) Interfaces and the driving force of hydrophobic assembly. *Nature*, 437, 640–647.
14. Gennis, R. B. (1988) Biomembranes: molecular structure and function, Springer advanced texts in chemistry.
15. Johnson, S. M., Bangham, A. D., Hill, M. W., and Korn, E. D. (1971) Single bilayer liposomes. *Biochim. Biophys. Acta*, 233, 820–826.
16. Roberts, M. F. (1996) Phospholipases: structural and functional motifs for working at an interface. *FASEB J, 10*, 11159-1172.
17. Payrastre, B., Missy, K., Giuriato, S., Bodin, S., Plantavid, M., and Gratacap, M. (2001) Phosphoinositides: key players in cell signalling, in time and space. *Cell. Signal.*, 13, 377–387.
18. Cockcroft, S., and De Matteis, M. A. (2001) Inositol lipids as spatial regulators of membrane traffic. *J. Membr. Biol.*, 180, 187–194.
19. Volwerk, J. J., Shashidhar, M. S., Kuppe, A., and Griffith, O. H. (1990) Phosphatidylinositol-specific phospholipase C from *Bacillus cereus* combines

intrinsic phosphotransferase and cyclic phosphodiesterase activities: a ^{31}P NMR study. *Biochemstry*, 29, 8056−8062.
20. Zhou, C., Qian, X., and Roberts, M. F. (1997) Allosteric activation of phosphatidylinositol-specific phospholipase C: specific phospholipid binding anchors the enzyme to the interface. *Biochemstry*, 36, 10089−10097.
21. Hondal, R. J., Zhao, Z., Kravchuk, A. V., Liao, H., Riddle, S. R., Yue, X., Bruzik, K. S., and Tsai, M. D. (1998) Mechanism of phosphatidylinositol-specific phospholipase C: a unified view of the mechanism of catalysis. *Biochemstry*, 37, 4568−4580.
22. Griffith, O. H., and Ryan, M. (1999) Bacterial phosphatidylinositol-specific phospholipase C: structure, function, and interaction with lipids. *Biochim. Biophys. Acta*, 1441, 237–254.
23. Read, T. D., Peterson, S. N., Tourasse, N., Baillie, L. W., Paulsen, I. T., et al. (2003) The genome sequence of *Bacillus anthracis* Ames and comparison to closely related bacteria. *Nature*, 423, 81–86.
24. Klichko, V. I., Miller, J., Wu, A., Popov, S. G., and Alibek, K. (2003) Anaerobic induction of *Bacillus anthracis* hemolytic activity. *Biochem. Biophys. Res. Commun.*, 303, 855–862.
25. Rhee, S. G., Suh, P. G., Ryu, S., and Lee, S. Y. (1989) Studies of inositol phospholipid-specific phospholipase-C. *Science*, 244, 546−550.
26. Kyei-Poku, G., Gauthier, D., Pang, A., and van Frankenhuyzen, K. (2007) Detection of *Bacillus cereus* virulence factors in commercial products of *Bacillus thuringiensis* and expression of diarrheal enterotoxins in a target insect. *Can. J. Microbiol.*, 53, 1283−1290.
27. Daugherty, S., and Low, M. G. (1993) Cloning, expression and mutagenesis of phosphatidylinositol-specific phospholipase C from *Staphylococcus aureus*: a potential staphylococcal virulence factor. *Infect. Immun.*, 61, 5078−5089.
28. Lehto, M. T., and Sharom, F. J. (2002) PI-specific phospholipase C cleavage of a reconstituted GPI-anchored protein: modulation by the lipid bilayer. *Biochemstry*, 41, 1398−1408.
29. Contreras, F. X., Sánchez-Magraner, L., Alonso, A., and Goñi, F. M. (2010) Transbilayer (flip-flop) lipid motion and lipid scrambling in membranes. *FEBS Lett.*, 584, 1779−1786.
30. Marques, M. B., Weller, P. F., Parsonnet, J., Ransil, B., and Nicholson-Weller, A. (1989) Phosphatidylinositol-specific phospholipase C, a possible virulence factor of *Staphylococcus aureus*. *J. Clin. Microbiol.,* 27, 2451−2454.
31. Weernink, P. A. O., Han, L., Jakobs, K. H., and Schmidt, M. (2007) Dynamic phospholipid signaling by G protein-coupled receptors. *Biochim. Biophys. Acta-Biomembranes*, 1768, 888−900.
32. Rebecchi, M. J., and Pentyala, S. N. (2000) Structure, function, and control of phosphoinositide-specific phospholipase C. *Physiol. Rev.*, 80, 1291−1335.
33. Rhee, S. G. (2001) Regulation of phosphoinositide-specific phospholipase C. *Annu. Rev. Biochemstry*, 70, 281−312.
34. Feng, J., Wehbi, H., and Roberts, M. F. (2002) Role of tryptophan residues in interfacial binding of phosphatidylinositolspecific phospholipase C. *J. Biol. Chem.*, 277, 19867−19875.

35. Feng, J., Bradley, W., and Roberts, M. F. (2003) Optimizing the interfacial binding and activity of a bacterial phosphatidylinositolspecific phospholipase C. *J. Biol. Chem.*, 278, 24651−24657.
36. Guo, S., Zhang, X., Seaton, B. A., and Roberts, M. F. (2008) Role of helix B residues in interfacial activation of a bacterial phosphatidylinositol-specific phospholipase C. *Biochemstry*, 47, 4201−4210.
37. Pu, M., Orr, A., Redfield, A. G., and Roberts, M. F. (2010) Defining specific lipid binding sites for a peripheral membrane protein in situ using subtesla field-cycling NMR. *J. Biol. Chem.*, 285, 26916−26922.
38. Goldstein, R., Cheng, J., Stec, B., and Roberts, M. F. (2012) Structure of the *S. aureus* PI-specific phospholipase C reveals modulation of active site access by a titratable π-cation latched loop. *Biochemstry*, 51, 2579−2587.
39. Jaeger, K. E., Ransac, S., Dijkstra, B. W., Colson, C., van Heuvel, M., and Misset, O. (1994) Bacterial lipases. *FEMS Microbiol. Rev.*, 15, 29–63.
40. Berg, O. G., Yu, B. Z., Rogers, J., and Jain, M. K. (1991) Interfacial catalysis by phospholipase A2: determination of the interfacial kinetic rate constants. *Biochemstry*, 30, 7283−7297.
41. Pu, M., Fang, X., Redfield, A. G., Gershenson, A. and Roberts, M. F. (2009) Correlation of vesicle binding and phospholipid dynamics with phospholipase C activity: Insights into phosphoatidylcholine activation and surface dilution inhibiton. *J. Biol. Chem. 284*, 16099-16107.
42. Carman, G. M., Deems, R. A., and Dennis, E. A. (1995) Lipid signaling enzymes and surface dilution kinetics. *J. Biol. Chem.*, 270, 18711–18714.
43. Zhou, C., Wu, Y., and Roberts, M. F. (1997) Activation of phosphatidylinositol-specific phospholipase C toward inositol 1,2-(cyclic)-phosphate. *Biochemstry*, 36, 347–355.
44. Volwerk, J. J., Filthuth, E., Griffith, O. H., and Jain, M. K. (1994) Phosphatidylinositol-specific phospholipase C from *Bacillus cereus* at the lipidwater interface: interfacial binding, catalysis, and activation. *Biochemstry*, 33, 3464–3474.
45. Shi, X., Shao, C., Zhang, X., Zambonelli, C., Redfield, A. G., Head, J. F., Seaton, B. A., and Roberts, M. F. (2009) Modulation of *Bacillus thuringiensis* phosphatidylinositol-specific phospholipase C activity by mutations in the putative dimerization interface. *J. Biol. Chem.,* 284, 15607–15618.
46. Cheng, J., Goldstein, R., Gershenson, A., Stec, B., and Roberts, M. F. (2013) The cation-π box is a specific phosphatidylcholine membrane targeting motif. *J. Biol. Chem. 283,* 14863-14873.
47. Qian, X., Zhou, C., and Roberts, M. F. (1998) Phosphatidylcholine activation of bacterial phosphatidylinositiol phospholipase C toward PI vesicles. *Biochemstry*, 37, 6513–6522.
48. Cheng, J., Goldstein, R., Stec, B., Gershenson, A., and Roberts, M. F. (2012) Competition between anion binding and dimerization modulates Staphylococcus aureus phosphatidylinositol-specific phospholipase C enzyme activity. *J. Biol. Chem. 287*, 40317-40327.
49. Chen, W., Goldfine, H., Ananthanarayanan, B., Cho, W., and Roberts, M. F. (2009) *Listeria monocytogenes* phosphatidylinositol-specific phospholipase C:

kinetic activation and homing in on different interfaces. *Biochemstry*, 48, 3578–3592.
50. Cho, W., Bittova, L., and Stahelin, R. V. (2001) Membrane binding assays for peripheral proteins. *Anal Biochem 296*, 153-161.
51. Feng, J., Wehbi, H., and Roberts, M. F. (2002) Role of tryptophan residues in interfacial binding of phosphatidylinositol-specific phospholipase C. *J. Biol. Chem. 277*, 19867-19875.
52. Rebecchi, M., Peterson, A., and McLaughlin, S. (1992) Phosphoinositide-specific phospholipase C-delta 1 binds with high affinity to phospholipid vesicles containing phosphatidylinositol 4,5-bisphosphate. *Biochemistry 31*, 12742-12747.
53. Qian, X., Zhou, C., and Roberts, M. F. (1998) Phosphatidylcholine activation of bacterial phosphatidylinositol-specific phospholipase C toward PI vesicles. *Biochemistry 37*, 6513-6522.
54. Jain, M. K., Egmond, M. R., Verheij, H. M., Apitz-Castro, R., Dijkman, R., and De Haas, G. H. (1982) Interaction of phospholipase A2 and phospholipid bilayers. *Biochim Biophys Acta 688*, 341-348.
55. Ladokhin, A. S., and Holloway, P. W. (1995) Fluorescence of membrane-bound tryptophan octyl ester: a model for studying intrinsic fluorescence of proteinmembrane interactions. *Biophys J 69*, 506-517.
56. Somerharju, P. (2002) Pyrene-labeled lipids as tools in membrane biophysics and cell biology. *Chem Phys Lipids 116*, 57-74.
57. Bazzi, M. D., and Nelsestuen, G. L. (1987) Association of protein kinase C with phospholipid vesicles. *Biochemistry 26*, 115-122.
58. Hixon, M. S., Ball, A., and Gelb, M. H. (1998) Calcium-dependent and - independent interfacial binding and catalysis of cytosolic group IV phospholipase. *Biochemistry 37*, 8516-8526.
59. Magde, D., Elson, E. L., and Webb, W. W. (1974) Fluorescence correlation spectroscopy. II. An experimental realization, *Biopolymers 13*, 29-61.
60. Rusu, L., Gambhir, A., McLaughlin, S., and Radler, J. (2004) Fluorescence correlation spectroscopy studies of Peptide and protein binding to phospholipid vesicles, *Biophys J 87*, 1044-1053.
61. Rhoades, E., Ramlall, T. F., Webb, W. W., and Eliezer, D. (2006) Quantification of alpha-synuclein binding to lipid vesicles using fluorescence correlation spectroscopy, *Biophys J 90*, 4692-4700.
62. Schuck, P. (1997) Use of surface plasmon resonance to probe the equilibrium and dynamic aspects of interactions between biological macromolecules, *Annu Rev Biophys Biomol Struct 26,* 541-566.
63. Heyse, S., Stora, T., Schmid, E., Lakey, J. H., and Vogel, H. (1998) Emerging techniques for investigating molecular interactions at lipid membranes, *Biochim Biophys Acta 1376*, 319-338.
64. Vegas, S., Abian, O., and Velazquez-Campoy, A. (2015) A unified framework basedon the binding polynomial for characterizing biological systems by isothermal titration calorimetry. *Methods 76*, 99-115.

Chapter 2

Materials and Methods

2.1. Materials

2.1.1. Molecular biology reagents

The pET-23a(+) vector and pET-28a(+) vector were obtained from Novagen. The pGEX-6p-1 GST expression vector was purchased from GE Healthcare. Restriction enzymes, IMPACT kit (including pTXB1 vector), Taq DNA polymerase, Quick Ligation kit, and Antarctic phosphatase were purchased from New England Biolabs. The QuikChange site-directed mutagenesis kit, Quikchange Lightening site-directed mutagenesis kit, competent cells used for cloning and mutagenesis (XL-1 blue or XL 10-gold), and overexpression (BL21 (DE3) Codonplus) were purchased from Agilent Technologies. The BL21 Star (DE3) One Shot competent cells were purchased from Invitrogen. The QIAprep spin miniprep kit, QIAquick PCR purification kit and QIAquick Gel Extraction kit were purchased from Qiagen. All the PCR primers were purchased from Eurofins MWG Operon. Pasmids pEVOL-pylT-PylRS and pEVOL-F2YRS were obtained from Dr. Wenshe Liu (Texas A&M) and Dr. Jiangyun Wang (Institute of Biophysics, Chinese Acadamy of Sciences), respectively.

2.1.2 Resin for purification

The Q Sepharose fast flow resin, phenyl sepharose resin and glutathione sepharose 4B resin were purchased from GE Healthcare. Micro bio-spin 6 columns and AG50W-X8 resin were purchased from Bio-Rad Laboratories. Ni-NTA agarose resin was purchased from Qiagen. Chitin resin was purchased from New England Biolabs.

2.1.3 Phospholipids

Most of the lipids used in this work were purchased from Avanti Polar Lipids Inc., and

used without further purification. These include the long chain lipids 1-palmitoyl-2-oleoyl-phosphatidylcholine (POPC), 1,2-dioleoyl-phosphatidylglycerol (DOPG), L-α-phosphatidylinositol (PI) from bovine liver, 1,2-dihexanoyl-*sn*-glycerol-3-phosphocholine (diC_6PC), 1,2-diheptanoyl-*sn*-glycerol-3-phosphocholine (diC_7PC) and 1,2-dibutyryl-*sn*-glycero-3-phophocholine (diC_4PC).

2.1.4 Molecular probes

Both the fluorescence labeling reagents Alexa Fluor 488 C5 maleimide (for cysteine labeling, AF488-Cys) and Alexa Fluor 488 carboxylic acid, succinimidyl ester (for N-terminal amino group, AF488-N-term), were purchased from Invitrogen.

2.1.5 Other chemicals

Tris(hydroxymethyl)aminomethane (Tris), 4-(2-hydroxyethyl)-1-piperazineethanesulfonic acid (HEPES), 2-(N-morpholino) ethane-sulfonic acid (MES), bovine serum albumin (BSA), dithiothreitol (DTT), β-mercaptoethanol (βME), deuterium oxide (D_2O), imidazole, sodium phosphate monobasic, sodium chloride, potassium chloride, magnesium sulfate, magnesium phosphate, manganese(II) chloride, calcium chloride, glycine, sodium pyruvate, ammonium acetate, ammonium sulfate, boric acid, ammonium persulfate (APS), N,N,N',N'-tetramethylethylenediamide (TEMED), 5,5'-dithiobis-(2-nitrobenzoic acid) (DTNB), pyridoxal 5'-phosphate (PLP), chloroform, methanol, acetic acid, glycerol, Triton X-100 (TX-100), M9 minimal salts, arabinose, leucine, polyethylene glycol 4000 (PEG4000) were obtained from Sigma-Aldrich. The 2,6-difluorophenol was purchased from ACROS. The Boc-L-pentafluorophenylalanine was purchased from Peptech Corporation. LB broth and LB agar were obtained from Fisher Scientific. Chloramphenicol, ampicillin and isopropyl β-D-1-

thiogalactopyranoside (IPTG) were purchased from American Bioanalytical, Inc. The detergent compatible (DC) BCA protein assay kit, molecular weight markers, agarose and 30% acrylamide/bisacrylamide solution were obtained from Bio-Rad Laboratories.

2.2 Preparation of fluorinated amino acids

2.2.1 Preparation of F-F_5

Boc-L-pentafluorophenylalanine (1 mmol) was dissolved in a mixture of 95/2.5/2.5 TFA/$^{i}Pr_3SiH/H_2O$ (10mL), and stirred at room temperature for 2 h. The solvents were then removed under rotary vacuum, and the residue was lyophilized and directly used for cell growth.

2.2.2 Synthesis of Y-F_2

Y-F_2 was synthesized following established methods [1]. Aliquots (1 mL) of *E. coli* cells for expression of tyrosine phenol lyase (TPL) were provided by Professor Jianmin Gao, Boston College. These were used to inoculate LB media (1 L containing 100 μg/ml ampicillin) at 37°C. The protein is constitutively expressed, so no induction is required. After 18 h at 37°C, the cells were harvested by centrifugation and re-suspended in 100 mM potassium phosphate, pH 7.0, 0.1 mM pyridoxal phosphate (PLP), 1 mM EDTA, and 5 mM β-mercaptoethanol (βME). Cells were lysed by sonication (10 x 30s) and the suspensions centrifuged. The clear lysate was used for enzymatic synthesis of Y-F_2.

To synthesize Y-F_2, the following reaction conditions, in a final volume of 1 L were used: 10 mM 2,6-difluorophenol, 60 mM sodium pyruvate, 40 μM PLP, 30 mM ammonium acetate and 5 mM βME. The pH of the mixture was adjusted to 8.0 with

ammonium hydroxide. The TPL lysate was added and the mixture was stirred at room temperature for 4 days in the dark.

2.2.3 Purification of Y-F_2

To purify the synthesized Y-F_2, the 1L reaction mixture was acidified to pH 3.0 with concentrated HCL, which precipitated the TPL. A 2 cm thick celite pad was prepared to filter the precipitated protein. The filtrate was extracted twice with 0.5 volume of ethyl acetate and the aqueous layer was loaded onto an AG50W-X8 cation exchange column (Bio-rad), which was equilibrated with 10 volumes water after pre-equilibration with 2 volumes of 6 N HCl. The column was then washed with another 8 volumes of distilled water. The Y-F_2 was eluted with 10% ammonium hydroxide; fraction sizes were 10 mL. Fractions that gave a positive ninhydrin (0.19% w/v ninhydrin, 95% v/v butanol, 0.5% v/v acetic acid and 4.5% v/v water) test were pooled and the volume reduced to 20 mL by rotary evaporation. The remaining solution was lyophilized overnight and stored at 4°C.

2.3 Cloning, expression and purification of *B. thuringiensis* and *S. aureus* PI-PLC

2.3.1 Cloning and construction of mutant proteins

The *S. aureus* PI-PLC (*Sa*PI-PLC) gene was cloned into a pET21a vector with a C-terimal His tag by previous lab member, Dr. Jiongjia Cheng. The *B. thuringiensis* PI-PLC (*Bt*PI-PLC) gene was originally cloned in the pHN1403 vector, and obtained from Dr. Ming-Daw Tsai (Ohio State University). To simplify the purification and increase the yield of fluorinated *Bt*PI-PLC, *Bt*PI-PLC gene was subcloned into a pET23b vector (Novagen) and expressed with a C-terminal His tag.

Figure 2-1. Molecular structures of fluorinated aromatic amino acids. (A) pentafluoro-Phe (F-F_5); (B) difluoro-Tyr (Y-F_2)

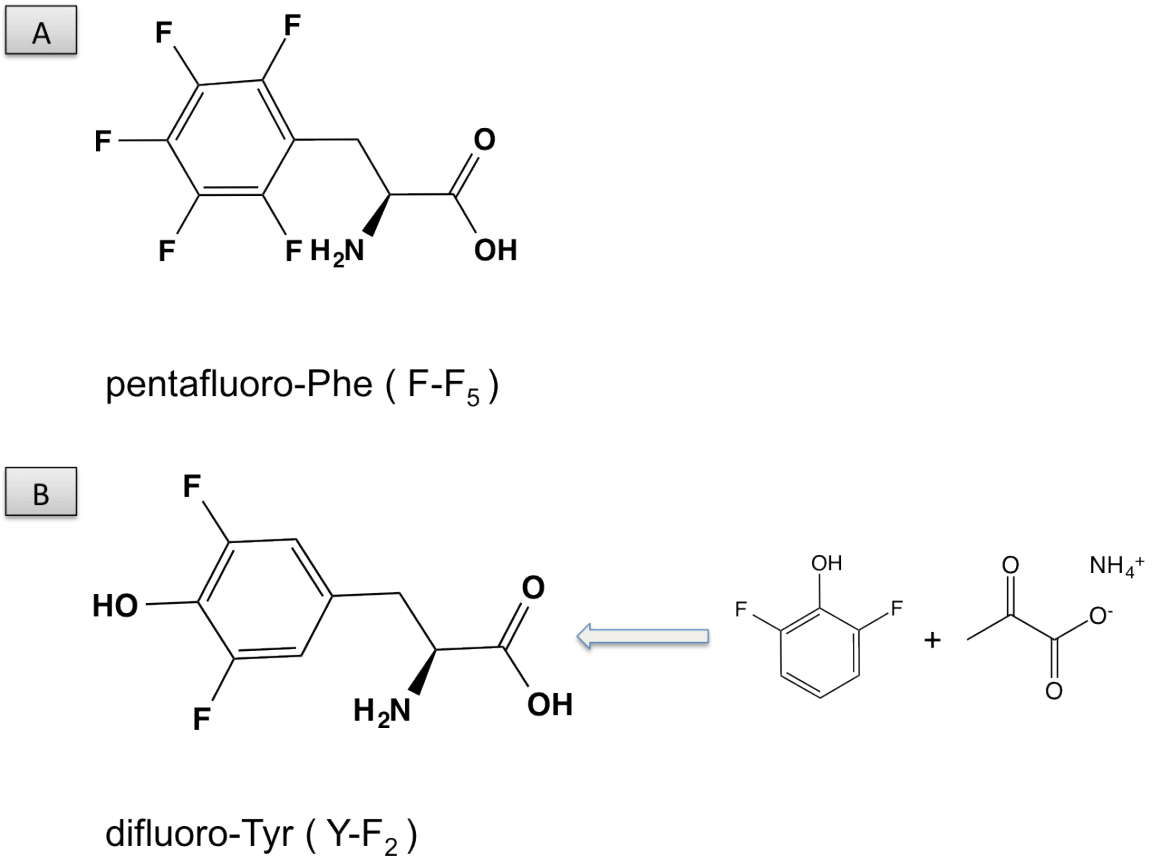

An NdeI restriction site was used for cloning the 5' end of the target gene, with a forward primer 5'-ggggaCATATGgctagctctgttaatgagctt-3' (NdeI site underlined). A XhoI restriction site was used for cloning the 3'end of the target gene with a reverse primer 5'-gcgaggCTCGAGttcttttattaatgacttata-3' (XhoI site underlined). Target genes flanked with NdeI and XhoI sites were amplified under Taq DNA polymerase by PCR. The PCR products were verified on a 1% agarose gel and further purified by the QIAquick Gel Extraction kit following the manufacturer's instructions. The purified products and empty pET23b vector were both doubly digested overnight with XhoI and

NdeI (New England Biolabs) at 37°C. Incubation for 2 h with alkaline phosphatase prevented self-ligation. The Quick ligation kit (New England Biolabs) was used to perform direct ligation of the digested PCR product into the empty pET23b vector. Molar ratios of 1:3 and 1:5 of vector to insert were tested. The ligation mixture was transformed into XL-10 gold competent cells for plasmid propagation and preparation. Resulting colonies were grown as minicultures, and purified DNA was sequenced to confirm the desired clone.

Both *Bt*PI-PLC and *Sa*PI-PLC mutants were constructed using QuikChange methodology [2], following the QuikChange instructions provided by Agilent Technologies. A pair of complementary primers were designed using the web-based program (http://www.genomics.agilent.com/primerDesignProgram.jsp). For mutants incorporating F-F_5 and Y-F_2, an amber codon was introduced into the desired site and primers with amber codon in the center were designed. All the primers used are listed in Table 2-1. Mutagenesis was carried out using the Quick Lightening site-directed Mutagenesis kit (Agilent), which contains PCR PfuTurbo DNA polymerase for primer extension and restriction enzyme DpnI for methylated parental DNA digestion. PCR products were transformed into XL-10 gold supercompetent cells for plasmid propagation. All mutant plasmids were minicultured and purified for DNA sequencing.

Figure 2-2. *B. thuringiensis* PI-PLC DNA and corresponding amino acid sequences.

```
  1  GCTAGCTCTGTTAAT GAGCTTGAAAATTGG TCAAAATGGATGCAA CCTATACCTGATAAT
  1   A  S  S  V  N   E  L  E  N  W   S  K  W  M  Q   P  I  P  D  N

 61  ATCCCGTTAGCACGA ATTTCAATTCCAGGA ACACACGATAGTGGG ACGTTCAAGTTGCAA
 21   I  P  L  A  R   I  S  I  P  G   T  H  D  S  G   T  F  K  L  Q

121  AATCCGATTAAGCAA GTGTGGGGAATGACG CAAGAATATGATTTT CGCTATCAAATGGAC
 41   N  P  I  K  Q   V  W  G  M  T   Q  E  Y  D  F   R  Y  Q  M  D

181  CATGGAGCTCGCATT TTTGATATAAGAGGA CGTTTAACAGATGAT AATACGATAGTTCTT
 61   H  G  A  R  I   F  D  I  R  G   R  L  T  D  D   N  T  I  V  L

241  CATCATGGGCCATTA TATCTTTACGTAACA CTGCATGAATTCATA AATGAAGCGAAACAA
 81   H  H  G  P  L   Y  L  Y  V  T   L  H  E  F  I   N  E  A  K  Q

301  TTTTTAAAAGATAAC CCGAGTGAAACAATT ATTATGTCTTTAAAA AAAGAGTATGAGGAT
101   F  L  K  D  N   P  S  E  T  I   I  M  S  L  K   K  E  Y  E  D

361  ATGAAAGGGGCAGAA GGTTCATTTAGTAGT ACGTTTGAAAAAAAT TATTTTGTTGATCCT
121   M  K  G  A  E   G  S  F  S  S   T  F  E  K  N   Y  F  V  D  P

421  ATCTTTTTAAAAACA GAAGGAAATATAAAA CTTGGAGATGCTCGT GGGAAAATTGTACTA
141   I  F  L  K  T   E  G  N  I  K   L  G  D  A  R   G  K  I  V  L

481  CTAAAAAGATATAGT GGTAGTAATGAATCT GGAGGATATAATAAT TTTTATTGGCCAGAT
161   L  K  R  Y  S   G  S  N  E  S   G  G  Y  N  N   F  Y  W  P  D

541  AATGAGACGTTTACC ACAACTGTAAACCAA AATGTAAATGTAACA GTACAAGATAAATAT
181   N  E  T  F  T   T  T  V  N  Q   N  V  N  V  T   V  Q  D  K  Y

601  AAAGTGAATTATGAT GAGAAAGTAAAATCT ATTAAAGATACGATG GATGAAACGATGAAC
201   K  V  N  Y  D   E  K  V  K  S   I  K  D  T  M   D  E  T  M  N

661  AATAGCGAGGATTTA AATCATCTATATATT AATTTTACAAGCTTG TCTTCTGGTGGTACA
221   N  S  E  D  L   N  H  L  Y  I   N  F  T  S  L   S  S  G  G  T

721  GCATGGAATAGTCCA TATTACTACGCTTCT TATATAAATCCTGAA ATTGCAAACGATATA
241   A  W  N  S  P   Y  Y  Y  A  S   Y  I  N  P  E   I  A  N  D  I

781  AAACAAAAGAATCCT ACAAGAGTAGGCTGG GTAATTCAAGACTAC ATAAATGAAAAGTGG
261   K  Q  K  N  P   T  R  V  G  W   V  I  Q  D  Y   I  N  E  K  W

841  TCACCATTATTGTAT CAAGAAGTTATAAGA GCGAATAAGTCATTA ATAAAAGAATAA
281   S  P  L  L  Y   Q  E  V  I  R   A  N  K  S  L   I  K  E  *
```

Figure 2-3. *S. aureus* PI-PLC DNA and corresponding amino acid sequences.

```
  1  TCAGATTCGTTGAGT AAAAGTCCAGAAAAT TGGATGAGTAAACTT GATGATGGAAAACAT
  1   S  D  S  L  S   K  S  P  E  N   W  M  S  K  L   D  D  G  K  H

 61  TTAACTGAGATTAAT ATACCGGGTTCACAT GATAGTGGCTCATTC ACTTTAAAGGATCCA
 21   L  T  E  I  N   I  P  G  S  H   D  S  G  S  F   T  L  K  D  P

121  GTAAAATCAGTTTGG GCAAAGACTCAAGAT AAAGATTACCTTACC CAAATGAAGTCGGGA
 41   V  K  S  V  W   A  K  T  Q  D   K  D  Y  L  T   Q  M  K  S  G

181  GTCAGGTTTTTTGAT ATTAGAGGTAGAGCA AGTGCTGATAATATG ATTTCAGTTCATCAC
 61   V  R  F  F  D   I  R  G  R  A   S  A  D  N  M   I  S  V  H  H

241  GGCATGGTTTATTTG CATCATGAATTAGGA AAATTTCTCGATGAT GCTAAATATTACTTG
 81   G  M  V  Y  L   H  H  E  L  G   K  F  L  D  D   A  K  Y  Y  L

301  AGTGCTTATCCAAAC GAAACAATTGTGATG TCTATGAAAAAGGAC TACGATAGCGATTCT
101   S  A  Y  P  N   E  T  I  V  M   S  M  K  K  D   Y  D  S  D  S

361  AAAGTTACGAAGACA TTTGAAGAAATTTTT AGAGAATATTATTAT AATAACCCGCAATAT
121   K  V  T  K  T   F  E  E  I  F   R  E  Y  Y  Y   N  N  P  Q  Y

421  CAGAATCTTTTTTAC ACAGGAAGTAATGCG AATCCTACTTTAAAA GAAACGAAAGGTAAA
141   Q  N  L  F  Y   T  G  S  N  A   N  P  T  L  K   E  T  K  G  K

481  ATTGTCCTATTCAAT AGAATGGGGGGTACG TACATAAAAAGTGGT TATGGTGCTGACACG
161   I  V  L  F  N   R  M  G  G  T   Y  I  K  S  G   Y  G  A  D  T

541  TCAGGTATTCAATGG GCAGACAATGCGACA TTTGAAACGAAAATT AATAATGGTAGCTTA
181   S  G  I  Q  W   A  D  N  A  T   F  E  T  K  I   N  N  G  S  L

601  AATTTAAAAGTACAA GATGAGTATAAAGAT TACTATGATAAAAAA GTTGAAGCTGTTAAA
201   N  L  K  V  Q   D  E  Y  K  D   Y  Y  D  K  K   V  E  A  V  K

661  AATTTATTGGCTAAA GCTAAAACGGATAGT AACAAAGACAATGTA TATGTGAATTTCTTG
221   N  L  L  A  K   A  K  T  D  S   N  K  D  N  V   Y  V  N  F  L

721  AGTGTAGCGTCTGGA GGCAGCGCATTTAAT AGTACTTATAACTAT GCATCACATATAAAT
241   S  V  A  S  G   G  S  A  F  N   S  T  Y  N  Y   A  S  H  I  N

781  CCTGAAATTGCAAAA ACGATTAAAGCAAAT GGGAAAGCTAGAACG GGTTGGCTGATTGTT
261   P  E  I  A  K   T  I  K  A  N   G  K  A  R  T   G  W  L  I  V

841  GACTATGCAGGATAT ACGTGGCCTGGATAT GATGATATCGTAAGT GAAATTATAGATAGT
281   D  Y  A  G  Y   T  W  P  G  Y   D  D  I  V  S   E  I  I  D  S

901  AATAAATAA
301   N  K  *
```

Table 2-1. Primers used in site-directed mutagenesis (reverse primers are not listed).

Mutant	Primer
***Bt*PI-PLC**	
WT* (N168C)	5′-gatatagtggtagt**TGT**gaatctggagg-3′
K38A	5′-cgatagtgggacgttc**GCG**ttgcaaaatccg-3′
K44A	5′-gcaaaatccgatt**GCG**caagtgtggggaatg-3′
V46K	5′-ccgattaagcaa**AAG**tggggaatgacgc-3′
R71A	5′-gatataagagga**GCT**ttaacagatg-3′
K122A	5′-gagtatgaggatatg**GCA**ggggcagaaggttc-3′
K201A	5′-cagtacaagataaatat**GCA**gtgaattatgatg-3′
K279A	5′-gactacataaatgaa**GCG**tggtcaccattattg-3′
Y246A	5′-gcatggaatagtcca**GCT**tactacgcttc-3′
Y247A	5′-gcatggaatagtccatat**GCC**tacgcttc-3′
Y248A	5′-gtccatattac**GCC**gcttcttatataaatcc-3′
Y251A	5′-ctacgcttct**GCT**ataaatcctgaaattgc-3′
N203Y	5′-gataaatataaagtg**TAT**tatgatgag-3′
Q40Y	5′-cgttcaagttg**TAT**aatccgattaagc-3′
G238W	5′-caagcttgtcttct**TGG**ggtacagcatgg-3′
Y246A/Y247A[a]	5′-ggaatagtccagct**GCC**tacgcttcttatataatcc-3′
Y86X	5′-gggccatta**TAG**ctttacgtaacactgc-3′
Y88X	5′-ccattatatctt**TAG**gtaacactgcatgaattc-3′
Y204X	5′-gataaatataaagtgaat**TAG**gatgagaaagtaaaatc-3′
Y246X	5′-gcatggaatagtcca**TAG**tactacgcttc-3′
Y247X	5′-ggaatagtccatat**TAG**tacgcttcttatataaatcc-3′
Y248X	5′-gtccatattac**TAG**gcttcttatataaatcc-3′
Y251X	5′-ctacgcttct**TAG**ataaatcctgaaattgc-3′
***Sa*PI-PLC**	
F249X	5′-ggaggcagcgca**TAG**aatagtacttataac-3′
Y253X	5′-gcatttaatagtact**TAG**aactatgcatcac-3′
Y253F	5′-gcatttaatagtact**TTT**aactatgcatcac-3′
H258F	5′-cttataactatgcatca**TTT**ataaatcctgaaattgc-3′
H258X	5′-ctatgcatca**TAG**ataaatcctgaaattgc-3′
N254Y/H258X[b]	5′-gtacttattattatgcatca**TAG**ataaatcctgaaattgc-3′

* All the other *Bt*PI-PLC mutant primers were based on N168C plasmid.
[a] This mutant was designed using Y246A as the parent plasmid.
[b] This mutant was designed using N254Y/H258Y as the parent plasmid.

2.3.2 Expression of native and unnatural amino acid containing PI-PLCs

The appropriate sequenced plasmid was transformed into BL21-codonplus (DE3)-RIL competent cells using the heat-shock method. A single colony was used to inoculate a 5ml LB media and the culture was shaken at 37°C overnight in the presence of appropriate antibiotics (34 μg/mL chloroamphenicol and 100 μg/mL ampicillin). This small culture was used to inoculate 1 L LB (with 34 μg/mL chloroamphenicol and 100 μg/mL ampicillin). Recombinant PI-PLC overexpression was induced by the addition of 0.8 mM IPTG (except for cysteine mutant where 0.4 mM IPTG were used) when the OD_{600} reached 0.7-0.8. The induced cell culture was incubated for another 20 h at 16°C. Cells were harvested by centrifugation and frozen at −20°C for storage.

To express PI-PLCs that incorporat F-F_5 or Y-F_2, *E. coli* BL21(DE3) Star one shot cells were cotransformed with pEVOL-pylT-PyIRs/pEVOL-F2YRS and mutant plasmids. A single colony was then selected and used to inoculate 30 mL of GMML supplemented with 34 μg/mL chloroamphenicol and 100 μg/mL ampicillin. Cells were grown at 37°C in an incubator (250 r.p.m.) and protein expression was induced when OD_{600} reached 0.6 by adding 1mM IPTG, 0.2% arabinose and 1mM F-F_5 or Y-F_2. The induced cell culture was incubated at 37°C for another 12 h. Cells were then harvested and frozen at −20°C for storage.

2.3.3 Purification of BtPI-PLC

Cell pellets were suspended in 20 mM Tris-HCl, pH 8.9, placed on ice and lysed by sonication. Cell debris was pelleted by centrifugation at 15,000 rpm (using a JA-17 rotor) for 35 min. The supernatant containing the enzyme was dialyzed against 20 mM Tris-HCl, pH 8.9 overnight, then it was applied onto a Q-sepharose fast flow (QFF) column

(15 mm x 15 cm) equilibrated with 20 mM Tris-HCl, pH 8.9. The PI-PLC protein was eluted using an increasing NaCl gradient from 0 to 0.6 M in 20 mM Tris-HCl, pH 8.0 at the flow rate of 2 mL/min. Fractions were collected and analyzed by SDS-PAGE (12% gels) to identify those with *Bt*PI-PLC. The protein was further purified using a phenyl-sepharose column (10 mm x 10 cm) equilibrated with 1 M NaCl in 20 mM Tris-HCl, pH 8.0. After the protein was loaded on the column, the PI-PLC was eluted with a decreasing NaCl gradient from 1.0 to 0 M at the flow rate of 1 mL/min. Fractions containing PI-PLC were collected and dialyzed against 20 mM Tris-HCl, pH 8.0, and then concentrated by using Vivaspin 20 mL 10 kDa cut-off filters (Vivaproducts, Inc). Purity of PI-PLC variants was >90% as monitored by SDS-PAGE. Protein concentrations were measured by both Lowry assays and the absorption at 280 nm. Extinction coefficients at 280 nm were calculated using the ProtParam tool (http://web.expasy.org/protparam [3]). For fluorescence correlation spectroscopy (FCS) experiments, a single Cys residue, N168C, was introduced into the protein. For these cysteine-containing proteins, DTT was added during the purification process and in the storage buffer.

2.3.4 Purification of unnatural amino acid containing PI-PLCs

Both His-tagged *Bt*PI-PLC and *Sa*PI-PLC were purified in the same way. The cell lysate with enzyme was prepared by suspending cell pellets in 40mL buffer of 20 mM Tris-HCl, 10 mM imidazole, pH 8.5, followed by sonication and then centrifugation. The cell extract was loaded onto a Ni-NTA agarose column at the flow rate of 0.4 ml/min then washed using 200 mL buffer (20 mM Tris-HCl, 10 mM imidazole, pH 8.5) at the flow rate of 1 mL/min and further washed with 200mL buffer at 2 mL/min. The UV signal was monitored during the washing and elution steps. The His-tagged protein was

eluted using 0.01 to 0.15 M imidazole gradient in 20 mM Tris-HCl, pH 8.5. Protein purity was monitored by SDS-PAGE and fractions with greater than 90% purity were pooled and concentrated. The concentrations of the PI-PLC enzymes were measured by the absorption at 280 nm using the calculated ProtParam tool.

2.4 CD Spectroscopy to monitor protein stability and overall folding

Secondary structure content and thermal stability of the PI-PLC variants were measured using far-UV circular dichroism (CD) spectra obtained on a model AVIV No. 202 CD spectrophotometer. All samples used for CD experiments were prepared by adding the desired amount of protein (0.05 mg/mL) to 10 mM borate, pH 8.0. In the wavelength scanning experiments at 25 ^{o}C, CD spectra were collected from 300 to 180 nm with 1 nm wavelength steps. Secondary structure content was analyzed with the CDNN program [4] using the calculated molar ellipticity in the 190-260 nm range. Thermal stabilities for all proteins were measured by monitoring the ellipticity at 222 nm (primarily α-helix) while increasing the sample temperature 1.0 ^{o}C per min from 20 to 90 ^{o}C, with 1 min equilibration time at each temperature.

2.5 Mass spectrometry to confirm the desired incorporation of F-F_5 and Y-F_2

Samples were analyzed using instrumentation at the University of Massachusetts Mass Spectrometry Center. Samples were dissolved initially in water and then diluted to 1-10 μM in acetonitrile/water/acetic acid (50:47:3 v/v/v). Intact protein molecular weights were determined with a MicrOTOF II ESI-TOF mass spectrometer (Bruker Daltonics, Inc.) using electrospray ionization in positive mode. MS/MS data were obtained using a SolariX 7T FT-ICR (Bruker Daltonics) using CID in the storage quadrupole (~ 5 V collision energy). The most intense charge state peak $[M+43H]^{43+}$ was selected for

isolation. Although complete top-down fragmentation data were not obtained, representative fragments enabled the site of modification to be confirmed. Interestingly, the fluorinated analogs tended to fragment with a significantly lower (2-3 V) collision energy and resulted in a quite different fragmentation pattern from the non-fluorinated version.

MS analysis of tryptic peptides was required to identify the position of the Y-F_2 in N254Y/H258Y-F_2. Tryptic peptides were also used to confirm the position of the fluorinated amino acid in H258F-F_5.

2.6 ^{19}F NMR to monitor fluorinated amino acid incorporation

^{19}F NMR was used to characterize the successful incorporation of the fluorinated aromatic amino acids in both *Bt* and *Sa* PI-PLCs. Appropriate amount of concentrated protein were frozen in liquid N_2, and then lyophilized overnight. The dried protein was rehydrated with Tris buffer (pH 8.5) to yield a final 0.2mM sample for ^{19}F NMR detection. Denaturation of samples in 2% SDS was also used in attempts to simplify the otherwise broad and powder-like ^{19}F spectra obtained using a Varian VNMRS 600 spectrometer. Acquisition parameters include 4.9 μs pulse width (90°), 8012.8 Hz sweep width, 1 delay time between pulse+acquisition times, and 10000 transients collected. Spectra were Fourier transformed with 25 Hz linebroadening.

2.7 Preparation of phospholipid vesicles

Small unilamellar vesicles (SUVs) used in enzyme kinetic experiments were prepared by sonication using a Branson Sonifier 250. The composition of the SUVs (PI, PI/PC, PG/PC) is noted by X_{PC}, the mole fraction of PC. Aliquots of phospholipids species in chloroform were mixed, then dried under N_2. The resultant film was lyophilized

overnight and stored at −20°C. The lipid film was rehydrated with appropriated buffer and the phospholipid solution was sonicated on ice for 30 x 20s, with a 20s rest between each sonication. The average radius for PI and PI/PC (X_{PC} =0.5) vesicles characterized by DynaPro NanoStar Dynamic Light Scattering (DLS) instrument (Wyatt Technology Corp) was 130 Å. Similar average radii for PG/PC SUVs were also documented. [5,6]

2.8 PI-PLC enzyme acitivity assayed by ^{31}P NMR spectroscopy

Specific activities of the PI-PLC enzymes were measured by ^{31}P NMR spectroscopy [7-10] using a VNMRS 600 spectrometer. For *Bt*PI-PLC, the activity assay was usually carried out in 50 mM HEPES pH 7.5, 1 mM EDTA, and 0.1 mg/mL bovine serum albumin (BSA) at 28 ^{o}C. For *Sa*PI-PLC, it was carried out in 50 mM MES, pH 6.5, with EDTA and BSA at 28 °C. The BSA was used to stabilize the protein at the very low concentrations used in these assays. The amount of enzyme added into different assay systems was adjusted so that <20% cyclic inositol phosphate product (cIP) was generated in 15 min for the fixed time method. The amount of *Bt*PI-PLC used was typically 0.1–0.25 μg/mL for mixed micelle assays, 0.2–2 μg/mL for PI cleavage when presented in vesicles, *Sa*PI-PLC concentrations used in assays ranged from 0.3 to 4 μg/mL. The increase in cIP under these conditions is linear with time indicative of an initial rate being measured. Because we are dealing with a vesicle and some fusion of SUVs as diacylglycerol (DAG) is produced, this is not the same as a steady-state rate with the substrate in solution, but it is operationally useful for comparing rates under different conditions (pH, concentration of enzyme, salt, etc.). Mixed micelles of PI with Triton X-100 (TX-100) or diC_7PC were prepared by addition of the detergent solution to dry PI which will turned optically clear after mixing. Mixed micelles examined were either PI (8

mM)/TX-100 (16 mM) or PI (8 mM)/diC$_7$PC (32 mM) for *Bt*PI-PLC and PI (4 mM)/TX-100 (8 mM) or PI (4 mM)/diC$_7$PC (16 mM) for *Sa*PI-PLC. For the specific activities of PI-PLCs toward PI in small unilamellar vesicles (SUVs), the enzyme and SUVs were incubated for a fixed length of time at 28 ^{o}C. The reaction was then quenched by the addition of a few drops of acetic acid (dropping the pH below 4) followed by TX-100 addition to solubilize the remaining lipids in mixed micelles. The relative integrated intensity of the cIP resonance versus the total phospholipid concentration (initial [PI] or [PI] + [PC]) was used to calculate PI-PLC specific activity (as shown in Fig. 2-4). For the enzymatic assays of cysteine mutant variants, 5 mM DTT was added to avoid formation of any protein dimers.

Figure 2-4. Characterization of PI-PLC enzymatic reaction by ^{31}P NMR. All the phosphorus species involved in the assay system are identified with arrows, including phosphatidylinositol (PI), phosphatidylcholine (PC), inositol 1,2-cyclic phosphate (cIP) the amount of enzyme was added so that less than 20% product was generated. X_{PC}=0.2.

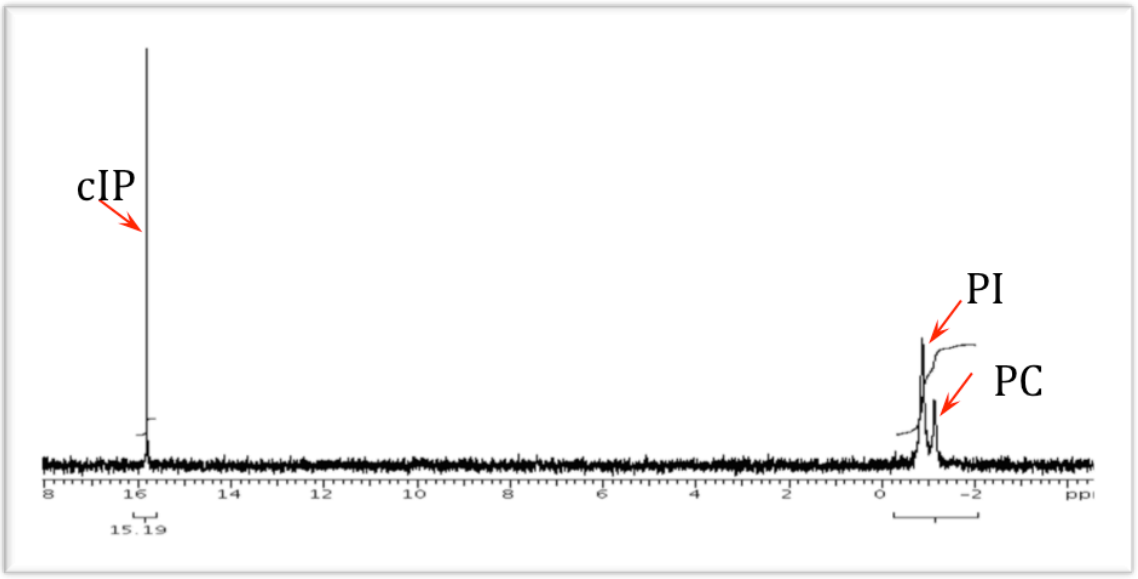

2.9 PI-PLC labeling with Alexa Fluor 488

Fluorescent labeling of proteins was carried out according to the manufacturer's protocol (Invitrogen); schemes for labeling chemistry are shown in Fig. 2-5. For *Bt*PI-PLC, N168C mutant proteins were specifically labeled at Cys168 with the hydrophilic dye Alexa Fluor 488 C5 maleimide (AF488-Cys). AF488-Cys was briefly centrifuged and prepared as a 25 mM stock solution in anhydrous DMSO and stored at −20°C until use. Prior to labeling, the proteins were incubated with 5 mM DTT at room temperature for 30 min to reduce any disulfide bonds. The excess DTT was removed using Micro Bio-Spin 6 columns, which were pre-equilibrated with 0.5mL buffer (20 mM Tris-HCl, pH 7.0). The dye was added immediately (mole ratio of dye:protein=3:1 to 5:1) and the solution was incubated in the dark at room temperature for 2 h. For different proteins, different amounts of dye and incubation time were needed for optimal labeling efficiency. For *Sa*PI-PLC, proteins were labeled with Alexa Fluor 488 carboxylic acid, succinimidyl ester (AF488-N-term). AF488-N-term dye was prepared as a 10 mM stock solution in anhydrous DMSO. This dye was added into the protein sample at a mole ratio of dye:protein = 5:1. To maximize preferential labeling of the N terminus rather than lysine residues, the *Sa*PI-PLC protein labeling reaction was carried out in phosphate buffer, pH 7.2. Unbound dye was removed using three micro-spin columns. The absorptions at 280 nm for protein plus dye and at 495 nm for the dye were used to estimate the labeling ratio. The equation used for calculating the labeling ratio was:

$$[D]/[P]=(\varepsilon_p/\varepsilon_d)*A_{495}/(A_{280}-0.1A_{495})$$

where ε_p was the extinction coefficient of PI-PLC at 280 nm (refer to *2.3.3*), ε_d was the extinction coefficient of AF488 at 495 nm (71,000 cm^{-1} M^{-1}) and 0.1 A_{495} was the

correction. All the *Bt*PI-PLC variants had a labeling ratio of 100±10%, and the *Sa*PI-PLCs typically had 90–100% dye incorporation.

Figure 2-5. Labeling schemes for Alexa Fluor 488 dyes. (A) Cysteine labeling with Alexa Fluor 488 C5 maleimide; (B) N-terminus labeling with Alexa Fluor 488 carboxylic acid, succinimidyl ester.

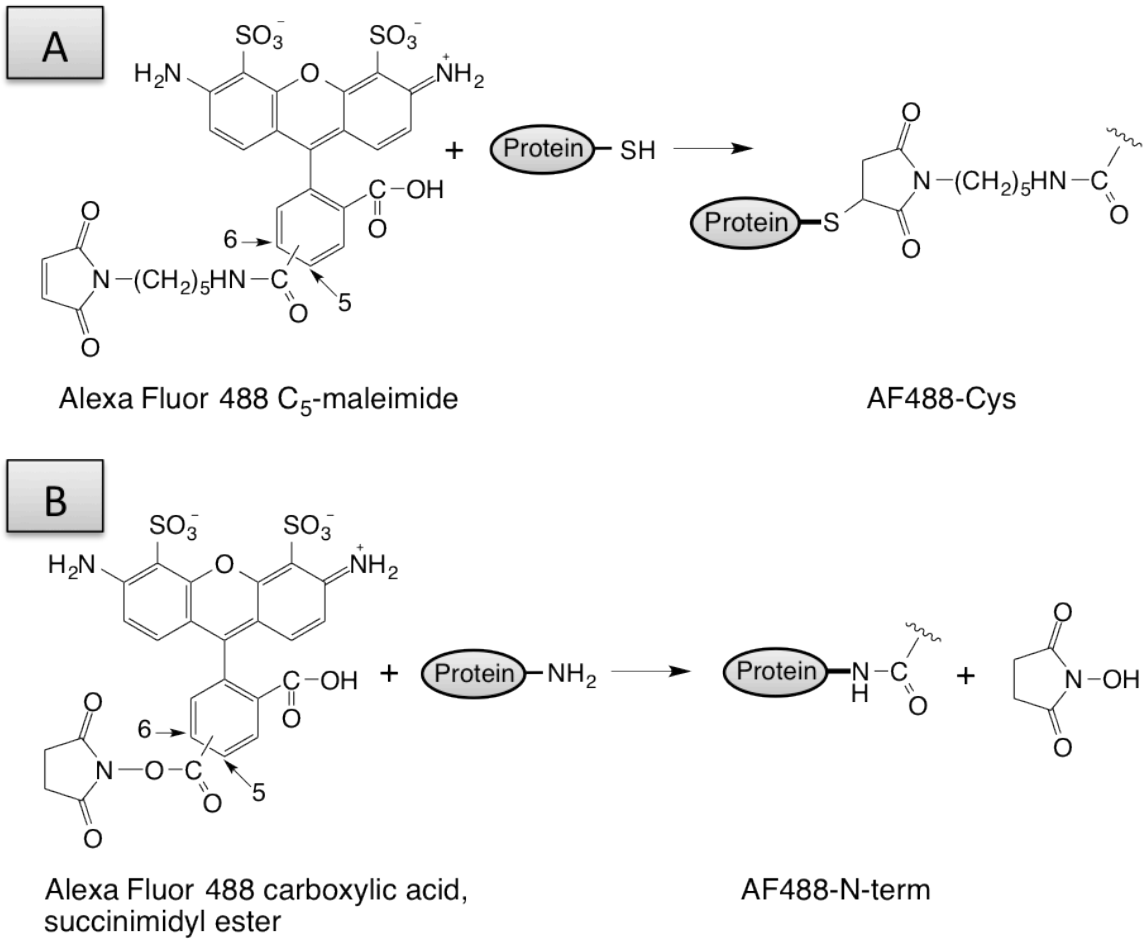

2.10 Binding of PI-PLCs to vesicles measured by fluorescence correlation spectroscopy (FCS)

FCS based binding assays were performed using a previously described [6] home-built confocal setup based on an IX-70 inverted microscope (Olympus) as shown in Fig. 2-5. Alexa Fluor 488 (AF488) fluorescence was monitored at 22 ^{o}C with samples placed in chambered coverglass wells (Lab-Tek, Nunc), containing 10 nM labeled *Bt*PI-PLCs plus 1 mg/mL BSA in 300 μl PBS, pH 7.4 for *Bt*PI-PLC; binding experiments with *Sa*PI-PLCs used 3.5 nM labeled protein and 1mg/ml BSA in 300 μl of 50 mM MES, pH 6.5. Prior to use, the chambers were coated with 10 mg/mL BSA and rinsed with desired buffer to prevent protein adhesion to the sides of the walls. The anionic substrate analog DOPG was used for all FCS experiments because the PI cleavage product DAG leads to vesicle fusion [7]. PG is a *Bt*PI-PLC substrate and can be cleaved over a period of days by mg/mL concentrations of PI-PLC. [8] However, at the low protein concentrations used in the FCS experiments, no detectable hydrolysis of PG occurred. To assess protein binding, SUVs containing DOPG and various mole fractions of POPC, X_{PC}, were titrated into the labeled PI-PLC solutions and fluorescence intensities were collected. For each X_{PC}, FCS titrations were run in triplicate and repeated a second time with different vesicle and protein preparations.

Data were analyzed as previously described [9-10]. The fitted diffusion coefficient for free, AF488-Cys labeled *Bt*PI-PLC was 54±5 μm^2 s^{-1} and AF488-N-term labeled *Sa*PI-PLC (D_{free}) was 50±2 μm^2 s^{-1}; the vesicle diffusion coefficient, D_{bound}, determined from analysis of vesicles containing fluorescently labeled Rhodamine lipids, was in the range of 12-15 μm^2 s^{-1}.

Figure 2-6. FCS experimental schematic. Individual laser lines from an air-cooled argon-krypton, multi-line laser are separated using a quartz prism P. The 488 nm laser line is isolated and expanded 5 times using two lenses, L1 and L2, in order to be reflected into the sample using a 500drlp dichroic D1. In the IX-70 inverted microscope, the 60X water objective, Obj, focuses the laser light into the sample and collects the emission. The emission passes through D1 and any remaining scattered laser light is blocked by a HQ505lp long pass filter F1. The emission is then focused onto a 30µm pinhole by the tube lens L3 in the microscope to limit the detection volume and collimated by lens L4. To calculate the cross-correlation, the fluorescence signal is split by a 50-50 beam splitter, BS2, and passes through HQ535/50 bandpass filters, F2 & F3, to be focused on two avalanche photodiodes, APD1 and APD2, by lenses L5 and L6, respectively. The box shows a typical observation volume (1 μm^3) with different species, free AF488 labeled protein and vesicle-bound AF488 labeled protein, diffusing in and out of the volume (as indicated in the cartoon on the right).

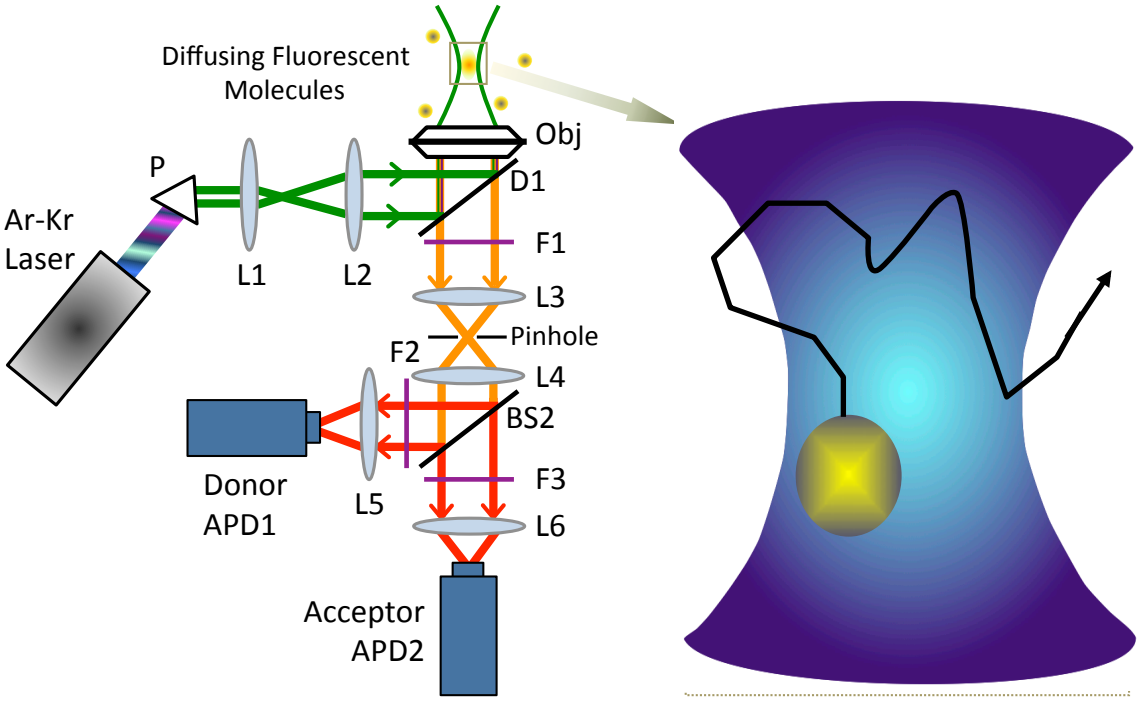

Figure 2-7. Representative normalized correlations and binding curves for *WT *Bt*PI-PLC. (A) Normalized correlation curves for 10 nM *WT *Bt*PI-PLC in solution (red), in the presence of 100 μM PC SUVs (open square), 400 μM PC SUVs (solid circle), 4700 μM PC SUVs (open circle) and fluorescent labeled PC SUVs (solid triangle). (B) Titration curves showing the fraction of *WT *Bt*PI-PLC bound to pure POPC SUVs (blue), DOPG/POPC (X_{PC} = 0.25) SUVs (orange). Error bars represent the S.D. from 3 independent sets of titrations.

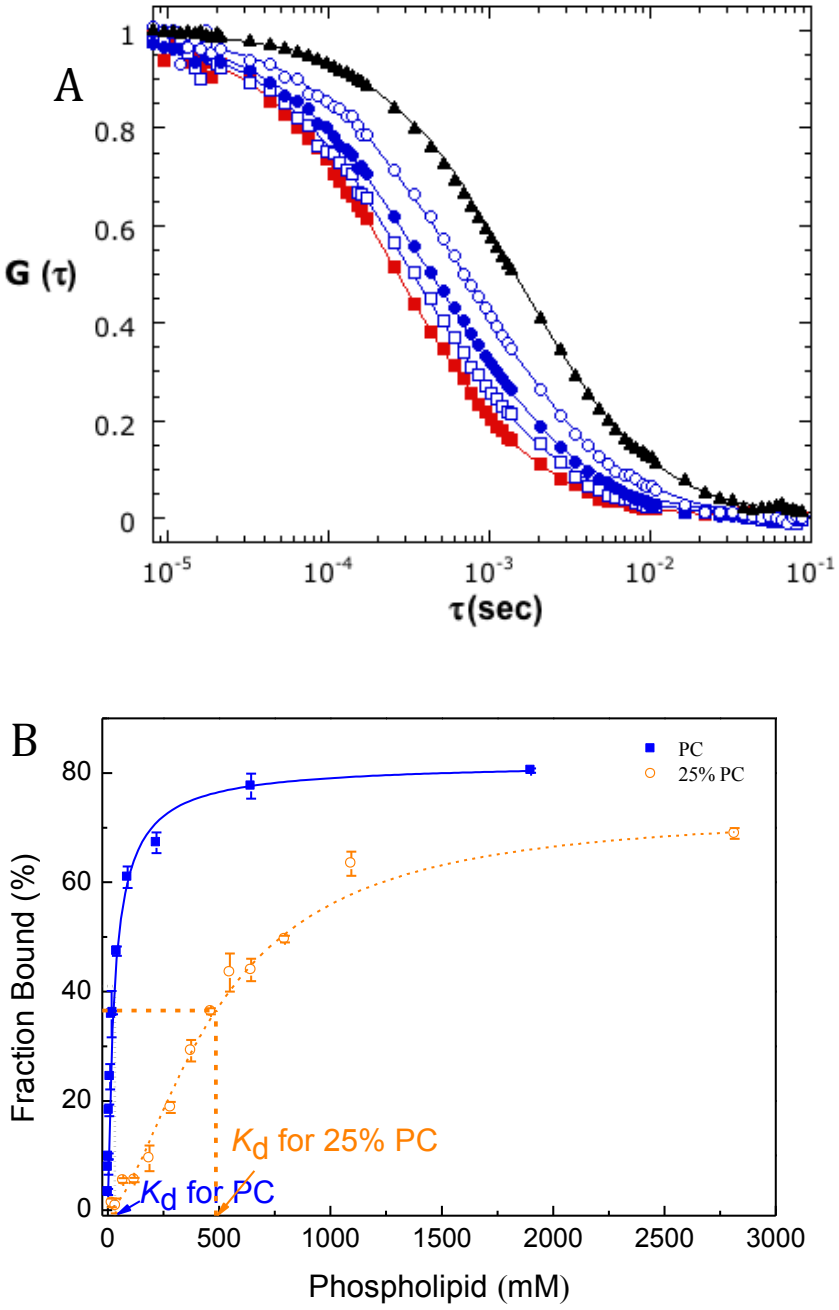

2.11 X-ray crystallography of *Sa*PI-PLC mutants H258F-F_5 and F249F-F_5

H258F-F_5 and F249F-F_5 were concentrated to 20 mg/mL and then combined with 200 mM *myo*-inositol. Before setting up crystallization trays, the protein solution was diluted to a final concentration of 10 mg/mL, with 100 mM *myo*-inositol and incubated on ice for a minimum of 2 h. The PI-PLC samples were crystallized at 4 °C by vapor diffusion, using 3 μL hanging drops against a reservoir solution containing 150 mM ammonium acetate, 100 mM sodium acetate, pH 4.6, with 10 mM magnesium nitrate, and 20-24% PEG 4000.

Data were collected at 100 K using a Rigaku MicroMax-07 HF high-intensity microfocus rotating Cu anode X-ray generator, coupled with Osmic VariMax Optics and a R-Axis IV++ image plate area detector. Data were indexed and reduced using d*TREK [12]. Both structures were solved by doing molecular replacement in PHENIX [13], using PHASER [15], with the *S. aureus* structure 3V18 as a starting model. All models were refined with Phenix.refine, with manual model building in COOT [14]. Maps were generated in PHENIX. Structural comparisons were made using SSM superposition [16] in COOT and alignment in Pymol [17]. Adit [18] was used for PBD deposition and validation.

Reference

1. Seyedsayamdost, M.R., Yee, C. S., and Stubbe, J. (2007) Site-specific incorporation of fluorotyrosines into the R2 subunit of *E. coli* ribonucleotide reductase by expressed protein ligation. *Nat. Protoc. 2*, 1225-1235.
2. Braman, J., Papworth, C., and Greener, A. (1996) Site-directed mutagenesis using double-stranded plasmid DNA templates. *Methods. Mol. Biol*., 57, 31–44.
3. Gasteiger, E., Hoogland, C., Gattiker, A., Duvaud, S., Wilkins, M. R., Appel, R. D., and Bairoch, A. (2005) Protein identification and analysis tools on the ExPASy server. Proteomics Protocols Handbook. J. M. Walker, editor. Humana Press, New York. 571–607.
4. Böhm, G., Muhr, R., and Jaenicke. R. (1992) Quantitative analysis of protein far UV circular dichroism spectra by neural networks. *Protein Eng.* 5, 191–195.
5. Pu, M., Fang, X., and Roberts, M. F. (2009) Correlation of vesicle binding and phospholipid dynamics with phospholipase C activity: insights into phosphatidylcholine activation and surface dilution inhibition. *J. Biol. Chem.*, 284, 16099–16107.
6. Liu, L., Mushero, N., Hedstrom, L., and Gershenson, A. (2006) Conformational distributions of protease-serpin complexes: a partially translocated complex, *Biochemistry*, 45, 10865-10872.
7. Goñi, F. M., and Alonso, A. (2000) Membrane fusion induced by phospholipase C and sphingomyelinases. *Biosci. Rep.*, 20, 443–463.
8. Volwerk, J. J., Filthuth, E., Griffith, O. H., and Jain, M. K. (1994) Phosphotidylinositol-specific phospholipase C from Bacillus cereus at the lipid-water interface: interfacial binding, catalysis, and activation, *Biochemistry*, 33, 3464-3474.
9. Pu, M., Roberts, M. F., and Gershenson, A. (2009) Fluorescence correlation spectroscopy of phosphatidylinositol-specific phospholipase C monitors the interplay of substrate and activator lipid binding. *Biochemstry*, 48, 6835–6845.
10. Cheng, J., Goldstein, R., Stec, B., Gershenson, A., and Roberts, M.F. (2012) Competition between anion binding and dimerization modulates *Staphylococcus aureus* phosphatidylinositol-specific phospholipase C enzymatic activity. *J. Biol. Chem.*, 287, 40317-40327
11. Zhou, C., Qian, X., and Roberts, M. F. (1997) Allosteric activation of phosphatidylinositol-specific phospholipase C: specific phospholipid binding anchors the enzyme to the interface. *Biochemstry*, 36, 10089−10097.
12. Otwinowski, Z., and Minor, W. (1997) Processing of X-ray diffraction data collected in oscillation mode. *Methods Enzymol. 276*, 207-236.
13. McCoy, A. J., Grosse-Kunstleve, R. W., Adams, P. D., Winn, M. D., Storoni, L. C., and Read, R. J. (2007) Phaser crystallographic software. *J. Appl. Crystallogr. 40*, 658−674.
14. Emsley, P., and Cowtan, K. (2004) Coot: model-building tools for molecular graphics. *Acta Crystallogr., Sect. D: Biol. Crystallogr. 60*, 2126−2132.
15. Adams, P. D., Afonine, P. V., Bunkóczi, G., Chen, V. B., Davis, I. W., Echols, N., Headd, J. J., Hung, L. W., Kapral, G. J., Grosse-Kunstleve, R. W., McCoy, A. J., Moriarty, N. W., Oeffner, R., Read, R. J., Richardson, D. C., Richardson, J. S.,

Terwilliger, T. C., and Zwart, P. H. (2010) PHENIX: a comprehensive Python-based system for macromolecular structure solution. *Acta Crystallogr., Sect. D: Biol. Crystallogr. 66*, 213−221.
16. Krissinel, E., and Henrick, K. (2004) Secondary-structure matching (SSM), a new tool for fast protein structure alignment in three dimensions. *Acta Crystallogr., Sect. D: Biol. Crystallogr. 60*, 2256−2268.
17. Ravichandran, K. R., Liang, L., Stubbe, J., and Tommos, C. (2013) Formal reduction potential of 3,5-difluorotyrosine in a structured protein: insight into multistep radical transfer. *Biochemistry 52*, 8907-8915.
18. Yang, H., Guranovic, V., Dutta, S., Feng, Z., Berman, H. M., and Westbrook, J. D. (2004) Automated and accurate deposition of structures solved by X-ray diffraction to the Protein Data Bank. *Acta Crystallogr. D Biol*. 60, 1833-1839.

Chapter 3

PC-cation/Tyrosine-π interactions in *Bt*PI-PLC

3.1 Introduction

Cation-π interactions are ubiquitous noncovalent interactions. They have been recognized as a major force for molecular recognition, playing an important role in macromolecule structure formation and stability as well as function [1-3]. In protein, cation-π interactions are typically observed between aromatic amino acid (phenylalanine, tryptophan, or tyrosine) sidechains and cationic ammonium or guanidinium groups from lysine and arginine [4]. Cation-π interactions are also important for substrate and ligand binding, particularly for molecules containing a choline group. For example, in the crystal structure of the human phosphatidylcholine transfer protein (PC-TP), the choline moiety of the lipid was involved in cation-π interactions with a cage of three tyrosine residues.

Cation-π interactions with phospholipids in cell membranes have been suggested to play a role in the structural stability and lipid specificity of integral membrane proteins. Using gramicidin dimer as a model for integral membrane proteins containing interfacial Trp residues for molecular dynamic simulations [5], Petersen and coworkers have shown that phosphatidylethanolamine (PE) and PC interact with interfacial tryptophans via cation-π interactions. Trp involvement in cation-π interactions with the membrane has also been observed in other simulations, both for short peptides [6,7] and for an amphitropic protein [8].

Compared to integral membrane proteins, peripheral membrane proteins do not span the lipid bilayer. They bind at the surface of cell membranes in order to perform their function. Thus the protein interactions with the phospholipid headgroups accounted for most of their affinity for the membranes. Tyrosine residues, like Trp, can in principle

engage in cation-π interactions with choline-containing lipids [9]. However, much less is known about these contributions to membrane binding by proteins. Recently, we reported that the *Sa*PI-PLC mutant N254Y/H258Y, constructed to contain a four Tyr strip mimicking *Bt*PI-PLC, exhibits greatly enhanced affinity for PC-containing membranes. In addition, both a X-ray crystal structure [10] and field cycling ^{31}P NMR [11] results showed that a specific PC binding site has been introduced into this phospholipase.

*Bt*PI-PLC has a plethora of Tyr residues in the protein membrane interface. To investigate the cation-π contributions of these residues, a method of combined MD simulation and mutagenesis studies was adopted.

3.2 *Bt*PI-PLC has much tighter vesicle binding than *Sa*PI-PLC

*Sa*PI-PLC binds to PC-rich membranes with much lower affinity than does the *Bt*PI-PLC, and it has virtually no affinity for pure PC vesicles [12]. For *Bt*PI-PLC, increasing X_{PC} up to 0.8 increases the protein affinity for SUVs, yielding μM K_d values [13]. In contrast, *Sa*PI-PLC binds SUVs at acidic pH, with mM K_d values [12]. Structural alignment shows that *Bt*PI-PLC has more surface tyrosine residues compared to *Sa*PI-PLC. The two long α-helices, F and G, as well as the neighboring α-helix B regions of *Bt*PI-PLC contain at least eight Tyr (Tyr86, Tyr88, Tyr200, Tyr204, Tyr246, Tyr247, Tyr248, Tyr251) and two Trp (Trp47, Trp242). Previous mutagenesis data for some of the helix G Tyr residues [14] showed that these aromatic residues are associated with tighter binding of *Bt*PI-PLC to PC-containing vesicles. These tyrosines could be involved in cation-π interactions with the choline head group of membrane PC. To bolster this interpretation, the *Sa*PI-PLC mutant N254Y/H258Y was constructed based on sequence and structural alignments of *Bt*PI-PLC and *Sa*PI-PLC enzymes to mimic a Tyr strip

(^{246}Y-Y-Y-A-S-^{251}Y) that is suggested by fc-P-NMR to be around the PC binding site for *Bt*PI-PLC [14]. The binding affinity of *Sa*PI-PLC N254Y/H258Y was 50-fold higher than WT at X_{PC}=0.8 and showed measurable binding affinity for pure PC vesicles [11]. However, even N254Y/H258Y is a much weaker vesicle binder when compared to *Bt*PI-PLC. The research goal of this project was to define the cation-π interactions between the *Bt*PI-PLC and the PC containing SUVs.

3.3 Molecular Dynamics (MD) simulations

Dr. Cedric Grauffel from University of Bergen, Norway, did all the MD simulations for *Bt*PI-PLC. Initially, simulations were carried out by docking *Bt*PI-PLC to an implicit anionic membrane model to predict the orientation of the protein at the membrane. Six PI-PLC orientations relative to the membrane, with each orientation corresponding to one face of a cube containing the enzyme, were screened. Half of these orientations led to an anchored PI-PLC at the model membrane. It was found that the anchorage was always achieved via helix B, in agreement with Dr. Mingming Pu's previous experimental data [13]. The simulation yielding the lowest IMM1-GC effective energy was then selected for further analysis. Decomposition of the binding energy shows that the hydrophobic interactions with residues in helix B contribute the most energy. It was also found that the interfacial Tyr residues showed no significant energetically favorable interactions with the implicit membrane, despite their proximity to the membrane plane. Considering that implicit membrane model has been reported to underestimate the interfacial interactions of aromatic amino acids, Dr. Grauffel switched simulation models to dimyristoylphosphatidylcholine (DMPC) bilayers.

Simulations of protein with an all-atom DMPC lipid bilayer were initiated using the *Bt*PI-PLC orientation predicted by the implicit membrane simulations. *Bt*PI-PLC showed very little structural change during the 500 ns MD simulation. Amino acid anchorage depth at the interfacial binding site was evaluated by calculating the distance between the residue centers of mass and the average plane defined by the position of the phosphorus atoms. The most deeply buried amino acids were located on helix B (Ile43, Pro42, Asn41) and on the β7-αG loop (Trp242, Thr240, Ala241 and Gly239), with an average penetration depth of 2 to 4 Å inside the plane defined by the phosphorus atoms (Figure 3-1A). Other amino acids of the interfacial binding site, including most tyrosines, were located on the other side of the phosphate plane.

Interactions between PI-PLC residues and the membrane phospholipid were monitored during the MD simulations. They showed that the frequency of aromatic amino acids, especially tyrosines, at the interface between PI-PLC and the membrane is strikingly high. Potential cation-π interactions between choline head group and aromatic groups were identified. The MD results suggested that the cation-π interactions involving Tyr88 and Tyr246 have the highest occupancy. Tyr86, Tyr118, Tyr204 and Tyr251 are involved in less persistent cation-π interactions that occur regularly throughout the simulation (Figure 3-1B). Tyr53, Tyr 247 and Tyr248 were observed mediating cation-π interactions with much less frequency. Tyr200 formed an interaction with the choline group of a lipid that occasionally sticks out of the bilayer and half-way into the active site. Among the four tyrosines (246, 247, 248 and 251) in helix G, three were involved in cation-π interactions (the exception was Y248, which has very low occupancy according to the simulations) and Y246 and Y251 were suggested to have rather strong interactions. Due to the

consecutive location on an α-helix, the side chains of Tyr246, Tyr247 and Tyr248 point in different directions and would interact with different lipids. However, the sidechains of Tyr247 and Tyr251 are on the same side of the helix, separated by one turn.

Figure 3-1. MD simulations of *Bt*PI-PLC binding to a DMPC bilayer. (A) IMM1 orientation of PI-PLC used to initiate the simulations with explicit lipids. Helices B, F and G are magenta, green and orange, respectively. (B) Occupancies of cation-π interactions for aromatic residues versus simulation time (occupancies >5% are shown). (C) Snapshot of a cation-π interaction collected along the simulation time course (representative frame taken between 400 and 500 ns).

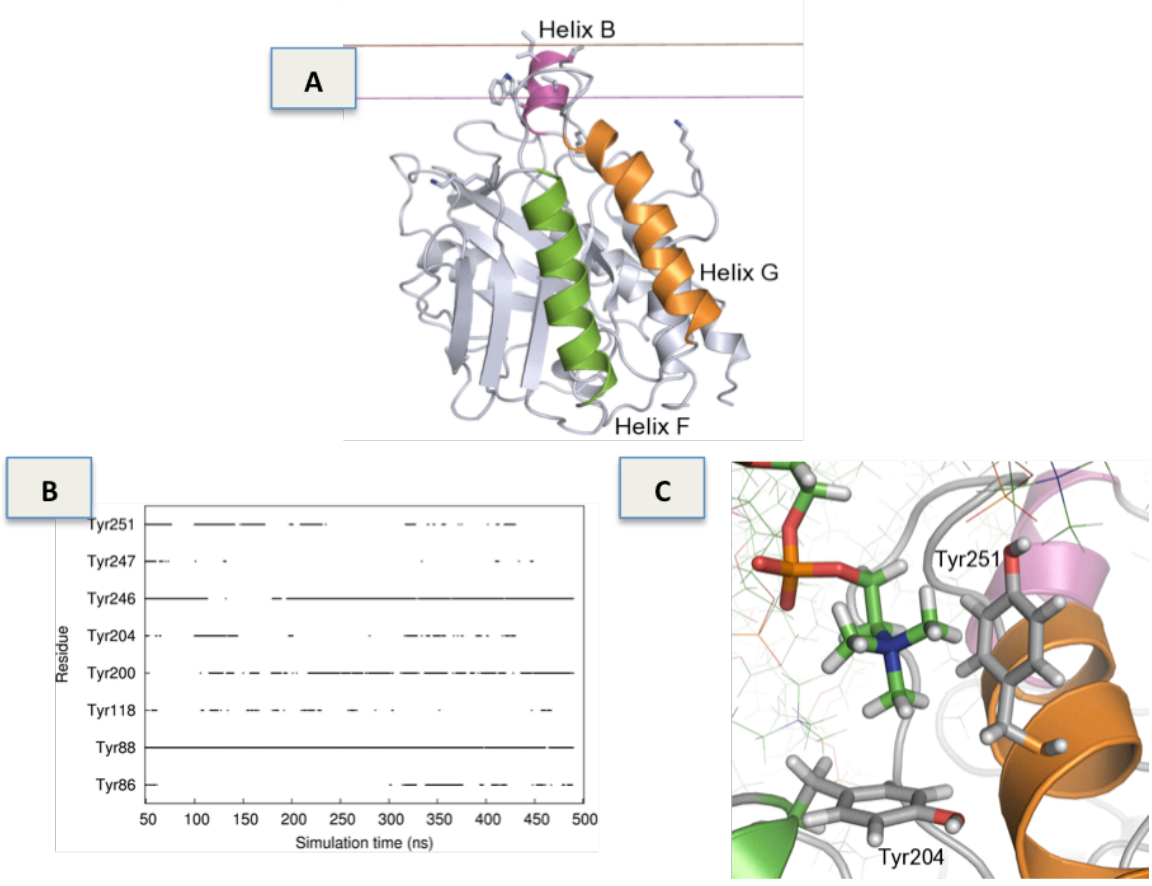

Thus, Tyr247 and Tyr251 could interact with the same phospholipid. Similarly, the orientations of Tyr204 on helix F and Tyr251 on helix G allow simultaneous interactions

with the same lipid (Figure 3-1C). Tyr248, also at the interfacial binding site, plays a slightly different role. It is almost never involved in interactions with phospholipid. Instead, it engages in long-lived intramolecular hydrophobic interactions with Leu235 and Pro245 that appear to maintain the structure and orientation of the rim loop.

3.4 Design and characterization of Tyrosine mutants

The MD simulation with a DMPC bilayer identified Tyr residues in the loop between β2 and helix D (86, 88), in helix F (204) and in helix G (246-247, 251) as important for cation-π interactions with PC choline head groups. These MD predictions were tested by mutating each Tyr to Ala or Ser, and measuring protein binding to SUVs using FCS. Tyr248, which appears to play a different role, was also tested. We also tried to design new cation-π interactions by introducing new Tyr or Trp into the rim loop region (at resides 40, 88, 203 and 238) of *Bt*PI-PLC. Mutants were constructed using site-directed mutagenesis and purified as previously described in Chapter 2, section 2.3. Secondary structure and thermal stability of the *Bt*PI-PLC variants were measured and all variants are well folded with similar CD spectra (Figure 3-2) and had no significant changes in secondary structure (Table 3-1). Thermal stabilities for all PI-PLC variants were similar to WT, except for Y204A containing mutants, which are less stable. Other helix B and rim loop mutants, including Y86A, Y88A, Y204S and Y248A, were made previously in the group by Dr. Su Guo. These were also included in studies of the effects of Tyr→Ala mutations.

Figure 3-2. Comparison of CD spectra for WT (□) and Y246A (●). Similar agreement with the WT far UV CD data is observed for all of the *Bt*PI-PLC mutants.

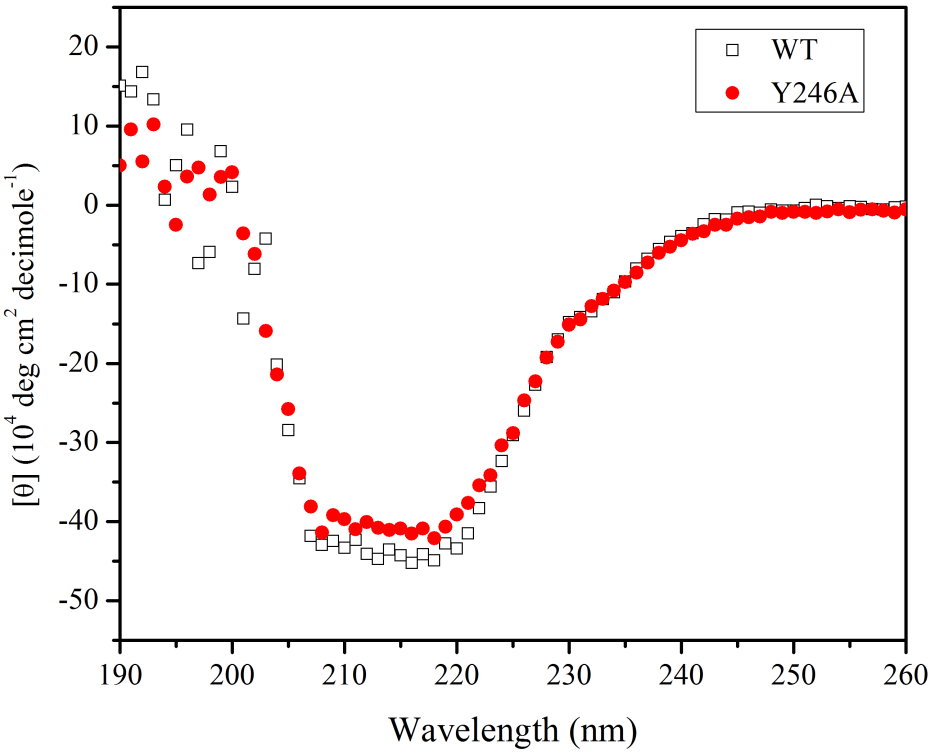

Table 3-1. Analysis of PI-PLC secondary structure and thermostability from far-UV circular dichroism (CD) data.

Variant[a]	α-helix(%)	β-sheet (%)	β-turn (%)	Random coil (%)	T_m (°C)
WT*	22.2	30.0	17.5	29.9	56.7
Y86A/Y88A*	19.1	34.1	17.1	29.7	56.5
Y204A/Y251A*	18.6	33.6	16.8	31.1	53.7
Y204S/Y248A*	21.8	31.5	17.5	29.1	52.9
Y246A*	20.9	31.6	17.2	30.2	53.1
Y247A*	19.5	34.3	17.2	29.1	52.6
Y246A/Y247A*	19.6	34.0	17.2	29.3	51.9

[a] The asterisk indicates that all variants contain the N168C mutation required for fluorescent labeling.

Figure 3-3. Approximate membrane binding geometry suggested by the explicit MD simulation. Important residues and helices B, F and G are labeled. The membrane is represented by a blue line. Top view is used here.

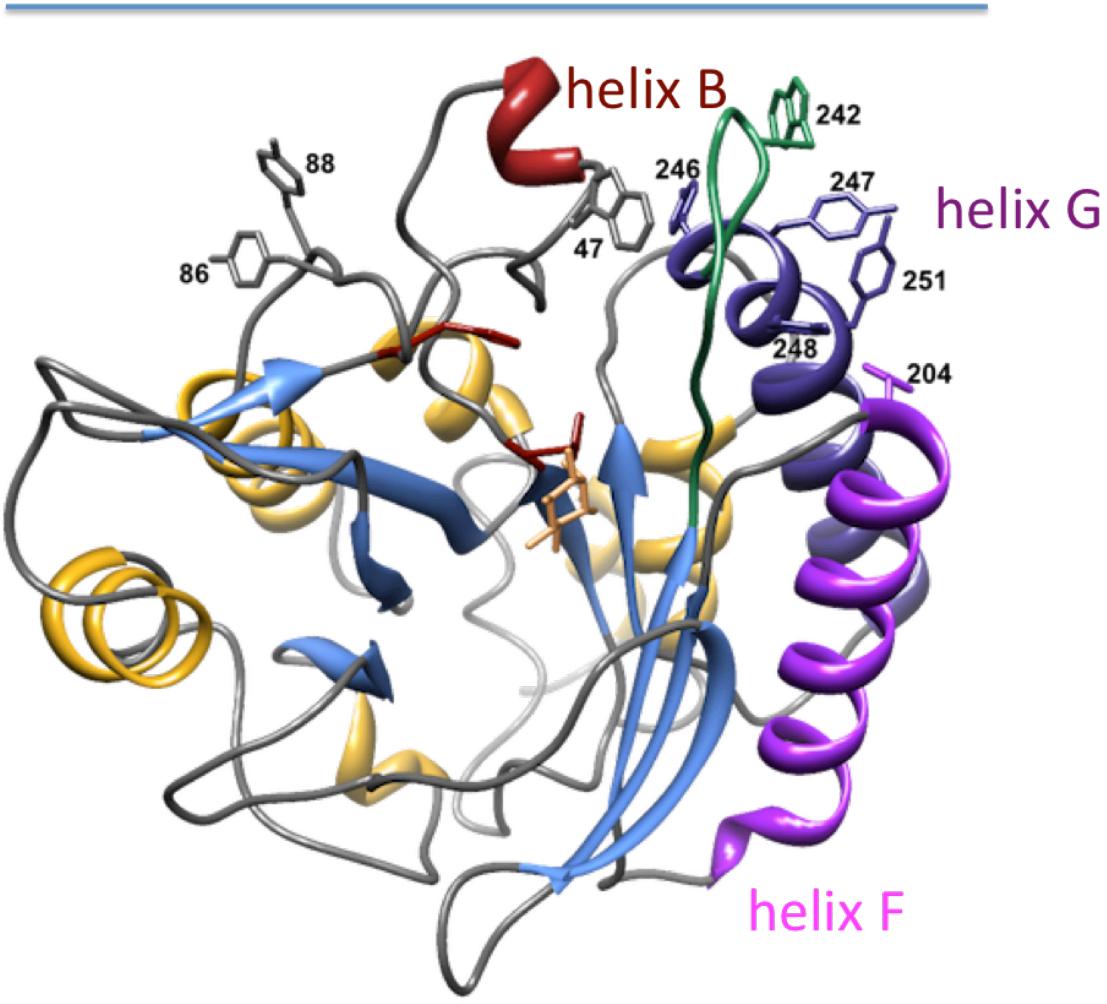

3.5 Effects of specific mutations on *Bt*PI-PLC binding to vesicles

*Bt*PI-PLC binds to SUVs with lower affinity for SUVs composed of pure anionic lipids or pure PC SUVs. Because of this apparent synergism, binding was measured as a function of X_{PC} (the mole fraction PC in the SUVs). The apparent K_d and ratio of the apparent K_d relative to the K_d for wild type (WT) protein are plotted in Figure 3-4 as a function of $X_{PC.}$ Apparent K_d values at $X_{PC} = 1$ are listed in Table 3-2.

In general, WT* PI-PLC and the Tyr* variants, (where the asterisk indicates the N168C mutation required for Cys-mediated fluorescent labeling of PI-PLC for FCS) have similar affinities for anionic SUVs containing only PG (Figure 3-4), and Tyr* defects in binding are greatest for SUVs at high X_{PC}. This is consistent with the simulations where most of the Tyr residues can mediate interactions with choline headgroups.

Both Tyr86 and Tyr88 are at the top of the barrel rim and could directly interact with membrane bilayer. Mutagenesis of Tyr88 to Ala (Y88A*) increases the apparent K_d by at least one order of magnitude for $X_{PC}>0.5$ while defects in binding of Y86A* are barely significant (Figure 3-4A). As might be expected, decreases in membrane affinity for the Y86A/Y88A* double mutant are dominated by the effect of mutating Tyr88. These results are consistent with the simulations where, compared to Tyr86, occupancies of cation-π interactions between Tyr88 and choline headgroups are much higher and are stabilized by additional interactions mediated by the phosphate group of the same phospholipid. It also suggests that, consistent with the MD simulations, Tyr86 is slightly farther away from the hydrocarbon boundary than Tyr88, which would result less interaction with choline head groups and consequently result in less PC dependence. It has been shown that the interactions between *Bt*PI-PLC and membranes are very dynamic

as shown in the single molecule spectroscopy measurement [15], so the difference of Y86A* and Y88A* is more likely caused by the slightly deeper insertion of Tyr88 into the interfacial region of the membrane.

Figure 3-4. Binding of *Bt*PI-PLC Tyr variants to SUVs. Apparent K_d (A) and apparent K_d relative to WT* (B, C and D) as a function of X_{PC}. The error bars are the largest uncertainties generated during the FCS data analysis, either the standard deviations from two independent repeats or the uncertainty generated by error propagation for the two independent data sets.

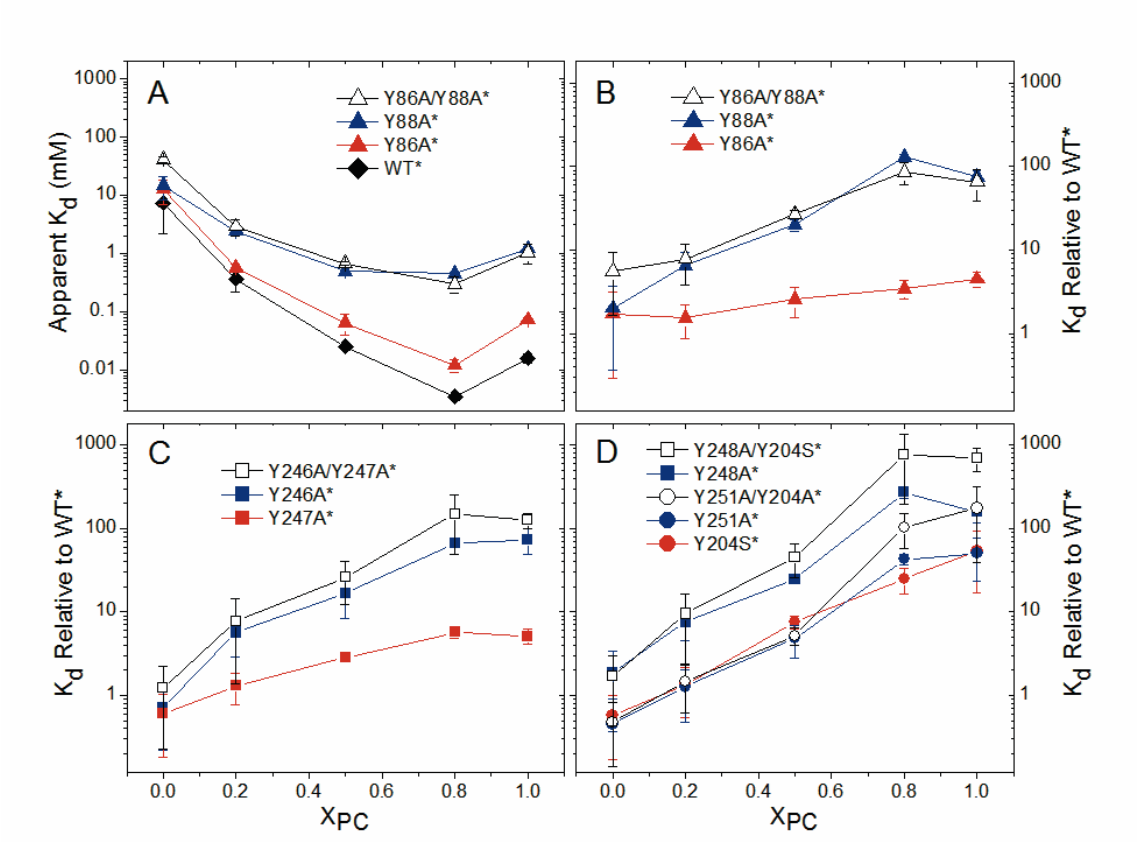

Tyr246 and Tyr247 are both on helix G. The Y246A* variant shows significant binding defects even at X_{PC} = 0.2 (Figure 3-4C). Mutagenesis of Tyr247 is much less perturbing, and Y247A* has apparent K_ds that at most 5-fold higher than WT* at X_{PC} > 0.8. Y246A* has apparent K_d values more than 60-fold larger than WT* at the same X_{PC}. As expected from these results, the double mutant, Y246A/Y247A*, has reduced binding affinity similar to that seen for Y246A*. This result is in consistent with the simulations where Tyr246 cation-π interactions have higher occupancies while Tyr247 mediates fewer cation-π interactions.

As for Tyr 204, Tyr248 and Tyr251, the binding results are more complicated. The Tyr204 and Tyr251 variants behave similarly (Figure 3-4D). Mutagenesis of either Tyr residue has little effect on binding at X_{PC} = 0 or 0.2, but increases the apparent K_d 5-fold for X_{PC} = 0.5 and at least an order of magnitude for vesicles with higher PC content. Additionally, the double mutant behaves similarly to either single mutant suggesting that the effects of these two mutations may not be cooperative. In both the *S. aureus* N254Y/H258Y structure (where *S. aureus* PI-PLC residues 254 and 258 correspond to *B. thuringiensis* PI-PLC residues 247 and 251, respectively), and in the simulations with DMPC, Tyr residues corresponding to *Bt*PI-PLC 204 and 251 can interact with the same choline ion diffused into the crystal. Thus, the mutagenesis data with the *Bt*PI-PLC suggest that disrupting one of these interactions may be sufficient to disrupt the other.

Mutating Tyr residues at positions 88, 246 or 248 has the largest effects on binding (Figure 3-4). However, unlike Tyr88 and Tyr246, whose experimental binding data correspond well with the MD simulation, the simulations and binding results for Y248A mutant do not correlate well. The serious losses in binding affinity for the Y248A*

variant when $X_{PC} > 0$ (Figure 3-4D) suggest that either the simulation underestimates the extent of interactions between 248 and PC or Tyr248 engages in other intramolecular interactions that stabilize the membrane-bound structure of the protein. The simulations indeed suggested Tyr248 was involved in other contacts that helped stabilize the orientation of the loop between β-strand 6 and α-helix G in water as shown in Figure 3-5. From the superposition of the three structures for WT and Y248A, it is clear that Tyr248 is critical for stabilizing the β7-αG loop in an orientation that is likely critical for correct membrane binding.

Figure 3-5. Structure of the interfacial binding sites of (A) WT PI-PLC and (B) Y248A after 20 ns MD simulations in water, from three independent simulations in each case.

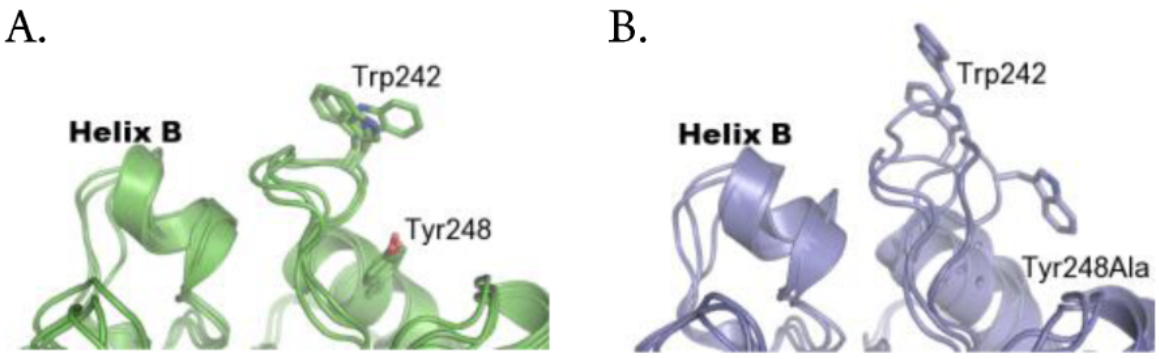

Combining the large effect of mutating either of these Tyr with the field cycling NMR data [16], as well as the engineered PC binding site in *Sa*PI-PLC N254Y/H258Y, we suggested that Tyr246, possibly aided and abetted by Tyr204 or Tyr251, forms the specific PC binding site that persists for at least one μs in the NMR experiments. The MD simulations only lasted a total of 0.5 μs. The fc-P-NMR did not reliably detect a persistent PC-Tyr88 interaction in 1:1 PMe (the anionic lipid analogue for PG since over

very long times PG is cleaved by the enzyme) /PC SUVs. Thus, even though the simulations with DMPC suggested such interactions occur, the NMR suggests that in the presence of significant anionic phospholipid, the Tyr88-PC choline interaction is not favored.

Since so many of the interfacial Tyr appeared to interact with choline, we decided to see if we could introduced a new cation-π site that would presumably enhance binding of *Bt*PI-PLC to vesicles. We mutated Gly238 and Tyr88 to Trp with the rationale that a larger aromatic residue might facilitate cation-π binding. Asn203 and Gln40 were mutated to Tyr since it looked like we could make these changes and not alter the other cation-π interactions of the protein with the bilayer. As shown in Figure 3-6, variant N203Y* shows a similar binding behavior to WT* protein, while all of the other variants G238W*, Y88W* and Q40Y* exhibit lower affinity than WT* at high X_{PC}. These results suggest that we failed to introduce new cation-π interactions to the system, which again indicates both the position and the local environment, including orientation, local conformation and mobility of the aromatic residue matter in order to design new cation-π interactions.

Figure 3-6. Apparent K_d of *Bt*PI-PLC rim loop region relative to WT* as a function of X_{PC}. The error bars are the largest uncertainties generated during the FCS data analysis, either the standard deviations from two independent repeats or the uncertainty generated by error propagation for the two independent data sets.

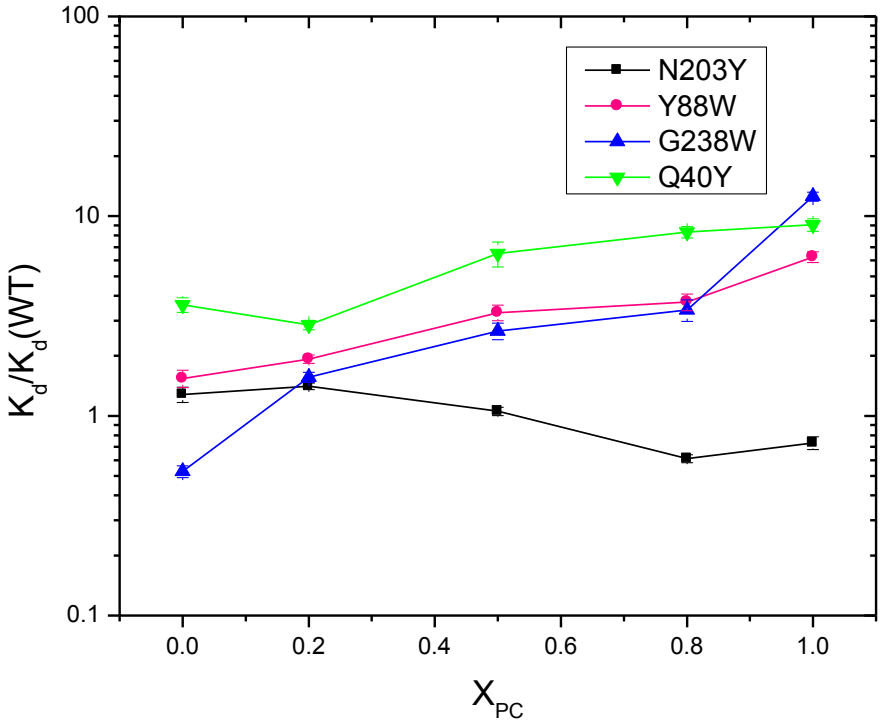

3.6 Specific enzymatic activity of Tyr mutants

Since most of the Tyr → Ala mutants had binding defects, it was of interest to see how this affected the enzymatic activity of PI-PLC. The phospholipase assays were performed using lipid concentrations that are 1.79 to 1250 times higher than the apparent K_d values for PG/PC SUVs, insuring that almost all of the protein partitions onto the vesicles in the presence of PC. All of the PI-PLC Tyr variants showed the same activity pattern as WT* (Figure 3-7).

Figure 3-7. Specific activity of unlabeled PI-PLC variants with 4 mM PI and increasing concentrations of PC: (1) WT* (2) Y86A* (3) Y88A* (4) Y86A/Y88A* (5) Y246A* (6) Y247A* (7) Y246A/Y247A* (8) Y204S* (9) Y248A* and (10) Y204S/Y248A*. All of these PI-PLC variants contain the N168C mutation used for fluorophore attachment.

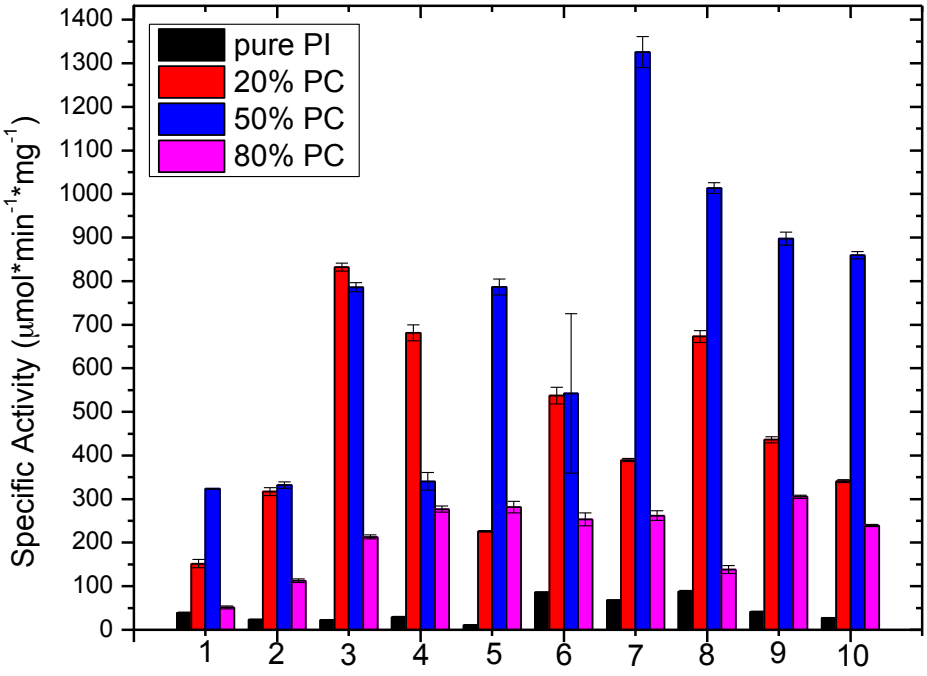

None of the mutations significantly inhibited the rate of PI cleavage in vesicles. Enzyme activity is low towards pure PI SUVs and increases significantly once PC is present. The decrease in specific activity at 80% PC has been observed for WT and other PI-PLC variants [13] and has been suggested to arise from protein sequestration from substrate in PC-rich vesicles (one can think of this as being below a 2-D K_m measured in mole fraction of substrate, here $X_{PI} = 0.2$) [17]. Although this 'surface dilution inhibition' occurs for all the tyrosine variants, the actual extent of loss of activity compared to the maximum activity (at $X_{PC} = 0.5$) varied suggesting that weakening vesicle binding at high X_{PC} increases the probability that either (i) substrate can more easily access the enzyme active site (perhaps high PC clusters around the protein preventing PI access) or (ii) the enzyme can dissociate from one vesicle and land on another more easily.

3.7 Two classes of Tyr in *Bt*PI-PLC involved in cation-π interactions.

The energetics of Tyr/PC cation-π interactions can be estimated by calculating ΔΔG, the loss in binding energy caused by the mutation, from comparing the apparent K_d for a given Tyr mutant to WT:

$$\Delta\Delta G = RT \ln \{K(mut)/K(WT)\} \quad \text{where } T = 295 \text{ K} .$$

Comparing the ΔΔG calculated from the apparent K_d values (Table 3-2) can also provide qualitative information about the type of interaction between tyrosines and PC. The tyrosine mutants fall into two classes: (i) those where $K_d(mut)/K_d(WT) \leq 5$ (Y86A*, Y247A*) and (ii) those where the ratio of mutant K_d to that of the WT was greater than 50 (Y88A*, Y204S*, Y246A*, Y248A*, Y251A*). The free energy change associated with Tyr86 and Tyr247 is approximately -1 kcal/mol. This value is comparable to that predicted by the Wimley-White scale (0.94±0.06 kcal/mol for the transfer of tyrosines

from water to POPC) and in the range of a hydrogen bonded interaction. It is also close to the Wimley-White scale for Tyr transfering to octanol (-0.71±0.11 kcal/mol), which reflects hydrophobic interactions. In contrast, removal of tyrosines 88, 204, 246 or 251 is linked to a higher energy cost: 2.5±0.2 kcal/mol, towards pure PC vesicles. These higher energies would be the values associated with PC cation – Tyr-π interactions. Removal of Ty248 has the highest energy cost of the single Tyr mutants: 3.0±0.1 kcal/mol, consistent with its hydrophobic interactions and role in stabilizing the β6-αG loop structure. An estimated upper limit of −3.6 kcal/mol for formation of a methylammonium-benzene cation-π interaction has been reported [18]. Altogether, these results strongly indicate the presence of these cation-π interactions between *Bt*PI-PLC and PC stabilizing the binding of this amphitropic protein to membranes.

Table 3-2. K_d and ΔΔG values for Tyr → Ala mutants of *Bt*PI-PLC.

Mutation	K_d (mM)	K_d(mut)/K_d(WT)	ΔΔG (kcal/mol)
WT	0.016±0.003		
Y86A*	0.072±0.005	4.5	0.88±0.04
Y88A*	1.2±0.1	75	2.53±0.05
Y204A*	0.87±0.58	54	2.3±0.5
Y246A*	1.2±0.3	75	2.5±0.2
Y247A*	0.082±0.007	5.1	0.96±0.05
Y248A*	2.5±0.5	156	3.0±0.1
Y251A*	0.81±0.41	51	2.3±0.3
Y86A/Y88A*	1.1±0.4	69	2.5±0.2
Y246A/Y247A*	2.0±0.1	125	2.83±0.03
Y248A/Y204A*	11±3	688	3.8±0.2
Y204A/251A*	2.8±2.1	175	3.0±0.6

3.8 Conclusion

The binding affinity between amphitropic proteins and the membrane lipids is typically the result of reversible interfacial interactions, most often referred to as the sum of electrostatics between basic amino acids (Lys, Arg) and the negative charged polar head group region of phospholipid, and hydrophobic interactions of aliphatic amino acids with the lipid tails. The role of interfacial aromatic amino acids is seldom mentioned despite the importance of these residues. Our results suggest that tyrosine residues are involved in interfacial cation-π interactions. The cation-π interactions are energetically equivalent to or stronger than hydrophobic interactions or electrostatic interactions. Cation-π interactions are thought to be less sensitive to the solvent dielectric constant than salt bridges [18], making them well-adapted for the interface between a low dielectric environment and a high dielectric environment. Our results suggest that overlooked cation-π interactions between membranes and aromatic amino acids of amphitropic proteins may play an important role not only in membrane binding but also in lipid recognition.

Reference

1. Ma, J. C.; Dougherty, D. A. (1997) The cation-π interaction. *Chem. Rev*., 97, 1303-1324
2. Dougherty, D. A. The cation-π interaction. (2013) *Acc Chem Res*. 46, 885-893.
3. Xiu, X, Puskar, N. L.; Shanata, J. A., Dougherty, D. A. (2009) Nicotine binding to bain receptors requires a strong cation-π interaction. *Nature*, 458, 534-537.
4. Gallivan, J. P.; Dougherty, D. A. (1999) Cation-pi interactions in structural biology. *Proc Natl Acad Sci*, 96, 9459-9464.
5. Peterson, F. N. R.; Jensen, M. O.; Nielsen, C. H. (2005) Interfacial Tryptophan residues: A role for the cation-π interactions? *Biophys J.*, 89, 3985-3996.
6. Aliste, M. P.; MacCallum, J. L.; Tieleman, D. P. (2003) Molecular dynamic simulations of pentapeptides at interfaces: salt bridge and cation-π interactions. *Biochemistry*, *42*, 8976-8987.
7. de Jesus, A. J.; Allen, T. W. (2012) The role of tryptophan side chains in membrane protein anchoring and hydrophobic mismatch. *Biochim Biophys Acta*, doi: 10.1016/j.bbamem.2012.09.009.
8. Broemstrup, T.; Reuter, N. (2010) How does proteinase 3 interact with lipid bilayers? *Phys Chem Chem Phys*, 12, 7487-96.
9. Sanderson, J., Whelan, E. J. (2004) Characterization of the interactions of aromatic amino acids with diacetyl phophatidylcholine. *Phys Chem Chem Phys*, 6, 1012-1017.
10. Rebecca, G.; Cheng, J.; Stec, B.; Roberts, M. F. (2012) Structure of the S. aureus PI-specific phospholipase C reveals modulation of active site access by a titratable π-cation latched loop. *Biochemistry*, 51, 2579-2587.
11. Cheng, J.; Goldstein, R.; Gershenson, A.; Stec, B.; Roberts, M. F. (2013) The cation-π box is a specific phosphatidylcholine membrane targeting motif. *J. Biol. Chem.* 288, 14863-14873.
12. Cheng, J.; Goldstein, R.; Gershenson, A.; Stec, B.; Roberts, M. F. (2012) Competition between anion binding and dimerization modulates Staphylococcus aureus phosphatidylinositol-specific phospholipase C enzymatic activity. *J. Biol. Chem.* 287, 40317-40327.
13. Pu, M.; Roberts, M. F.; Gershenson, A. (2009) Fluorescence correlation spectroscopy of phosphatidylinositol-specific phospholipase C monitors the interplay of substrate and activator lipid binding. *Biochemistry*, 48, 6835-6845.
14. Shi, X.; Shao, C.; Zhang, X.; Zambonelli, C.; Redfield, A.; Head, J. F.; Seaton, B. A.; Roberts, M. F. (2009) Modulation of Bacillus thuringiensis phosphatidylinositol-specific phospholipase C activity by mutations in the putative dimerization interface. *J. Biol. Chem*. 284, 15607-15618.
15. Yang, B.; Pu, M.; Khan, H. M.; Friedman, L.; Reuter, N.; Roberts, M. F.; Gershenson, A. (2014) Quantifying transient interactions between Bacillus phosphatidylinositol-specific phospholipase C and phosphatidylcholine-rich vesicles. *J. Am. Chem. Soc*., 137, 14-17.
16. Pu, M.; Orr, A.; Redfield, A. G.; Roberts, M. F. (2010) Defining specific lipid binding sites for a peripheral membrane protein in Situ using subtesla field-cycling NMR. *J. Biol. Chem*., 285, 26916-26922.

17. Pu, M.; Fang, X.; Redfield, A. G.; Gershenson, A.; Roberts, M. F. (2009) Correlation of vesicle binding and phospholipid dynamics with phospholipase C activity: insights into phosphatidylcholine activation and surface dilution inhibition. *J. Biol. Chem*., 284, 16099-16107.
18. Gallivan, J. P.; Dougherty, D. A. (2000) A Computational Study of Cation-pi Int Interactions vs. Salt Bridges in Aqueous Media: Implications for Protein Engineering. *J. Am. Chem. Soc.*, 122 (5), 870-874.

Chapter 4

Distinguishing cation-π interactions from simple insertion of an aromatic side chain into a membrane – *Sa*PI-PLC

4.1 Introduction

Peripheral membrane proteins can be targeted to membrane via interactions with specific phospholipids (e.g., phosphatidylserine [1], phosphoinositides [2,3], phosphatidic acid [4]). Although phosphatidylcholine (PC), a major component of eukaryotic membranes, is usually considered a structural lipid, it can also serve as a specific anchor for amphitropic proteins. As an example, the extracellular *B. thuringiensis* PI-PLC binds poorly to vesicles of anionic phospholipids, but with increasing avidity to vesicles containing PC. The targets of this enzyme are GPI-anchored proteins in the external leaflet of the plasma membrane, and affinity for PC would aid in directing the enzyme to its mammalian cell target. As discussed in Chapter 3, mutagenesis, NMR, and MD simulations are consistent with choline cation / tyrosine π complexes providing a significant amount of the binding energy for *Bt*PI-PLC. However, none of these experiments absolutely distinguishes nonspecific side-chain insertion from very specific formation of a cation-π complex with PC. Alanine substitution of tyrosines produces a large change in the side chain volume and cannot identify the source of lost binding affinity. The NMR experiments localized long-lived PC binding sites, but could not define the complex explicitly as a cation-π complex. The MD simulations suggest such complexes can occur but many are transient in nature. Clearly, a more direct experimental method is needed to prove the existence of such interactions.

We have developed a method to separate the two membrane binding modes which uses site-specific incorporation of fluorinated amino acids, in this case pentafluorophenylalanine (F-F_5) and 3,5-difluorotyrosine (Y-F_2). The fluorinated amino acids are more hydrophobic [5] and are therefore likely to enhance binding by insertion.

However, the altered electrostatics of the fluorinated aromatic ring should destabilize cation-π interactions [6].

4.2 *Sa*PI-PLC Model System

The method alluded to section 4.1 is first tested with the related *Staphylococcus aureus* PI-PLC, which has little affinity for PC and binds preferentially to membranes rich in anionic phospholipids [7,8]. However, the introduction of two tyrosines, at Asn-254 and His-258 (N254Y/H258Y), to mimic the *Bacillus* enzyme, leads to choline binding specificity, presumably due to cation-π complexes since a crystal structure (PDB: 4I90) exists of N254Y/H258Y with two choline bound [9] (Figure 4-1). Site 1 uses Tyr212 and H258Y to form the cation-π site for the choline trimethylammonium group (Figure 4-1). It requires a large rotation of the Tyr211 side chain to form the binding site. Choline in site 2 makes similar cation-π interactions with Trp287 and Tyr290. The rotation of H258Y forms the right side of binding pocket 1, as well as the left side of binding pocket 2. A crystal of N254Y/H258Y soaked with dibutyroyl-PC (diC_4PC) showed only site 2 occupied by the PC choline moiety (Figure 4-2) and the quaternary amines of the choline and diC_4PC ligand are completely superimposable, strongly suggesting that this is the site for the PC choline when the protein docks to membranes. Tyr258 in particular appears critical for choline binding, either by direct interaction or by aligning other aromatic residues.

In contrast to tyrosine residues thought to be involved in specific choline binding, a phenylalanine (Phe249) in a surface loop around the active site is thought to contribute to binding by inserting into the membrane [7,8](Figure 4-3). With this in mind, introducing a fluorinated Tyr at residue 258 would weaken the protein binding to PC-rich vesicles

(since Tyr258 contributes to choline cation/Tyr π interactions) while a fluorinated Phe at 249 would enhance vesicle binding for all vesicle compositions.

Figure 4-1. Overlay of the *Sa*PI-PLC N254Y/H258Y structure without choline (dark blue, PDB 4I8Y) and with choline bound (pale cyan, PDB 4I90) showing that choline site 2 (orange) is preformed, whereas site 1 (yellow) requires rotamer changes in side chains.

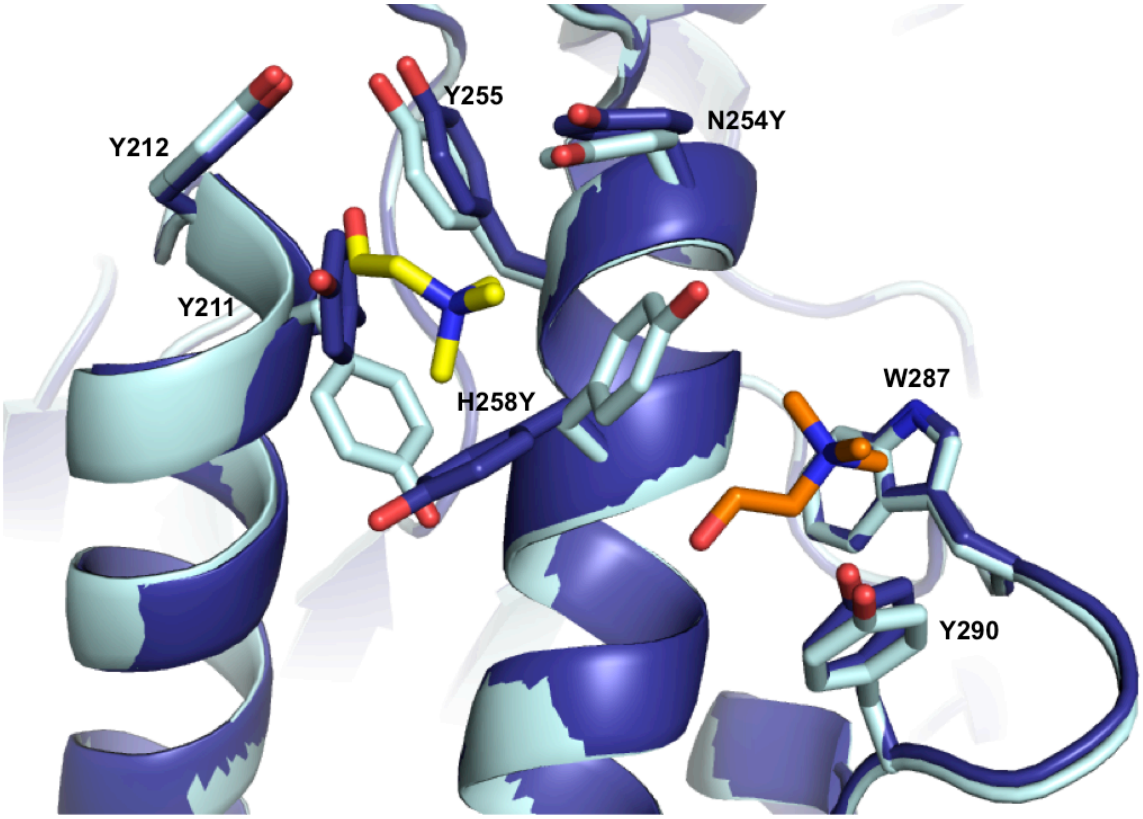

Figure 4-2. Overlay of the *Sa*PI-PLC N254Y/H258Y structure without diC_4PC (dark blue, PDB 4I8Y) and with diC_4PC bound (pale cyan, PDB 4I9J) showing the lipid in site 2 (orange).

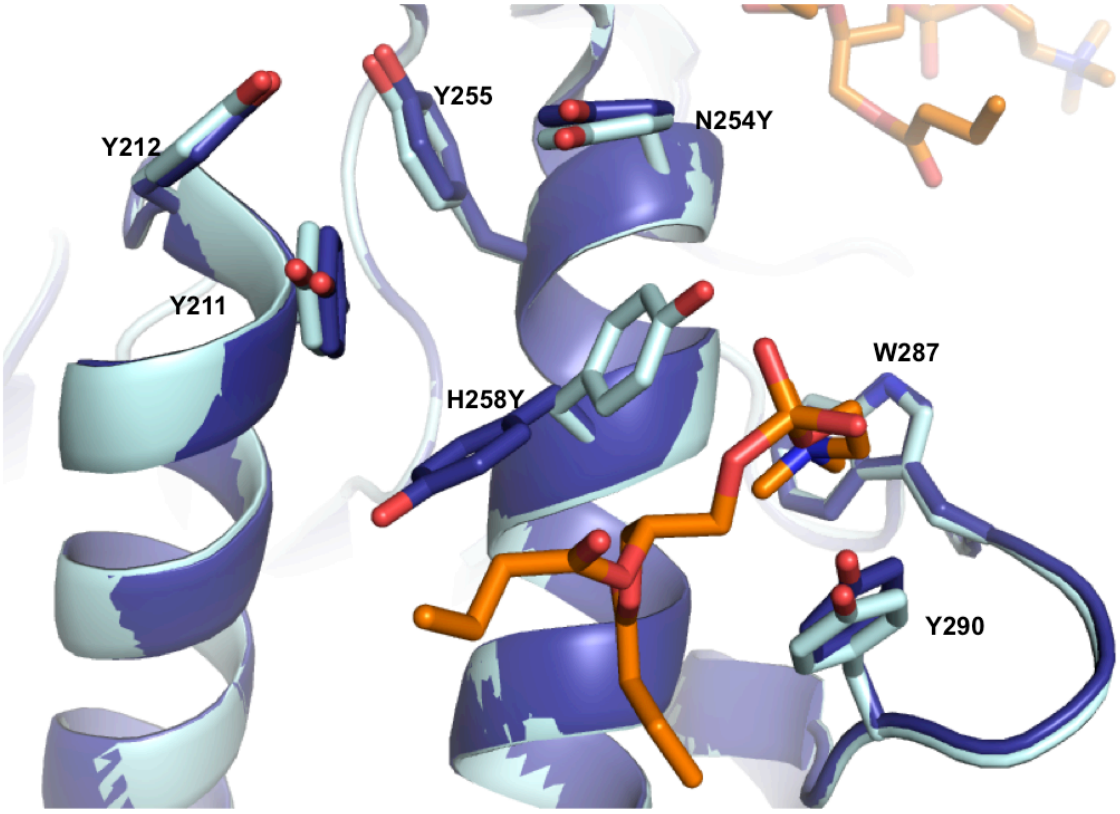

Figure 4-3 Overlay of the acidic pH (magenta, PDB 3V16) and basic pH (cyan, PDB 3V18) structures of *Sa*PI-PLC. The red circle highlights the mobile rim loop and the large conformational change in it with pH. Phe249 and His258 are labeled. *myo*-Inositol is depicted in red space-filling representation. A gray bar represents the membrane interface.

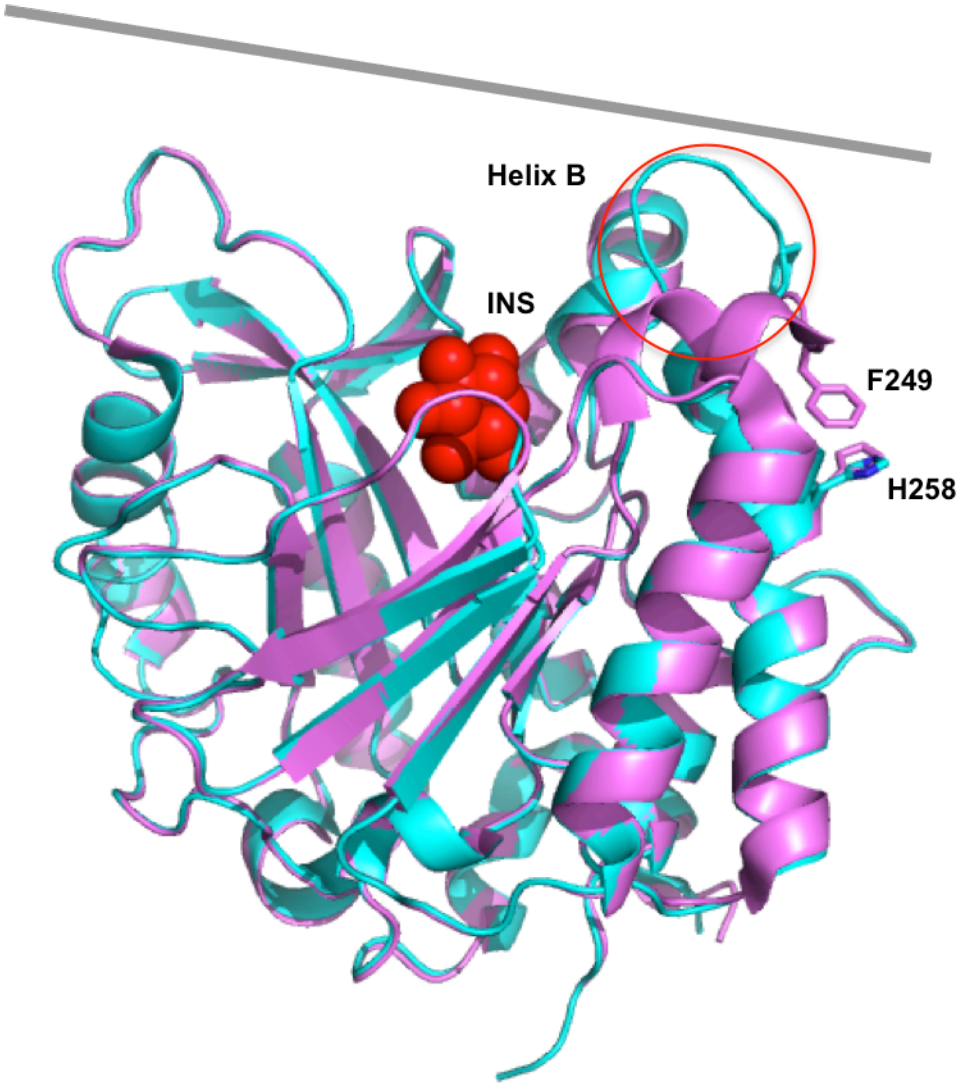

4.3 Fluorinated amino acid incorporation strategy

F-F_5 was incorporated at residue 249 and 258 to make single mutant F249F-F_5 and H258F-F_5, Y-F_2 was incorporated at residue 258 to make variant N254Y/H258Y-F_2. By comparing the binding affinity and enzyme specific activity of fluorinated protein to the control (F249F-F_5 to WT, H258F-F_5 to H258F, N254Y/H258Y-F_2 to N254Y/H258Y), we directly assess if the specific residue was involved in cation-π interations or membrane insertion.

4.4 Secondary structure of fluorinated protein variants

F-F_5 and Y-F_2 were prepared as previously described in Chapter 2, section 2.2. F249F-F_5, H258F-F_5 and N254Y/H258Y-F_2 were constructed, expressed and purified as described in Chapter 2, section 2.3, with WT, H258F and N254Y/H258Y purified and used as control, respectively. The fluorinated *Sa*PI-PLC yield was 4-6 mg/L, compared to the 60mg/L yield of native protein.

Secondary structure and thermal stability of the above SaPI-PLC variants were measured and all variants were well folded with similar CD spectra (Figure 4-4) and secondary structure (Table 4-1). However, the fluorinated variants showed slightly less thermal stability compared to their native controls. Since the proteins irreversibly denature in these experiments, this small difference could reflect increased hydrophobicity of the fluorinated variants. Overall, the CD experiments indicate that the F-F_5 or Y-F_2 substitutions are tolerated well by the protein.

Table 4-1. Analysis of PI-PLC secondary structure and thermostability of *S. aureus* PI-PLC and its variants.

Variant	α-helix (%)	β-sheet (%)	β-turn (%)	Random (%)	T_m (^oC)
WT	18.2	33.9	16.6	31.3	64
F249F-F_5	20.1	31.1	16.9	31.9	61
H258F	18.2	33.9	16.8	31.1	62
H258F-F_5	20.3	29.0	16.5	34.2	61
N254Y/H258Y	18.0	33.9	16.5	31.6	63
N254Y/H258Y-F_2	18.4	32.5	16.5	32.6	60

Figure 4-4. Comparison of CD spectra for WT (□) and N254Y/N254Y-F_2 (●).

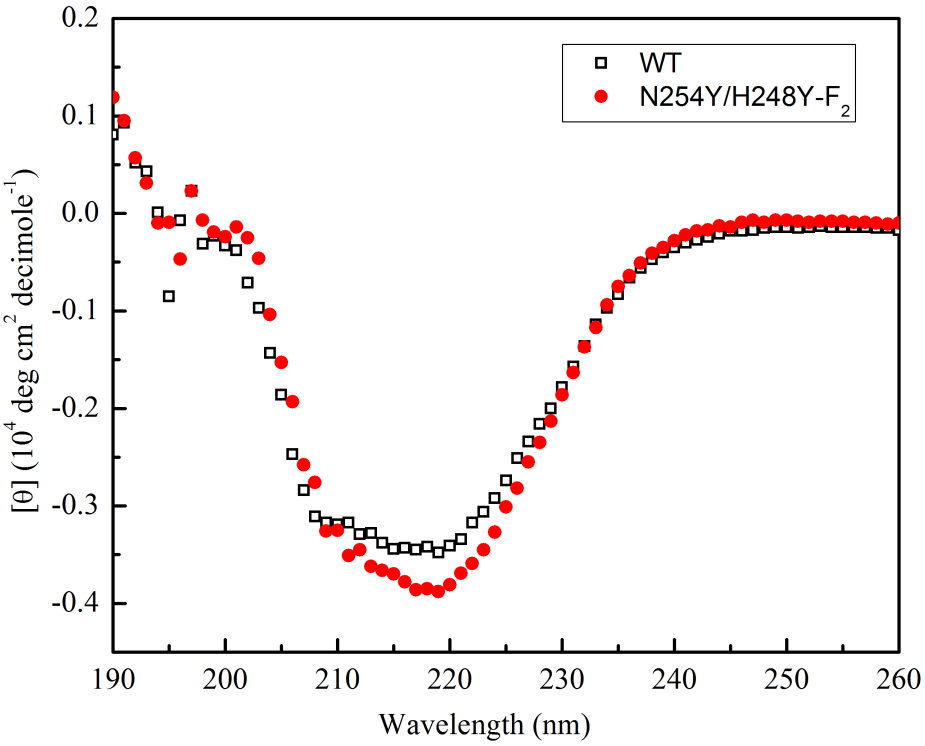

4.5 Analysis of the incorporation of F-F_5 and Y-F_2 into *S. aureus* PI-PLC

ESI-TOF MS analysis was used to show that the fluorinated amino acids were incorporated into *S. aureus* PI-PLC F249F-F_5 and H258F-F_5. F249F-F_5 gave an observed average mass of 36,807 Da and H258F-F_5 an average mass of 36,819, while WT has an observed mass of 36,719 (Figure 4-5). These results were in agreement with the calculated mass. MS/MS analysis of the collision-induced dissociation (CID) also confirmed the fluorinated modification at these desired sites. Figure 4-5B shows peptide fragments of the protein with the fluorinated residue. Thus, the ESI-MS and MS/MS together confirmed successful incorporation of F-F_5 at site 249 and 258.

Mutant N254Y/H258Y-F_2 showed a high avidity for salts. This in turn precluded successful analysis by ESI-TOF. Instead, the protein containing Y-F_2 was trypsinized and the mixture examined for fluorinated peptides to determine the site of fluoro-compound incorporation. Figure 4-5C show the ions corresponding to fragments of the tryptic peptide containing Y-F_2 at residue 258 in *S. aureus* PI-PLC. Lists of the MS/MS fragments detected for both N254Y/H258Y-F_2 and H258F-F_5 are provided in Tables 4-2 and 4-3.

Figure 4-5. MS confirmation of fluorinated amino acid incorporation in *S. aureus* PI-PLC. (A) Intact MS analysis of wildtype, F249F-F_5 and H258F-F_5 proteins. (B) MS/MS and collision-induced dissociation analysis of *S. aureus* PI-PLC, F249F-F_5 and H258F-F_5. (C) MS/MS identification of the tryptic peptide fragments containing the fluorinated tyrosine in N254Y/H258Y-F_2. Red and blue indicate the b (N-terminal) and y (C-terminal) ions, respectively.

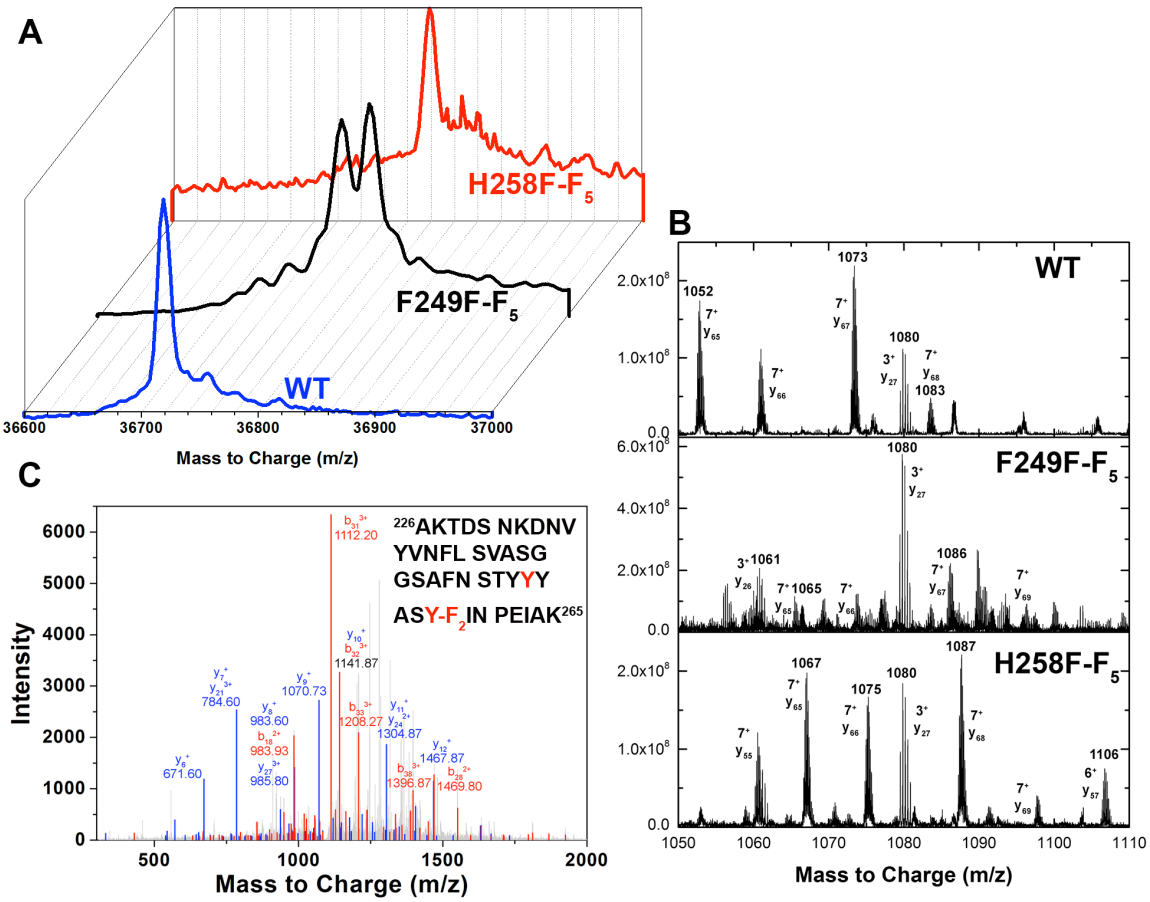

Table 4-2. MS/MS fragments of the tryptic peptide containing the N254Y/H258Y-F_2 mutation with intensities >900. The full peptide sequence is ^{226}AKTDS NKDNVYVNFL SVASGGSAFN STY**Y**YAS **Y-F $_2$**IN PEIAK^{265} and the MS/MS data, including all identified peptides, are shown in Figure 4-5C.

C-term Fragment	Fragment Sequence	Predicted Mass (Da)	Measured Mass (Da)
y_6^+	^{260}N PEIAK^{265}	671.37	671.60
y_7^+	^{259}IN PEIAK^{265}	784.46	784.60
y_8^+	^{258} **Y–F $_2$** IN PEIAK^{265}	983.50	983.60
y_9^+	^{257}S**Y-F $_2$**IN PEIAK^{265}	1070.53	1070.73
y_{10}^+	^{256}AS **Y-F $_2$**IN PEIAK^{265}	1141.57	1141.87
y_{11}^+	^{255}YAS**Y-F $_2$**IN PEIAK^{265}	1304.63	1304.87
y_{12}^+	^{254}**Y**YAS**Y-F $_2$**IN PEIAK^{265}	1467.70	1467.87
y_{21}^{3+}	^{245}GGSAFN STY**Y**YAS**Y-F $_2$**IN PEIAK^{265}	784.69	784.60
y_{24}^{2+}	^{242}VASGGSAFN STY**Y**YAS**Y-F $_2$**IN PEIAK^{265}	1305.10	1304.87
y_{27}^{3+}	^{239}FLSVASGGSAFNSTY**Y**YAS**Y-F $_2$**IN PEIAK^{265}	986.13	985.80
N-term Fragment			
b_{18}^{2+}	^{226}AKTDS NKDNVYVNFL SVA^{242}	983.99	983.93
b_{28}^{2+}	^{226}AKTDSNKDNVYVNFLSVASGGSAFN STY^{253}	1469.69	1469.80
b_{31}^{3+}	^{226}AKTDS NKDNVYVNFL SVASGGSAFN STY**Y**YA^{256}	1112.52	1112.20
b_{32}^{3+}	^{226}AKTDS NKDNVYVNFL SVASGGSAFN STY**Y**YAS^{257}	1141.53	1141.87
b_{33}^{3+}	^{226}AKTDS NKDNVYVNFL SVASGGSAFN STY**Y**YAS **Y-F $_2$**^{258}	1207.88	1208.27
b_{38}^{3+}	^{226}AKTDS NKDNVYVNFL SVASGGSAFNSTY**Y** YAS **Y-F $_2$**IN PEI^{263}	1396.64	1396.87

Table 4-3. MS/MS fragments of the tryptic peptide containing the H258F-F_5 mutation. The full peptide sequence is ^{226}AKTDS NKDNVYVNFL SVASGGSAFN STYNYAS**F-F_5**IN PEIAK^{265} and the MS/MS data are shown in Figure 4-5.

C-term Fragment	Fragment Sequence	Predicted Mass (Da)	Measured Mass (Da)
y_5-	^{261}PEIAK^{265}	557.33	557.33
y_6-	^{260}N PEIAK^{265}	671.37	671.40
y_7-	^{259}IN PEIAK^{265}	784.46	784.47
y_8-	^{258}**F-F_5**IN PEIAK^{265}	1021.48	1021.47
y_9-	^{257}S**F-F_5**IN PEIAK^{265}	1108.51	1108.60
y_{10}-	^{256}AS**F-F_5**IN PEIAK^{265}	1179.55	1179.60
y_{11}-	^{255}YAS**F-F_5**IN PEIAK^{265}	1342.61	1342.60
y_{12}-	^{254}NYAS**F-F_5**IN PEIAK^{265}	1456.65	1456.60
y_{13}-	^{253}YNYAS**F-F_5**IN PEIAK^{265}	1619.72	1619.73
y_{15}-	^{251}STYNYAS**F-F_5**IN PEIAK^{265}	1807.80	1807.40
y_{16}-	^{250}N STYNYAS**F-F_5**IN PEIAK^{265}	1921.84	1921.40

^{19}F NMR was also used to establish incorporation of the fluorinated amino acid. Both F249F-F_5 and N254Y/H258Y-F_2 in solution exhibited an asymmetric and fairly broad pattern consistent with restricted motion of the fluorinated amino acid side chain on the 34 kDa protein (and also enhanced aggregation at the concentration of protein, 7 mg/mL, used for the solution ^{19}F NMR experiments). In 2% SDS, protein exhibited a considerably narrower spectrum (Figure 4-6), although there is still evidence of slower motion and for N254Y/H258Y-F2 the two ^{19}F on the tyrosine ring have different environments in the SDS micelles. These spectra indicate that Y-F_2 and F-F_5 have been incorporated into *S. aureus* PI-PLC.

Figure 4-6. ^{19}F-NMR spectra (600MHz) confirm the incorporation of fluorinated amino acid in *Sa*PI-PLCs. (A) Y-F_2; (B) N254Y/H258Y-F_2 in 2% SDS, Tris pH 8.5; (C) native N254Y/H258Y-F_2 in Tris pH8.5; (D) F-F_5; (E) F249F-F_5 in 2% SDS, Tris pH 8.5. Both protein concentrations were 7 mg/ml (0.2 mM).

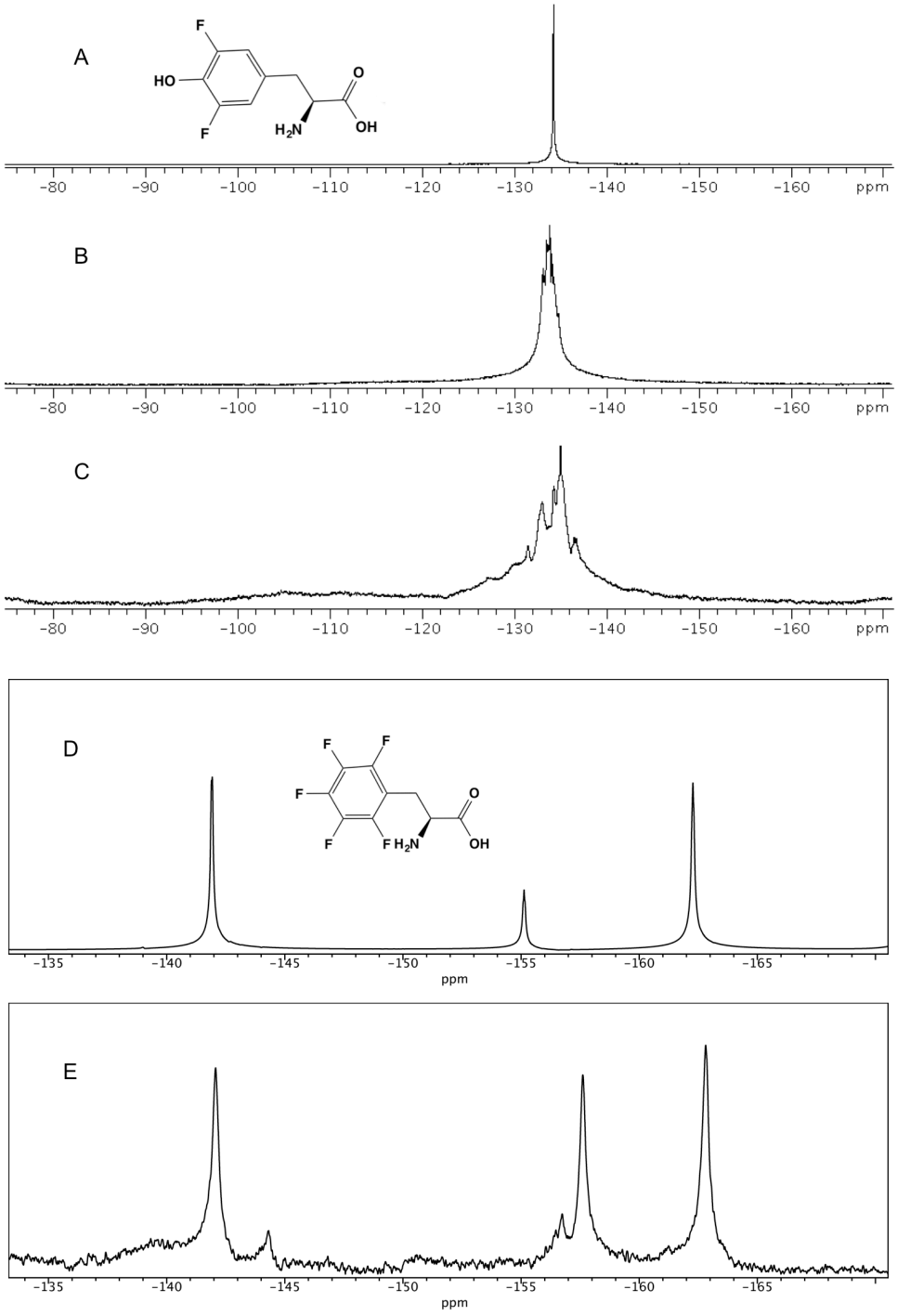

4.6 Crystallography and comparison of structures

F249F-F_5 and H258F-F_5 crystals were grown and data collected as described in Chapter 2, section 2.11 (Table 4-4). Replacement of Phe with the fluorinated analog F-F_5 should destabilize cation-π interactions. To test this, we took advantage of the observation that an intramolecular cation-π interaction between Phe249 and His258 is seen for the WT protein when crystallized under acidic conditions. The structure of F249F-F_5 was solved and compared to the structure for WT obtained under acidic pH conditions. Electron density is contoured to 1σ for the aromatic residues near the mutation in Figure 4-7A to show the quality of the data. The cation-π interaction between Phe249 and the cationic His258 has a planar stacking distance of 3.5 to 4.3 Å between the aromatic rings [7]. With the F-F_5 introduced at position 249, the cation-π complex can no longer form (Figure 4-7C), and F249F-F_5 adopts a conformation similar to that of the WT structure crystallized at basic pH [7]. However, the mobile loop preceding helix G is in a different orientation. This feature of the structure, variable in many of the *S. aureus* mutant crystal structures [7,8,9], is near protein contacts in the crystal. The specific orientation of the loop for F249F-F_5 likely aids in stabilizing the more hydrophobic F-F_5 side chain in the crystal (Figure 4-8).

H258F-F_5 was also crystallized under acidic conditions; Figure 4-7B provides an example of the electron density. Since His258 has been replaced, the intramolecular cation-π interaction cannot form. In this variant, the loop with Phe249 adopts a conformation close to that seen for H258Y [7] (Figure 4-7D). More importantly, the Tyr at residue 258 is nearly superimposable with the F-F_5 indicating that introduction of the fluorinated amino acid had virtually no effect on helix G. These structures show that the

electrostatics of the fluorinated Phe preclude formation of cation–π complexes but otherwise have little effect on the overall structure.

Table 4-4. Full refinement and model statistics for F249F-F_5 and H258F-F_5 structures.

	F249F-F_5 (PDB 4S3G)	H258F-F_5 (PDB 4RV3)
diffraction data		
resolution range (Å)	42.26-2.5	49.87-2.0
no. of reflections	12823	22307
no. of reflections in free set	623	1139
space group	$P4_32_12$	$P4_32_12$
unit cell		
a (Å)	60.05	59.85
b (Å)	60.05	59.85
c (Å)	191.33	180.41
completeness	99.7	96.6
R_{merge}	0.053	0.056
refinement		
R_{cryst} [a]	0.212	0.180
R_{free} [b]	0.291	0.238
no. of residues	301	302
no. of non-hydrogen protein atoms	2408	2433
no. of H_2O molecules	54	161
no. of non-hydrogen inositol atoms	12	12
no. of ions	1	1
rmsd bonds (Å)	0.010	0.007
rmsd angles (deg)	1.337	1.020
ave B-factor (Å^2)	49.0	29.0

[a] $R_{work} = \{\sum||F_o| - |F_c||)/|F_o|\}$, where $|F_o|$ and $|F_c|$ are the observed and calculated structure factor amplitudes, respectively.
[b] R_{free} is calculated from a set of 5% randomly-selected reflections that were excluded from the refinement.

Figure 4-7. Representative electron densities of (A) part of the rim loop in the mutant F249F-F_5 and (B) part of the helix G in the mutant H258F-F_5 structures, shown in grey and contoured at 1σ. Overlay of the pH 4.6 structures for (C) WT (yellow, PDB: 3V16) and F249F-F_5 (red, PDB: 4S3G), (D) H258Y (magenta, PDB: 3V1H) and H258F-F_5 (cyan, PDB: 4RV3) *S. aureus* PI-PLC. Key residues are labeled. *myo*-Inositol is depicted in space-filling representation.

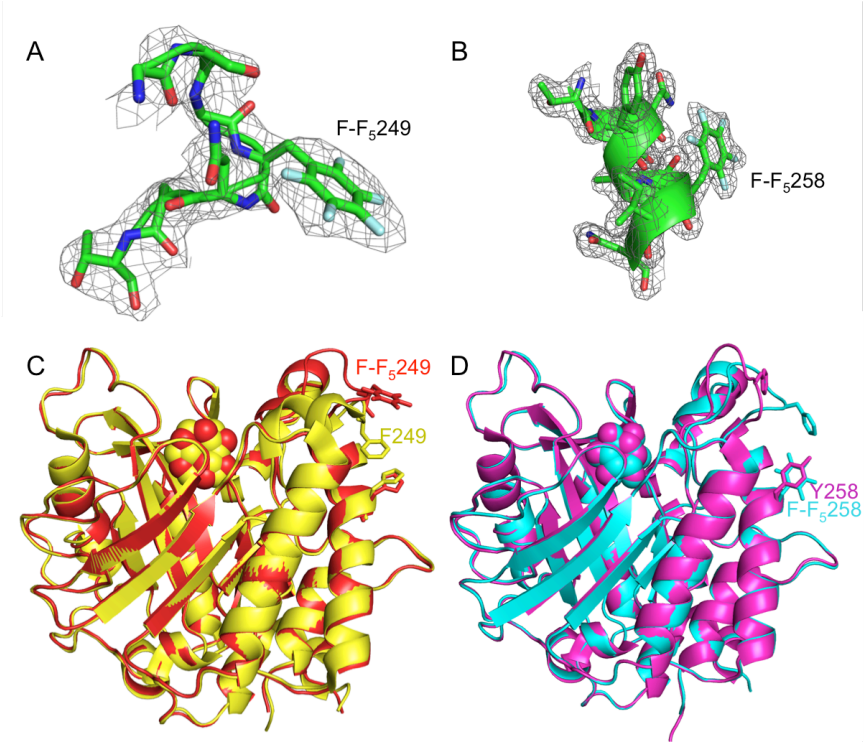

Figure 4-8. Crystal packing for WT (3V16) and mutant F249F-F_5 (4S3G) PI-PLC. The rim loop region containing residue Phe-249 or Phe-F-F_5 is circled in magenta and indicated with arrows in respective unit cell. This shows that the hydrophobic residue in the rim loop affects the packing of monomers in the crystal.

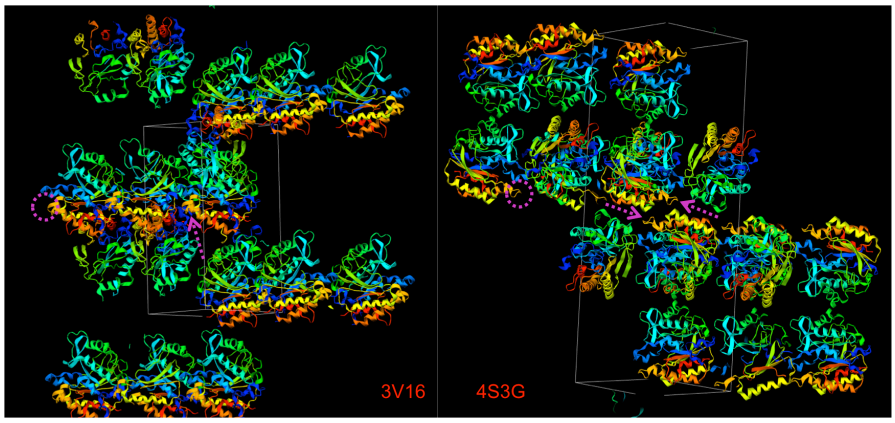

4.7 *S. aureus* fluorinated PI-PLC binding to vesicles

Binding of *S. aureus* PI-PLC proteins to PG/PC SUVs was monitored by FCS at a pH of 6.5, the pH optimum of the enzyme. WT protein has weak affinity for PC as shown in Figure 4-9A (open circles). The apparent K_d decreases substantially as X_{PC} increases. Phe249 has been postulated to insert into membranes and its replacement with alanine weakens binding [7]. Replacing that aromatic residue with F-F_5 enhances binding across the vesicle composition (Figure 4-9A, filled circles). The enhanced binding affinity is shown in Figure 4-9D where the ratio of K_d for F249F-F_5 is compared to the WT K_d. The increased affinity of F249F-F_5 for all vesicles correlates with better partitioning of the more hydrophobic F-F_5 into the bilayer.

The affinity of H258F for the SUVs is comparable to WT protein (within a factor of two across the range of compositions). The binding of H258F-F_5 compared to H258Y (Figure 4-9B) is similar for $X_{PC} \leq 0.5$. However, at high X_{PC} H258F-F_5 binding is five-fold weaker than H258F. Not enough binding of H258F-F_5 was measured at $X_{PC} = 0.9$ to generate a K_d. In this case, although WT has low affinity for PC-rich membranes, its affinity is further reduced with incorporation of F-F_5. Since structurally H258F-F_5 is very similar to H258Y, the loss of affinity at high X_{PC} might suggest that in H258F there is some tendency for that Phe to interact with choline headgroups. Formation of such a complex would be weak, requiring significant PC in the bilayer.

N254Y/H258Y, as reported previously, shows a dramatic increase in affinity for PC-rich SUVs indicative of the introduction of a PC-site with these mutations [9]. As the PC content increases above X_{PC}=0.5, tight binding of N254Y/H258Y is observed (Figure 4-9C). The shape of the curve is consistent with a PC cation / Tyr-π interaction contributing

to binding in the PC-rich region and electrostatic interactions dominating binding in PG-rich vesicles. Rather than introduce F-F_5 at this position we chose to incorporate Y-F_2. However, substituting Y-F_2 for a surface tyrosine can also alter the electrostatic distribution, because the Y-F_2 hydroxyl pK_a is shifted to around 7.5 [10]. Since *S. aureus* PI-PLC is optimally acidic at pH 6.5, and the binding was measured at that pH, deprotonation of the hydroxyl should not dominate the binding. For the most anionic SUVs, where introduction of a negative charge on the protein should have the strongest effect on binding (X_{PC} = 0 and 0.2), the K_d for N254Y/H258Y-F_2 is the same as that for N254Y/H258Y (Figure 4-9C). As SUVs become enriched in PC, N254Y/H258Y-F_2 loses much of the binding affinity compared to N254Y/H258Y. This is easily seen in Figure 4-9D where the ratio of K_d for N254Y/H258Y-F_2 is compared to its control N254Y/H258Y. From the ratio of K_d for the fluorinated enzyme compared to its control, we can estimate the free energy lost with incorporation of the Y-F_2. At X_{PC} = 0.65, 0.8 and 0.9, $\Delta\Delta G$ values are +1.46, +1.36 and +1.82 kcal/mol, respectively. This very dramatic loss of affinity is consistent with the role of Tyr258 in cation-π complexes with choline headgroups [9].

Interestingly, for pure PC SUVs, $\Delta\Delta G$ is +0.65 kcal/mol when the Tyr is fluorinated. The lower $\Delta\Delta G$ and the fact that N254Y/H258Y-F_2 binding could still be measured towards pure PC vesicles might suggest that the cation-π interaction has been weakened but still forms to some extent. Perhaps this is not surprising since only two F atoms were incorporated into the ring. However, another interpretation is that the large $\Delta\Delta G$ values for N254Y/H258Y-F_2 binding to SUVs with some PG indicate that the cation-π complex requires PG binding in the active site for optimal formation.

Figure 4-9. Apparent dissociation constants for *S. aureus* PI-PLC variants with fluorinated aromatic amino acids binding to PG/PC SUVs as a function of mole fraction PC: (A) F249F-F_5 (●) compared to WT (○); (B) H258F-F_5 (▲) compared to H258F (Δ); and (C) N254Y/H258Y-F_2 (■) compared to N254Y/H258Y (❒). In (D) is shown the ratio of the K_d for the fluorinated protein to the K_d of its control as a function of X_{PC}; symbols are the same as in A through C.

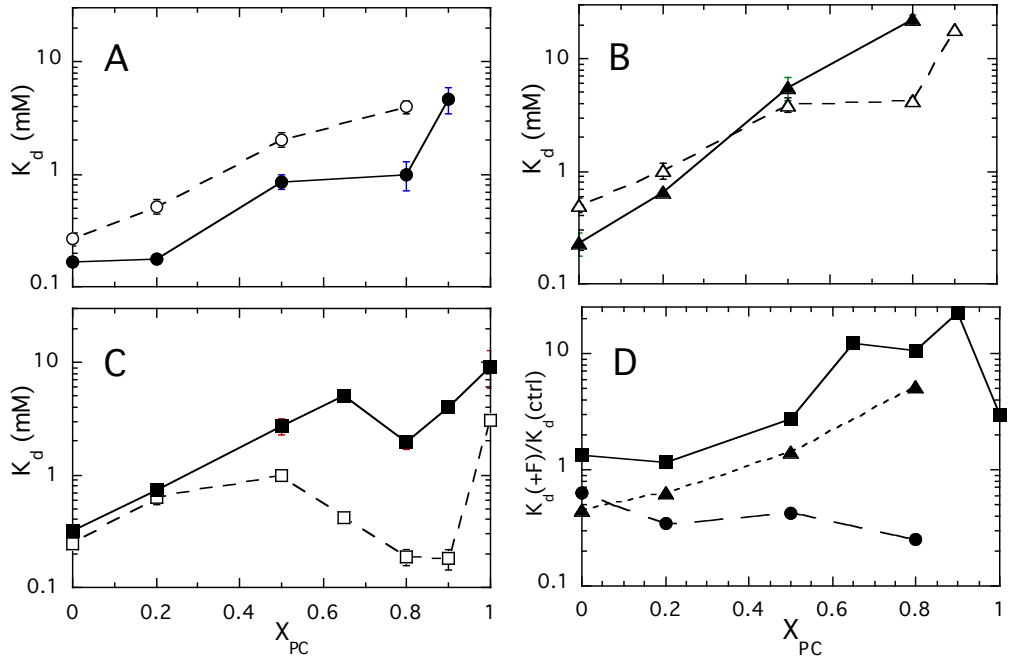

4.8 Enzyme activity of fluorinated *Sa*PI-PLC

With the exception of the pure PI SUVs, enzymatic activities for all the *S. aureus* PI-PLC variants were carried out under conditions where the total amount of phospholipid is significantly above the apparent K_d measured by FCS for PG/PC SUVs. Thus, nearly all the proteins should be partitioned on the vesicles. Specific activities all increase with increasing PC content (Figure 4-10). For WT this is not due to a specific PC interaction with the protein but rather because the zwitterionic species reduces the surface PI (PG, or PA as well) concentration and prevents the anionic lipid from binding to an cationic site adjacent to the active site that antagonizes dimerization [8]. Therefore, all mutants

exhibited higher activities with increasing X_{PC}. However, superimposed on that behavior were some interesting trends. F249F-F_5 had higher activity than WT towards PI in vesicles with $X_{PC} \leq 0.5$, while H258F-F_5 had lower specific activity than H258F. N254Y/H258Y-F_2 had lower activity than its control, N254Y/H258Y, at all X_{PC}. The increased activity for F249F-F_5 correlates with increasing the hydrophobicity of a side chain that partitions into the membrane.

These differences in specific activities under conditions where the proteins are bound to the vesicles indicate that PC cation – protein π interactions, while they do contribute to bulk binding, must also enhance either substrate access or hydrophobic product exit from the active site of the anchored protein.

Figure 4-10. Specific activities of *S. aureus* PI-PLC mutants towards PI/PC SUVs as a function of mole fraction PC (X_{PC}): WT (■), F249F-F5 (///), H258F (■), H258F-F_5 (:::), N254Y/H258Y (❒), and N254Y/H258Y-F2 (\\\\). PI was fixed at 4 mM with increasing amounts of PC. Protein concentrations were adjusted to 0.3-4 μg/ml to ensure less than 20% cleavage of the PI (4 mM).

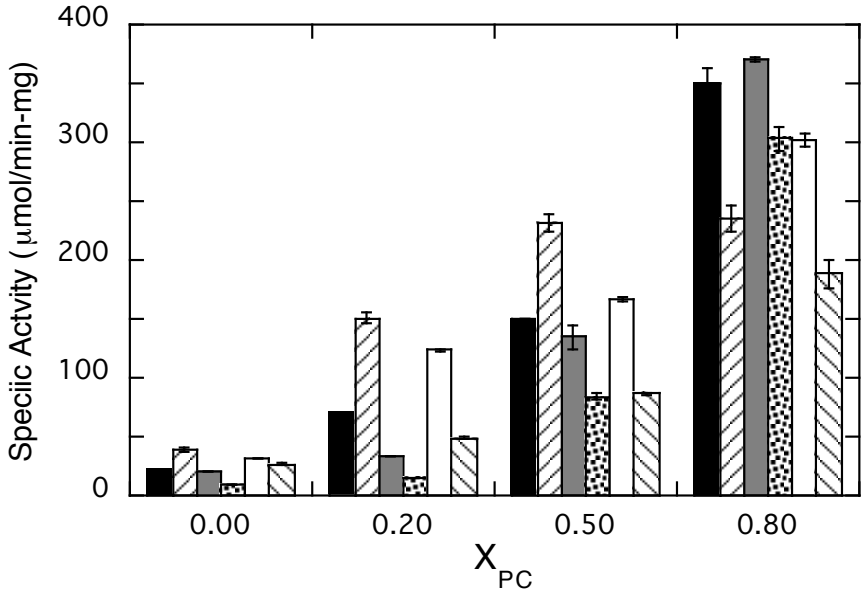

4.9 Conclusion

The incorporation of fluorinated amino acids into the *S. aureus* PI-PLC has allowed us to assess directly the specific interaction mode of aromatic residues with membranes. The loss of binding affinity correlates with F-F_5 or Y-F_2 indicates participation in a choline caton – aromatic π interaction. Enhanced vesicle binding correlates with better partitioning of a side chain into the target bilayer. For this particular enzyme the results also suggest that Phe249 nonspecific insertion into the membrane and cation-π complexes with Tyr258 are not only relevant to bulk partitioning of the enzyme on surfaces but to how a given phospholipid substrate reaches the active site.

Since crystal structures of the *S. aureus* PI-PLC exist with choline and dibutyroyl-PC, we had evidence for the role of Phe249 and Tyr258 in nonspecific and specific, respectively, interactions with membranes. Thus, the incorporation of F-F_5 and Y-F_2 served as a proof of principle for the method. The success clearly shows that this approach should be useful in providing a direct test of predictions from MD simulations and in designing membrane binding interfaces based on PC cation – protein π interactions.

Integral membrane proteins have aromatic residues at the membrane surface and these may also engage in cation–π interactions with the membrane. For example, PC modulation of an aspartate transporter from *Pyrococcus horikoshii* is postulated to occur through a cation-π interaction with a surface Tyr and the lipid headgroup. In that case, the interaction influences conformational flexibility of the oligomerization domain which in turn modulates the rate of transport [11]. Use of Y-F_2 in such a system could provide direct evidence for such as cation-π interaction.

Reference

1. Lemmon, M. A. (2008) Membrane recognition by phospholipid-binding domains. *Nat. Rev. Mol. Biol*. *9*, 99-111.
2. Kutateladze, T. G. (2010) Translation of the phosphoinositide code by PI effectors. *Nat. Chem. Biol*. *6*, 505-553.
3. Krick, R., Busse, R. A., Scacioc, A., Stephen, M., Janshoff, A., Thumm, M., and Kühnel, K. (2012) Structural and functional characterization of the two phosphoinositide binding sites of PROPPINs, a β-propeller protein family. Proc. *Natl. Acad. Sci. U.S. A. 109*, E2042-E2049.
4. Karathanassis, D., Stahelin, R. V., Bravo, J., Perisic, O., Pacold, C.M., Cho, W., and Williams, R.L. (2002) *EMBO J. 21*, 5057-5068.
5. Pace, C.J., and Gao, J. (2013) Exploring and exploiting polar-π interactions with fluorinated aromatic amino acids. *Acct. Chem. Res. 46*, 907-915.
6. Dougherty, D. A. (2013) The cation-p interaction. *Acc. Chem. Res. 46*, 885-893.
7. Goldstein, R., Cheng, J., Stec, B., and Roberts, M. F. (2012) Structure of the *S. aureus* PI-specific phospholipase C reveals modulation of active site access by a titratable π-cation latched loop. *Biochemistry 51*, 2579-2587.
8. Cheng, J., Goldstein, R., Stec, B., Gershenson, A., and Roberts, M. F. (2012) Structure of the S. aureus PI-specific phospholipase C reveals modulation of active site access by a titratable π-cation latched loop. *J. Biol. Chem. 287*, 40317-40327.
9. Cheng, J., Goldstein, R., Gershenson A., Stec, B., and Roberts M. F. (2013) The cation-π box is a specific phosphatidylcholine membrane targeting motif. *J. Biol. Chem*. *288*, 14863-14873.
10. Ravichandran, K. R., Liang, L., Stubbe, J., and Tommos, C. (2013) Formal reduction potential of 3,5-difluorotyrosine in a structured protein: insight into multistep radical transfer. *Biochemistry 52*, 8907-8915.
11. McIlwain, B. C., Vandenberg, R. J., and Ryan, R. M. (2015) Transport rates of a glutamate transporter homologue are influenced by the lipid bilayer. *J. Biol. Chem. 290*, 9780-9788.

Chapter 5

Identifying which Tyr in *Bt*PI-PLC form cation-π complexes with PC

5.1 Introduction

Given the success in using fluorinated aromatic amino acid incorporation to distinguish aromatic side chain partitioning into a bilayer from PC cation-π interactions, we examined the PI-PLC from *B. thuringiensis*. MD simulations suggested the tyrosine residues on *Bt*PI-PLC surface and choline headgroups form short-lived cation-π interactions at the protein-membrane interface. Our mutagenesis study by changing Tyr to Ala suggested that the tyrosines involved in membrane binding fell into two different categories: (i) removal of tyrosines at positions 86 and 247 was associated with 1 kcal/mol (4.2 kJ/mol) energy cost while removal of tyrosines at positions 204, 246, 247, 248 and 251 was associated with 2.5±0.2 kcal/mol (10.5±0.8 kJ/mol) energy cost. As we know aromatic residues could also form hydrophobic interactions with membrane lipids, and replacing a Tyr with a smaller Ala would also show a binding defect if the Tyr was partitioning into the bilayer. This being said, are the above energy costs caused by loss of specific cation-π interactions or nonspecific side-chain portioning into the membrane? Is there a direct way to tell if these are cation-π interactions?

In this chapter, I describe a further application of fluorinated amino acid incorporation to differentiate cation-π interations from membrane insertion. Instead of changing Tyr → Ala, We constructed seven Y-F_2 variants (Y86Y-F_2, Y88Y-F_2, Y204Y-F_2, Y246Y-F_2, Y247Y-F_2, Y248Y-F_2 and Y251Y-F_2) and examined their binding to PG and PC SUVs at pH 7.4, the optimal pH for enzyme activity. At that pH the hydroxyl group of each surface Y-F_2 will be around 50% ionized introducing a partial negative charge in the vicinity of the bilayer. That is likely to affect affinity of the proteins for PG surfaces (quantified by the K_d for pure PG SUVs) but have a modest effect on binding to a

zwitterionic bilayer (pure PC SUVs). For the latter, a reduction in the K_d value would indicate nonspecific partitioning of that Tyr into the bilayer, while an increase in K_d would indicate lost participation of that Tyr in PC cation-π binding.

5.2 Cloning, purification and characterization of *Bt*PI-PLC

The original *Bt*PI-PLC plasmid was cloned into a pET23b vector to add a C-teriminal His tag to the BtPI-PLC protein, as described in Chapter 2, section 2.3. This was added to simplify the purification process and decrease the protein loss during purification steps. The non-tagged protein was purified by an anion exchange column followed by a hydrophobic column, which was not suitable for Y-F_2 incorporated proteins with increased hydrophobicity. The overexpression and purification of fluorinated *Bt*PI-PLC was also described in Chapter 2, section 2.3. Protein yield was only 1-2 mg/L, compared to the 40 mg/L yield of native *Bt*PI-PLC. A large drop in the yield of purified *Sa*PI-PLC was also observed upon fluorinated amino acid incorporation.

Figure 5-1. SDS-PAGE of purified His-tagged *Bt*PI-PLC Y246Y-F_2 fractions.

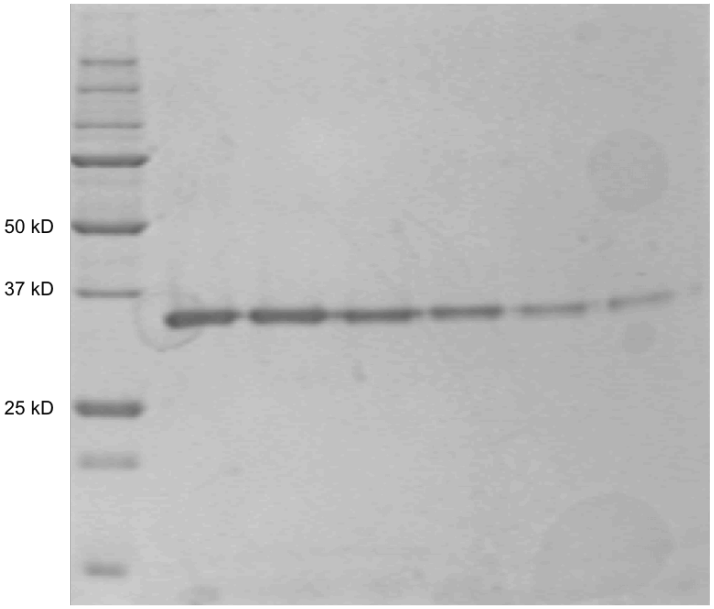

The purified BtPI-PLC variants were subjected to ^{19}F NMR (600MHz) analysis to confirm the success incorporation of Y-F_2. All of the variants showed similar ^{19}F broad spectra (Figure 5-2) with powder pattern characteristics (three 'peaks' that actual reflect a ^{19}F tensor describing the chemical shift environment for the two fluorine nuclei). This suggests significant aggregation of the fluorinated proteins. As such the native protein ^{19}F spectra are difficult to interpret. Denaturation of proteins should at least indicate the presence of the fluorinated amino acid (since the sharper free amino acid would appear as a spike on these broader patterns). In 2% SDS, protein exhibited a narrower spectrum, although an asymmetric pattern still exists. This reflects either (i) the two fluorines on the tyrosine ring still have different environments in the SDS micelles or (ii) the micelles with the protein are still large enough to not average the dipolar pattern. These spectra indicate that Y-F_2 has been incorporated into each of the *Bt*PI-PLC mutants.

Figure 5-2. ^{19}F spectra of Y-F_2 molecule (top), Y246Y-F_2 in 2% SDS (middle) and native Y246Y-F_2 (bottom). All other variants have similar patterns.

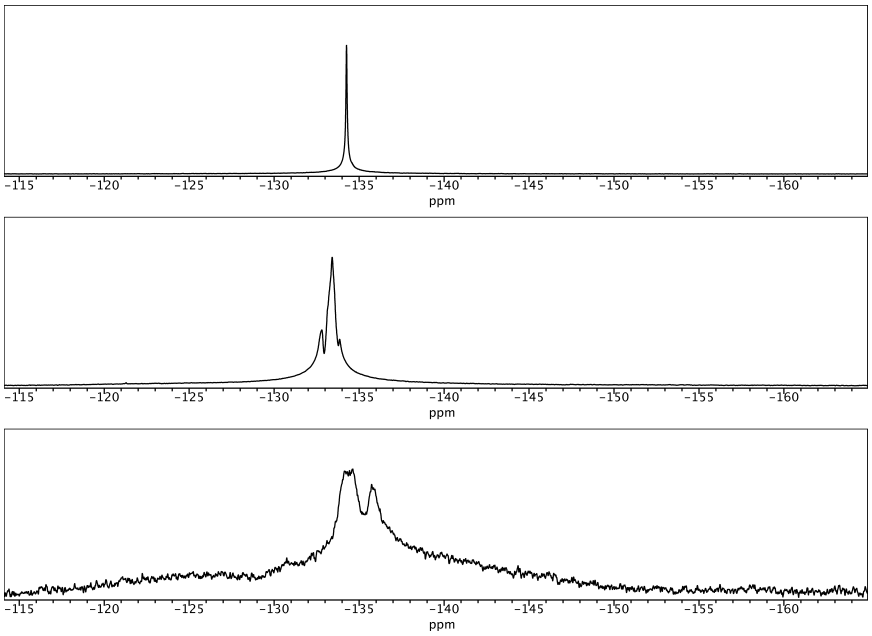

5.3 Fluorinated *Bt*PI-PLC binding to vesicles

Binding of *Bt*PI-PLC to vesicle surfaces (measured with FCS) reflects the first step in enzyme activity. All Y-Y_2 variants show impaired binding to PG SUVs, the apparent K_d increasing from 5.6 mM for WT to 30-40 mM (Table 5-1). The average ΔΔG for the effect of incorporation of Y-F_2 in these proteins is +1.05±0.12 kJ/mol in binding energy. That positive ΔΔG represents the electrostatic cost of placing a fluorinated ring (and partial negative charge) of the protein at an anionic interface.

Table 5-1. Apparent K_d value for *Bt*PI-PLC Y→Y-F_2 mutants and extrapolated ΔΔG for loss of binding.

PI-PLC	PG SUVs K_d (mM)	ΔΔG (kcal/mol) (PG) [a]	PC SUVs K_d (mM)	ΔΔG (kcal/mol) (PC) [a]	% occupancy cation-π [b]	PC SUVS, K_d for YnnnA [b] (mM)
WT	5.60±0.04		0.030±0.006			
Y86Y-F_2	41.2±1.2	1.17	0.62±0.03	1.77	22	0.072±0.005
Y88Y-F_2	30.3±1.5	0.86	0.78±0.07	1.60	96	1.2±0.3
Y204Y-F_2	36.9±5.5	1.12	1.04±0.06	2.08	26	0.87±0.58
Y246Y-F_2	34.5±10.1	1.08	1.09±0.02	2.10	77	1.2±0.3
Y247Y-F_2	28.2±1.4	0.96	0.053±0.004	0.33	8.9	0.082±0.007
Y248Y-F_2	40.2±9.4	1.17	2.31±0.07	2.53	1.9	2.5±0.5
Y251Y-F_2	28.7±8.6	0.96	0.69±0.46	1.84	36	0.8±0.4

[a] Extrapolated from the ratio of K_d(mutant)/K_d(WT) at 22 °C.
[b] From Chapter 2.

In contrast to the uniform behavior of these variants with a PG vesicle, the K_d values for pure PC SUVs covered a much wider range. The Y247Y-F_2 K_d was less than two-fold higher than WT and indicated it is not contributing significantly to cation-π interactions. The largest increase was for Y248Y-F_2 (from 0.03 to 2.3 mM). However, the MD simulations suggest this is not because of cation-π interactions but destabilization of the loop conformation that positions W242 in the membrane [1]. Y204Y-F_2 and Y246Y-F_2

show the next largest increases in K_d, followed by Y86Y-F_2, Y88Y-F_2 and Y251Y-F_2 (Figure 5-3). All of these contribute cation-π interactions in the simulations but with different occupancies. The important observation is that none of the K_d values for Y-F_2 variants decreased with PC SUVs. Therefore, for this PI-PLC, the surface tyrosines do not partition into the membrane but can engage in cation-π interactions to different degrees.

Figure 5-3. Apparent dissociation constants for *Bt*PI-PLC variants with fluorinated aromatic amino acids binding to PG/PC SUVs as a function of mole fraction PC: WT (●), Y86X (○), Y88X (❒), Y204X (Δ), Y246X (▲), Y247X (■), Y248X (▼), Y251X (◆). X represents for Y-F_2. The grey line indicates the total phospholipid concentration used in activity assay, 8mM PI plus increasing concentrations of PC (Figure 5-5).

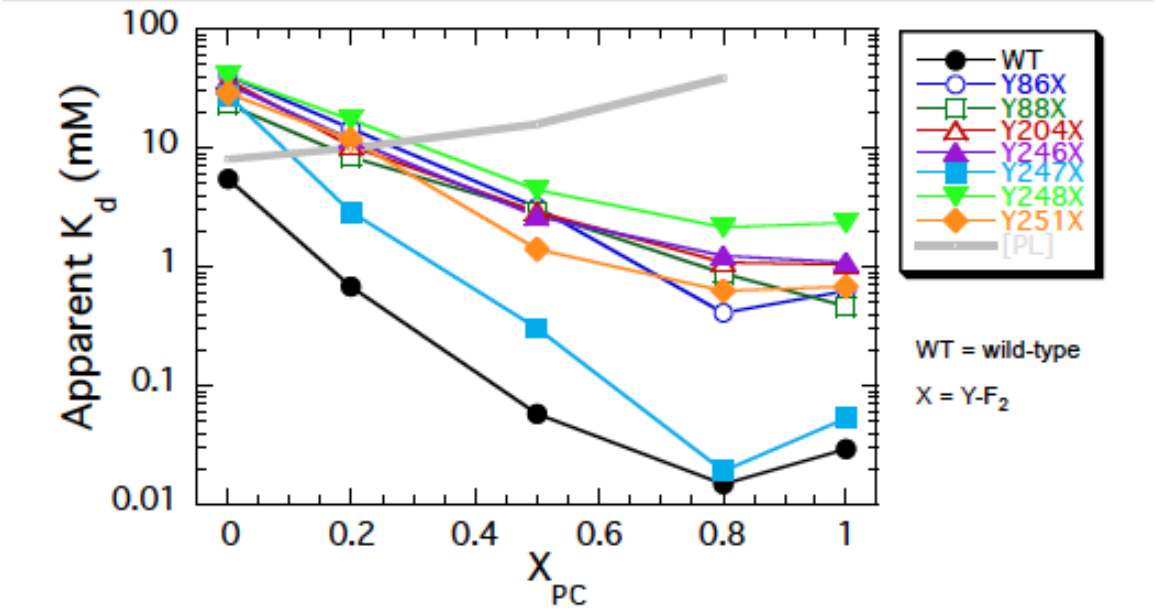

With the exception of Y86A and Y86Y-F_2, the K_d values for the Y-F_2 variants also correlate well with those for the alanine variants (Table 5-1). For both types of

substitutions (Ala or Y-F_2), there is a very qualitative correlation of the loss of binding affinity with cation-π occupancy observed in the MD simulations (Figure 5-4).

Figure 5-4. The change in free energy upon binding to vesicles for Tyr → Ala (blue circle) and Tyr → Y-F_2 (red solid circle) mutations in *Bt*PI-PLC as a function of the cation-π occupancy extracted from MD similations of the protein binding to pure PC SUVs.

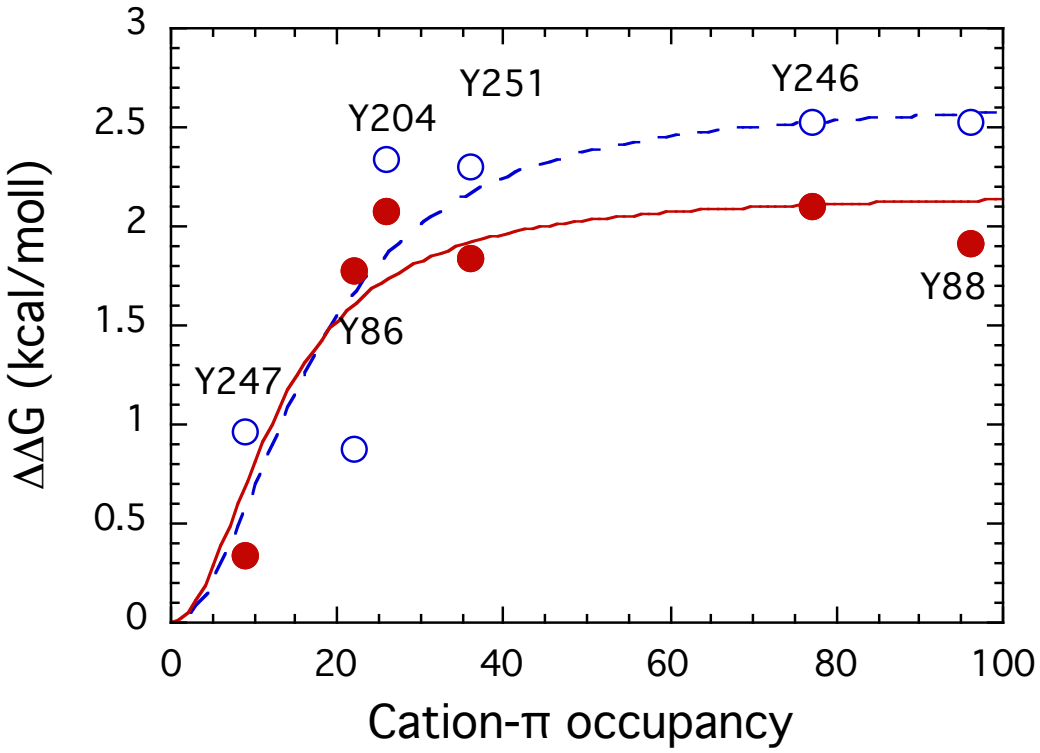

What is particularly interesting in the plot is that it is not linear, which one might expect if the Tyr residues contributed to separate complexes with a PC headgroup. For example, the occupancy for Tyr204 is low in the simulation but significant energy is lost when it is replaced. A possible explanation is that two Tyr can form a complex with the same PC. In the simulation [1], there is a small occupancy of such two Tyr complexes. However, in reality these may be much more prevalent over the time scale the protein likely residues on a given vesicle (100-400 ms [2]). An alternative explanation is that a

lower occupancy Tyr such as Tyr86 is involved in stabilizing a longer-lived cation-π complex but not by directly acting as a ligand. Regardless of the explanation, this work shows that only Tyr247 does not contribute to PC cation-π interactions that aid in the protein binding to membranes.

5.4 Enzyme activity of fluorinated *Bt*PI-PLC

PC is a kinetic activator for *Bt*PI-PLC towards monomer, micelle and vesicle substrates [3,4,5]. As shown in Figure 5-5, the specific activities of all the fluorinated species increase with increasing PC content.

Figure 5-5. Specific activities of *Bt*PI-PLC mutants towards PI/PC SUVs as a function of mole fraction PC (X_{PC}): WT (●), Y86X (○), Y88X (❒), Y204X (Δ), Y246X (▲), Y247X (■), Y248X (▼), Y251X (◆). X stands for Y-F_2. PI was fixed at 4 mM with increasing amounts of PC. Protein concentrations were adjusted to 0.3-4 μg/ml to ensure less than 20% cleavage of the PI (4 mM).

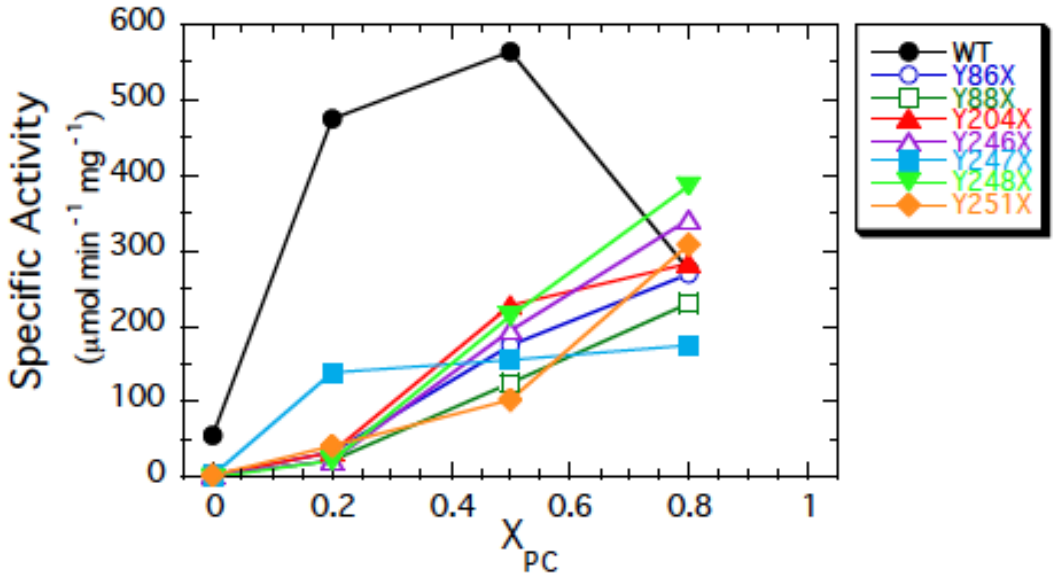

All mutants have lower activity towards PI-rich vesicles, which is largely because of weaker binding to these vesicles, caused primarily by the partial negative charge of Y-F_2.

At low X_{PC} = 0.2, only Y247Y-F_2 shows a large increase in activity with a small amount of PC added. All the other mutants containing Y-F_2 show more gradually increasing specific activity as the total phospholipid concentration exceeds K_d values. At both X_{PC} = 0.5 and 0.8 all the protein is vesicle bound, yet there is a substantial increase in specific activity for all mutants but Y247Y-F_2. Interestingly, Y247Y-F_2 specific activity reaches a plateau at X_{PC} = 0.2. Once the protein is partitioned onto a vesicle, an individual substrate molecule has to partition into the active site. Thus, while Tyr247 does not participate in cation-π interactions with PC that aids in bulk binding, the presence of the Y-F_2 at that site affects binding or positioning of the anionic substrate (or product) in the active site in a way that reduces the overall activity of this enzyme.

Another interesting difference in fluorinated enzymes versus wild type is the lack of 'surface dilution inhibition' [6]. For *Bt*PI-PLC, the activity toward PI in PC-rich SUVs decreases from its maximum around X_{PC} = 0.5. There are many reasons that could explain this behavior, (1) An individual PC molecule may have some affinity for the active site but only partition into it in at high X_{PC}. (2) In PC-rich vesicles, the mole fraction PI is less than the two-dimensional affinity of the protein for PI, measured in terms of mole fraction PI, so the protein is not 'saturated even though it is bound to the vesicle surface [7]. (3) PC clusters around the protein preventing PI access into the active site. Whatever the reason, the fluorinated proteins are not affected by lowering the mole fraction of PI in the substrate vesicle. The fluorinated mutants do have weaker binding to PC_rich SUVs than wildtype enzyme, so perhaps PC clustering and excluding PI access contributed to the observed surface dilution inhibition of *Bt*PI-PLC.

5.5 Conclusion

The incorporation of fluorinated amino acids into both *Sa*PI-PLC and *Bt*PI-PLC has allowed us to unambiguously assess the specific interaction modes of aromatic residues with membranes as either membrane insertion of cation-π interactions.

Combining the data in this chapter with MD simulations, mutagenesis studies and previous field cycling ^{31}P NMR results, we suggest that Tyr88 and Tyr246 are involved in frequent and more persistent cation-π interactions, followed by Tyr86, Tyr204 and Tyr251. Tyr247 does not contribute to the cation-π complexes (nor does it partition into the membrane). Tyr248 forms intramolecular hydrogen bonds that stabilize the orientation of the large interfacial loop and helix G. For PC-rich bilayers, cation-π interactions, are ideal for transiently anchoring these protein long enough to search an initial area for their GPI-anchored substrates, to cleave ~10 substrates followed by hopping to a new region on the PC-rich outer plasma membrane. This type of interaction would be necessary since the outer membrane of eukaryotic cells has regions where phospholipids and proteins constrained, the former in rafts and the latter via cytoskeletal interactions. An extracellular protein cannot simply diffuse around the membrane since it is not a homogenous sea of lipids and proteins. Models of the plasma membrane [8] have treated the surface as a series of corrals that constrain movements of membrane proteins and lipids. Frequent hops of the PI-PLC after a limited 2D-search would be the best way to find its target substrates.

Reference

1. Grauffel, C., Yang, B., He, T., Roberts, M. F., Gershenson, A., and Reuter, N., (2013) Cation-π interactions as lipid specific anchors for phosphatidylinositol-specific phospholipase C. *J. Am. Chem. Soc. 135*, 5740-5750.
2. Yang, B., Pu, M., Friedman, L., Reuter, N., Roberts, M. F., and Gershenson, A. (2015) Quantifying transient interactions between Bacillus phosphatidylinositol-specific phospholipase-C and phosphatidylcholine-rich vesicles. *J. Am. Chem. Soc. 137*, 14-17.
3. Zhou, C., Wu, Y., and Roberts, M. F. (1997) Activation of phosphatidylinositol-specific phospholipase C toward inositol 1,2-(cyclic)-phosphate. *Biochemistry, 36*, 347-355.
4. Zhou, C., Qian, X., and Roberts, M. F. (1997) Allosteric activation of phosphatidylinositol-specific phospholipase C: specific phospholipid binding anchors the enzyme to the interface. *Biochemistry, 36*, 10089-10097.
5. Qian, X., Zhou, C., and Roberts, M. F. (1998) Phosphotidylcholine activation of bacterial phosphatidylinositol-specific phospholipase C toward PI vesicles. *Biochemistry, 37*, 6513-6522.
6. Pu, M., Fang, X., Redfield, A. G., Gershenson, A., and Roberts, M. F. (2009) Correlation of vesicle binding and phospholipid dynamics with phospholipase C activity. *J. Biol. Chem, 284*, 16099-16107.
7. Berg, O. G., Gelb, M. H., Tsai, M. D., and Jain, M. K. (2001) Interfacial enzymology: the secreted phospholipase A(2)-paradigm. *Chem. Rev. 101*, 2613-2654.
8. Suzuki, K. G. N., Fujiwara, T. K., Edidin, M., and Kusumi, A. (2007) GPI-anchored receptor clusters transiently recruit Lyn and G for temporary cluster immobilization and Lyn activation: single-molecule tracking study 1. *J. Cell Biol. 177*, 717-730.

Chapter 6

Electrostatic interactions of *Bt*PI-PLC with membranes

6.1 Introduction

The association of peripheral membrane proteins with biological membranes is classically described as an electrostatically-driven approach followed by the intercalation of hydrophobic side groups into the lipid bilayer. Long-range nonspecific electrostatic forces between the negatively charged membrane and clusters of basic amino acids are thought to bring the protein into a binding-competent orientation relative to the lipid bilayer and play a major role for numerous prototypical peripheral membrane proteins [1-4]. Once the protein is in the vicinity of the membrane, other interactions enhance protein binding via more specific contacts (hydrophobic partitioning, hydrogen bonding, or cation-π interactions) of key residue side-chains. Experimental and computational pioneering studies have evaluated nonspecific electrostatics to contribute a few kilocalories per mole to the overall affinity and estimated that each basic amino acid contributes up to 1 kcal/mol to the binding free energy [2,5].

*Bt*PI-PLC is a secreted virulence factor that binds specifically to PC-containing negatively charged lipid bilayers. The affinity of *Bt*PI-PLC has been measured to be tightest for vesicles containing 20% anionic lipids (X_{PC}=0.8). In these conditions, the affinity is 4 times more favorable than for neutral vesicles (pure PC) while higher anionic lipid content decreases the affinity considerably. Its interfacial binding site consists of a small α-helix (helix B) and two neighboring loops rich in tyrosines that we have shown in Chapter 3 and Chapter 5 engaged in cation-π interactions with the choline groups of PC lipids in membrane bilayers. These cation-π interactions provide a likely molecular mechanism for *Bt*PI-PLC PC specificity but do not account for its preference for bilayers containing a small fraction of anionic lipids.

The *Bt*PI-PLC interfacial binding site includes five lysines (Lys38, Lys44, Lys122, Lys201, Lys279) and one arginine (Arg71). Lys44 on helix B has been previously observed to mediate membrane binding by the electrostatic interactions with anionic phospholipids [6]. Together with the other four lysines and one arginine, these basic amino acids have been identified by MD simulations as aiding in electrostatic interactions of the protein to the anionic lipids bilayer. In this chapter, we combined MD simulations and mutagenesis to investigate the electrostatic effect these residues have on membrane binding and enzyme activity. Furthermore, by combining electrostatic interactions with cation-π interactions, we can formulate a complete model of PI-PLC membrane binding using the interplay of these two interactions.

6.2 MD simulations and mutant design of *Bt*PI-PLC

The implicit membrane model simulations MD simulation (done by Dr. Cedric Grauffel, University of Bergen, Norway, described in Chapter 3, section 3.2) was used to evaluate the energy contribution for all membrane interacting residues (Figure 6-1B) The interactions could be separated into two groups (i) those dominated by hydrophobic interactions and (ii) those with electrostatic interactions. This result can be better visualized by anchoring the protein into the implicit membrane (Figure 6-1A). Several cationic residues (Lys38, Lys44, Lys 201 and Lys 279) were identified by MD simulation as aiding in electrostatic interactions of the protein with the anionic lipid bilayer. Lys38 is in a loop right before helix B placing it near the rim of the αβ-barrel and above the active site. Arg71 is at top of β-strand but away from the membrane binding surface, and this arginine as well as Lys44 are conserved in the bacterial PI-PLCs of various species (e.g., *Staphylococcus aureus, Enterococcus faecalis, Erwinia amylovora*). Residues that

contributed to the hydrophobic component of binding were Pro42, Ile43, Val46 and Trp47 in helix B, which were already studied in our previous work [7]. During the interaction with the anionic head group of phospholipids, the electrostatic force is thought to orient the protein and thus initiate the binding.

Explicit (atomistic) MD simulations with a DMPG bilayer carried out by Hanif M. Khan (University of Bergen, Norway) show that *Bt*PI-PLC docked to pure DMPG bilayers has much loose binding compared to DMPC-containing bilayers. In one the simulations, the protein completely detaches from the bilayer within 200 ns (Figure 6-2). In the other simulations, the protein remains bound but the structure of the rim loop becomes distorted (Figure 6-3). This simulation result is in agreement with the observed weak binding affinity of *Bt*PI-PLC for pure PG vesicles and with the low enzyme activity towards pure PI. Simulations with DMPC: DMPG bilayers (X_{PC}=0.5, 0.8, 1) yielded stable BtPI-PLC anchorage. Protein regions helix B and rim loop β7-αG anchor the protein in bilayer interface (Figure 6-4) at similar depths, and together with the β2-αD loop they mediate most of protein with lipid.

According to above MD simultions, residues Lys38 (right before helix B), Lys44 (helix B), Lys279 and Arg71 (on top of β2-αD loop) were mutated to alanine to measure their effect on membrane binding and enzymatic activity. According to their positions, one would expect Lys44 and Lys38 to have the most effect followed by Lys279 and Arg71 the least in contributing to electrostatic binding (we chose not to generate K201A since its relative placement with respect to the phospholipid negative charges was between Lys38 and Lys279). Meanwhile, V46K was designed to see if an additional positive charge could enhance enzymatic activity and vesicle binding.

Figure 6-1. MD simulation results shown by structural and energy decomposition models. (A) View of the insertion of PI-PLC into the implicit membrane. The limit of the interior region of the membrane is represented in brown, and the position of the negative charge in magenta. A color gradient going from blue to red is used to describe the residues having respectively a favorable or an unfavorable hydrophobic contribution to binding. (B) Plot representing the same energy decomposition (in kcal/mol). The Gouy-Chapman terms that account for electrostatic interactions are represented with black bars, while boxes represent the hydrophobic contacts.

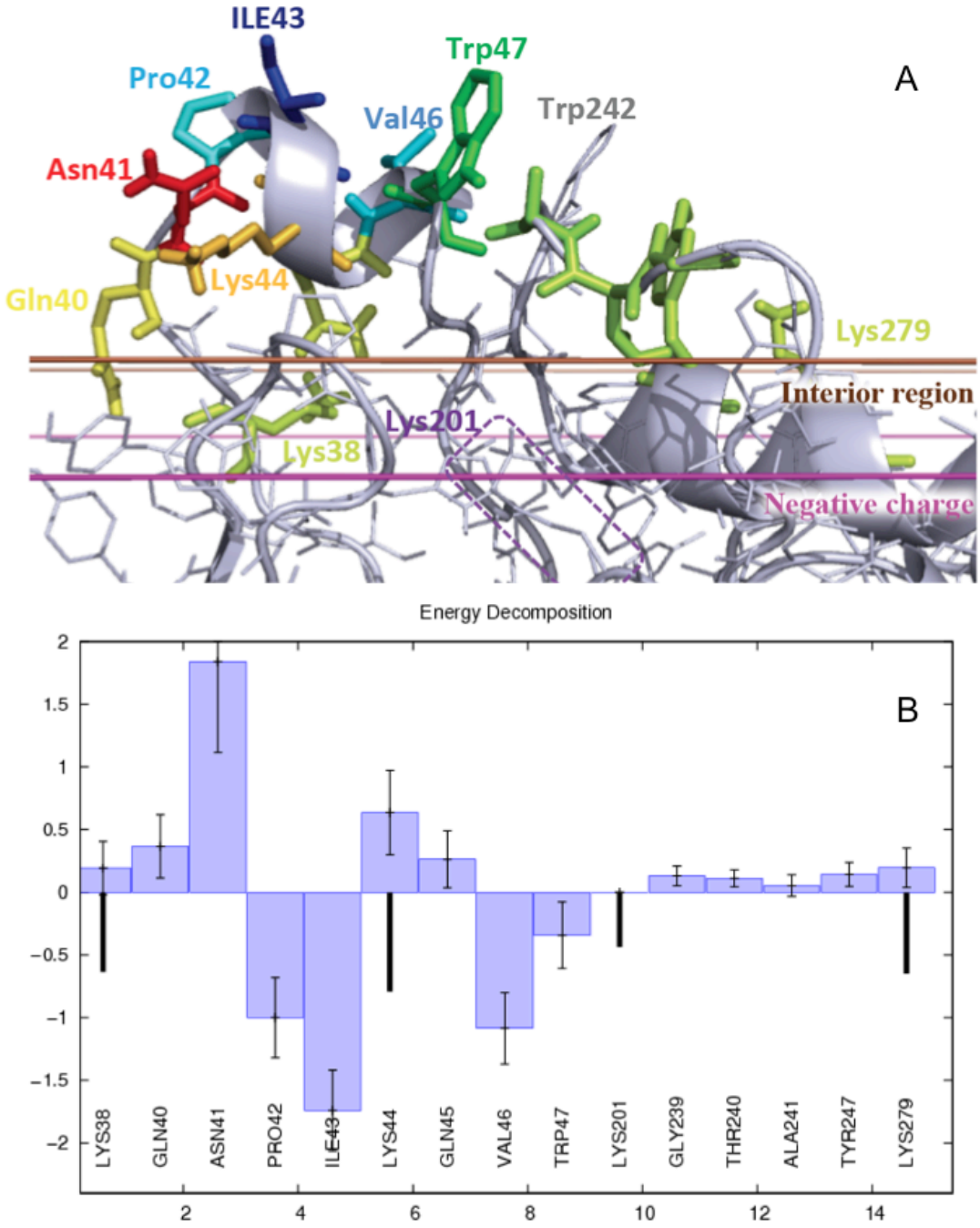

Figure 6-2. Snapshots from one of the MD simulations of WT *Bt*PI-PLC on a DMPG bilayer (X_{PC}=0, replica 2). (A) System at the beginning of the production run, (B) system after 200 ns. *Bt*PI-PLC is represented by cartoons and the lipids with sticks. helix B (αB, brown), helix D (αD, magenta), helix F (αF, cyan), helix G(αG, yellow).

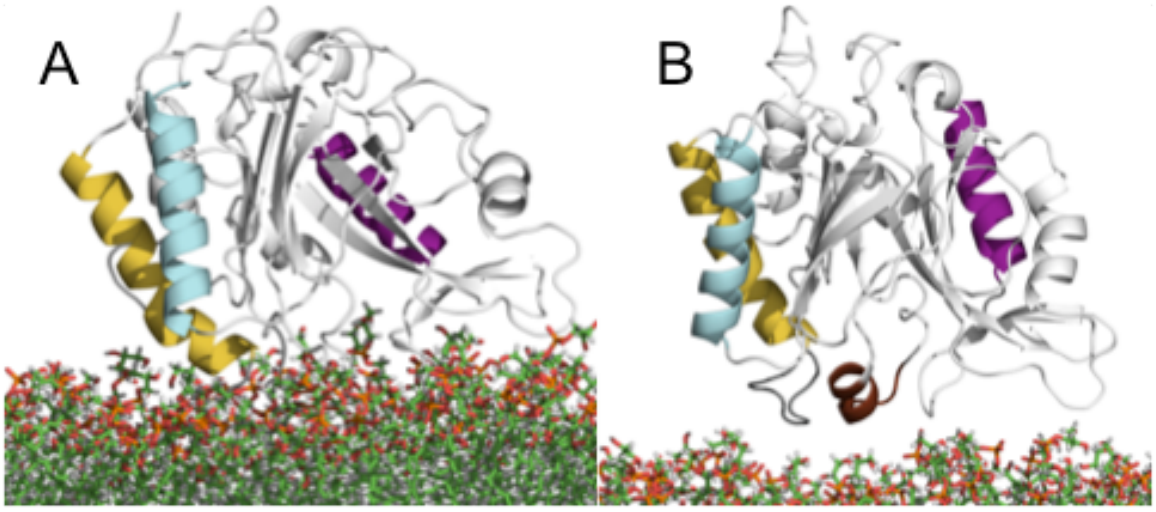

Figure 6-3. Comparison of the *Bt*PI-PLC membrane bound secondary structure after a 500 ns simulation for X_{PC}=0 (red, pure DMPG) and X_{PC}=0.5 (blue). The essential intramolecular interactions within the rim loop are lost at X_{PC}=0 causing a distorted loop structure (arrow).

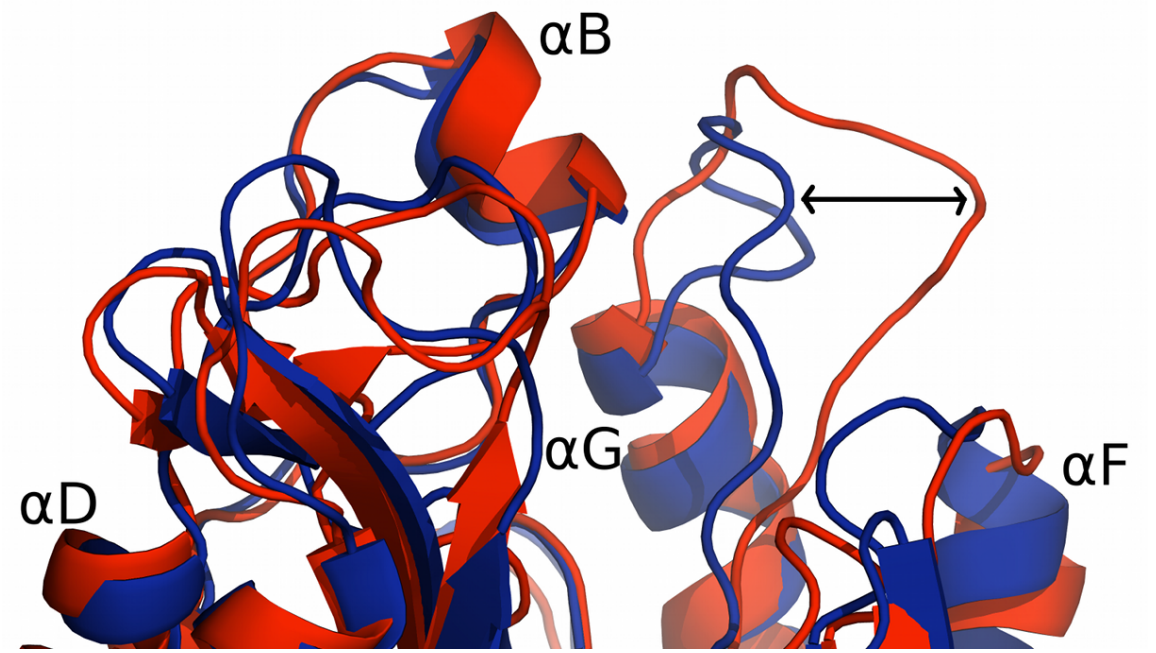

Figure 6-4. *Bt*PI-PLC secondary structure elements and their predicted insertion at the interface of a mixed DMPC:DMPG bilayer (X_{PC}= 0.5). The average phosphate plane (brown) is constructed from MD simulation data.

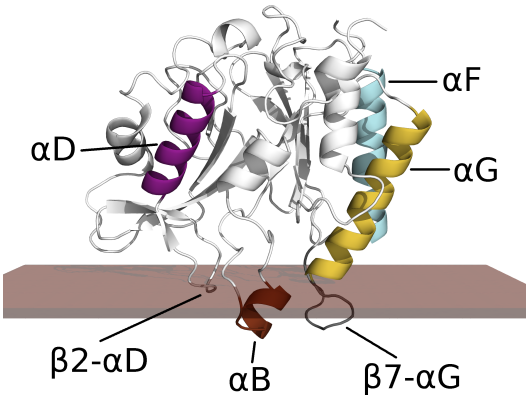

6.3 Secondary structure of *Bt*PI-PLC variants

All alanine variants expressed well and had similar secondary structures and thermal stabilities to WT protein indicating that removal of these cationic groups does not affect the overall structure of the *Bt*PI-PLC (Table 6-1).

Table 6-1. Comparison of secondary structure contents and T_m values of WT and mutant *Bt*PI-PLCs.

Protein	*α*-Helix (%)	*β*-Sheet (%)	*β*-Turn (%)	Random Coil (%)	T_m (^oC)
WT	20.6	32.2	17.2	30.0	57.1
K38A	20.2	32.5	17.1	30.1	57.3
K44A	21.6	30.9	17.4	30.1	60.3
R71A	21.4	30.9	17.2	30.3	56.8
K44A/R71A	21.9	30.9	17.4	29.8	58.8
K279A	20.8	31.8	17.2	30.1	56.0
V46K	20.7	31.6	17.2	30.6	55.4

Interstingly, K44A appeared slightly more stable to thermal unfolding than WT protein. V46K, a mutant constructed to introduce another cationic side chain in the membrane binding site, was the least stable of the variants expressed.

6.4 The affinity of *Bt*PI-PLC variants for vesicles

The results of FCS experiments measuring affinity of the mutants for PC/PG SUVs are shown in Figure 6-5 and listed in Table 6-2. As expected, all proteins have the lowest binding affinity for pure PG vesicles. Addition of PC led to decreases in the apparent K_d for all proteins, again with a minimum around $X_{PC} = 0.8$. For pure PC SUVs, R71A and K279A have K_d values only 1.5-fold higher than WT protein. K38A and K44A had K_d towards PC SUVs that were 10- and 20- fold higher than WT, indicating more than electrostatics was altered with these alanine substitutions. At $X_{PC} \geq 0.5$ R71A and K279A had apparent K_d values that approached WT protein. These two mutants recover binding affinity at higher X_{PC}, presumably due to the increased contribution of specific tyrosine mediated cation-π interactions with PC compared to the electrostatic contribution to binding. This indicates their role is almost exclusively an electrostatic contribution to vesicle binding. The K38A mutation is much more perturbing with an approximately 10–fold higher K_d relative to WT for SUVs containing PC. Even more detrimental is the K44A mutation. Whereas all the other proteins showed an increase in K_d from $X_{PC} = 0.8$ to 1.0, the K44A K_d stayed relatively constant between X_{PC} of 0.5 to 1.0. For K44A binding to X_{PC}=0.5 SUVs, the K_d was approximately 60 times higher than that of WT while the relative increase for K38A was approximately 20-fold. Lys44, which is an interfacial residue, has multiple contributions to membrane binding. Its position in the phospholipid headgroup region allows it to have more than just electrostatic interactions,

it could also participate in hydrophobic interactions with the lipid tails and to hydrogen bond with the phosphate group of a phospholipid.

Table 6-2. Apparent K_d values for *Bt*PI-PLC mutans.

	K_d (mM)				
PI-PLC	$X_{PC} = 0$	0.2	0.5	0.8	1.0
WT	12±1	0.31±0.01	0.016±0.001	0.0064±0.0008	0.026±0.005
K38A	32±1	2.2±0.2	0.30±0.05	0.037±0.002	0.24±0.06
K44A	22±4	8.8 [a]	1.0±0.3	0.35[a]	0.51±0.07
K44A/R71A		19.7±1.3	2.22±0.33	0.626±0.078	1.05±0.34
R71A	43±5	1.8±0.2	0.13±0.05	0.030±0.008	0.042±0.009
K279A	31±7	0.87±0.04	0.092±0.011	0.012±0.002	0.034±0.008
V46K	22±2	1.4±0.2	0.74±0.11	1.11±0.176	21±2

[a] Data for K44A binding at X_{PC}=0.2 and 0.8 was interpolated from data between X_{PC} = 0.1 and 0.3 (14.7±2.6 and 5.43±2.13, respectively) and X_{PC} = 0.7 and 0.9 (0.42±0.06 and 0.33±0.03, respectively).

Figure 6-5. Binding of PI-PLC WT and cationic amino acids mutants to SUVs. The apparent K_d is plotted as a function of X_{PC}. K_d values are provided in Table 6-2. Blue line indicates the total phospholipid concentrations used in enzymatic assays (see Figure 6-8).

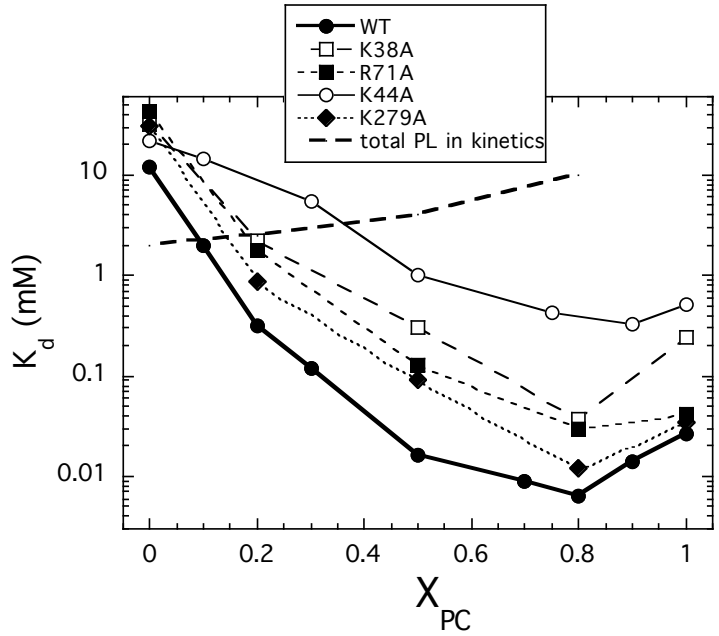

For each mutant protein, its apparent K_d can be compared to the apparent K_d for WT protein (Figure 6-6B shows such a plot for several of these mutant proteins). A value of $\Delta\Delta G$ for the loss (or gain) of binding affinity in the mutant can then be estimated from $\Delta\Delta G = RT \ln \{K_d(\text{mutant})/K_d(\text{WT})\}$. The dependence of $\Delta\Delta G$ on X_{PC} is shown in Figure 6-7A. It is apparent that the $\Delta\Delta G$ values for single Lys or Arg mutant proteins are relatively constant from $X_{PC} = 0.2$ to 0.8. This is what would be expected if the mutations only altered electrostatic and hydrophobic interactions with phospholipids but not cation-π contributions to membrane binding. In support of this, preliminary analysis of the MD simulations at $X_{PC} = 0$, 0.5 and 0.8 (Hanif Khan and Nathalie Reuter, University of Bergen, Norway) show that both electrostatic and hydrophobic interactions of the protein with the membrane do not vary with the amount of PC in the membrane.

Two other cation mutations were constructed: K44A/R71A, to see if removal of cationic groups was additive, and V46K, to see how introduction of another positive charge affect PG/PV SUV binding. As shown in Figure 6-6A, the double mutant binds more poorly than K44A. The loss of binding energy for K44A/R71A Experimental is fairly close to the sum of the $\Delta\Delta G$ for each single mutation (Figure 6-7B). Values for the double mutant are in general slightly lower than the sum of $\Delta\Delta G$ for the single mutants with the largest difference at $X_{PC} = 0.5$. Thus, it appears the electrostatic contributions are additive.

Figure 6-6. (A) Variation of apparent K_d with mole fraction PC in PG/PC SUVs for double mutant K44A/R71A and the single mutants K44 and R71A and for V46K which introduced a second positive charge in helix B. (B) Comparing the mutant K_d values to that of the WT protein.

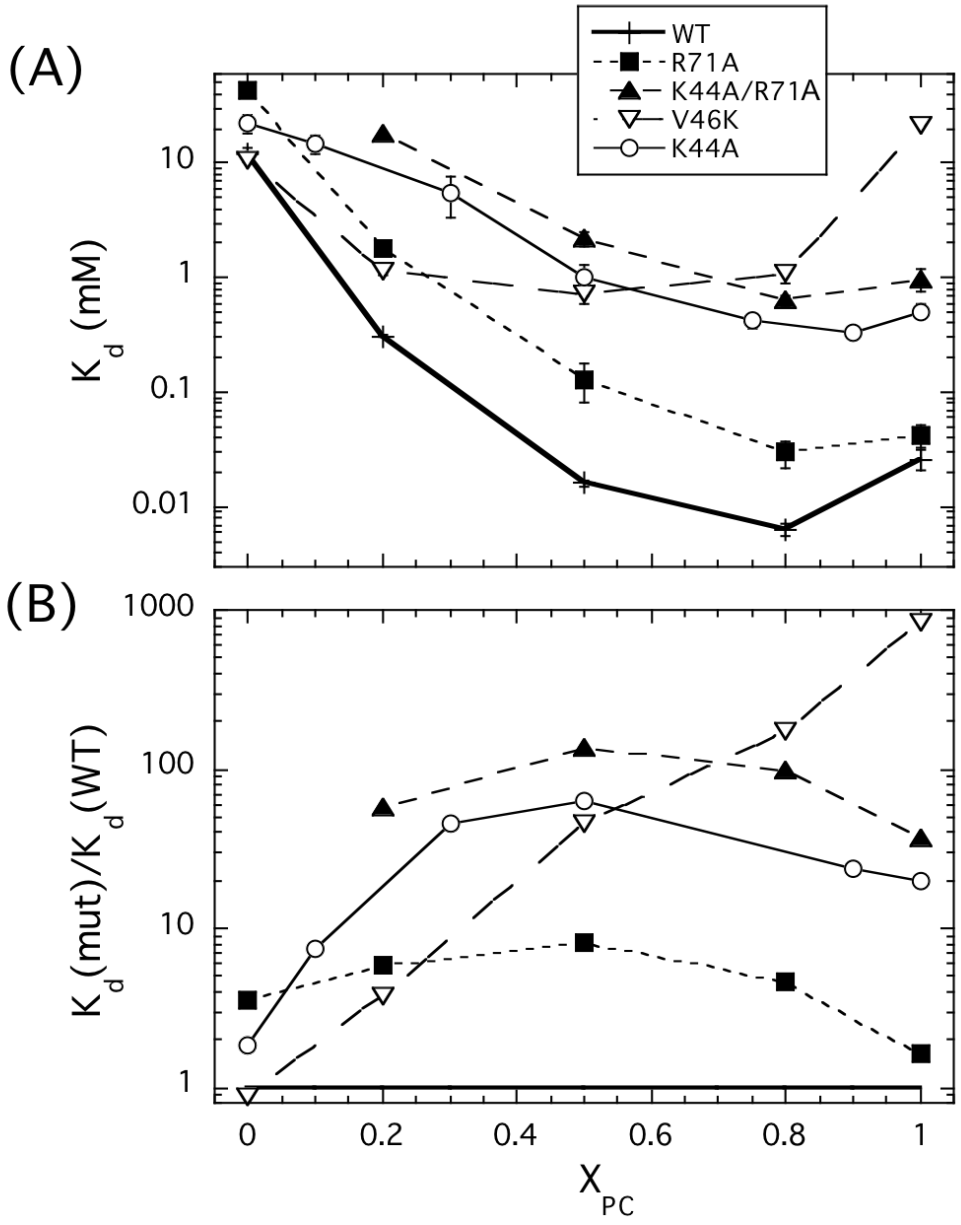

Figure 6-7. (A) ΔΔG values estimated for all K→A or R→A mutations binding to PG/PC SUVs as a function of mole fraction PC. (B) Comparison of ΔΔG for K44A/R71A (filled triangle) to the sum of the individual singe mutant proteins (open triangle).

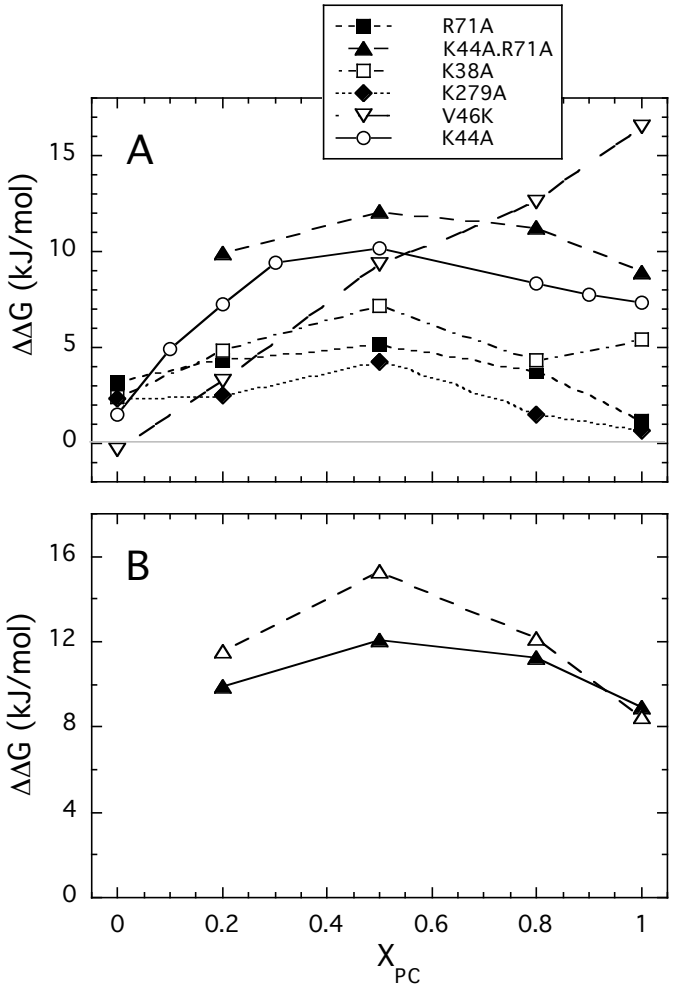

Ile43 is the most deeply embedded side chain of helix B. Introducing a positive charge at residue 46 should position the side chain near the phosphate moieties of the phospholipids and enhance electrostatic binding. There is a very small increase in affinity for V46A binding to pure PG SUVs, but V46K shows a dramatic loss of affinity towards pure PC SUVs. Shown in Figure 6-7A is the estimated ΔΔG for this mutation, which shows almost a linear loss of binding energy with X_{PC}. This strongly suggests that a

second Lys at residue 46 must also interfere with cation-π interactions (which according to MD simulations increase with increasing X_{PC}. Exactly how this happens is unclear, since Trp47 was not implicated in cation-π interactions in the MD simulation.

6.5 Enzyme activity of *Bt*PI-PLC variants

Removal of cationic residues alters vesicle binding, but does this affect the activity of this enzyme? As shown in Figure 6-8, all single mutant proteins show only slightly reduced enzymatic activity relative to WT at X_{PC} = 0.5. The lower specific activity towards X_{PC} = 0 and 0.2 SUVs correlates with loss of binding affinity provided by altering the electrostatics. Among the single cationic residue mutations, K44A has the lowest specific activity at low X_{PC} and the highest for PC-rich SUVs. Since analysis of vesicle binding suggests that K44A contributes more than just electrostatic interactions (its removal has the highest ΔΔG of any of the single cationic residue mutations), it would be expected to have the lowest specific activity at X_{PC} = 0.2. Its position in helix B, which is anchored in the membrane, could have the methylenes contribute hydrophobic binding energy. Since its ΔΔG is relatively constant from X_{PC} = 0.2 to 1.0, it would not appear that it has no significant effects on cation-π interactions.

At high X_{PC}, all the cationic residue mutations exhibit surface dilution inhibition. . The weakest binding proteins (V46K, K44A/R71A, and K44A) show the highest specific activities, commonly seen with other *Bt*PI-PLC mutants [8]. This likely reflects a better ability to dissociate from one vesicle and find another when interfacial substrate is rare.

Figure 6-8. Specific activity of *Bt*PI-PLC variants towards PI/POPC SUVs with 2 mM PI and varying X_{PC}: WT (solid circle), K38A (open square), K44A (open circle), R71A (solid square), K279A (solid diamond), V46K (inverted triangle), and K44A/R71A (solid triangle). Protein concentrations were adjusted to between 0.15-2 g/ml to ensure less than 20% cleavage of the PI.

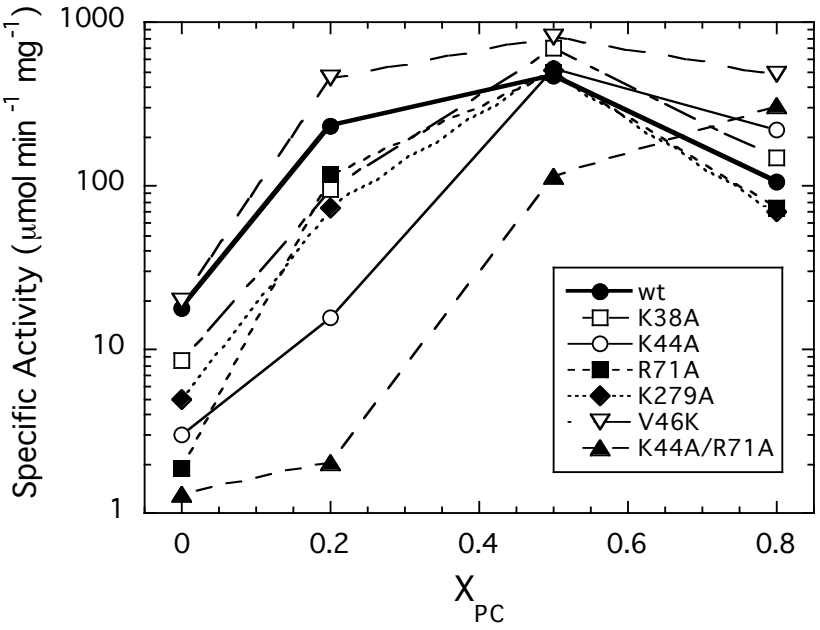

6.6 Conclusion

Polybasic motifs on amphitropic proteins surfaces are essential for binding to negatively charged lipid bilayers through electrostatic interactions with the negative charged headgroups of membrane lipids [9]. This not the case for *Bt*PI-PLC, which carries an overall negative net charge and does not present any obvious cluster of basic amino acids at its interfacial binding site. Previous results have shown that as little as 10% anionic phospholipid is enough to aid in driving the *Bt*PI-PLC protein to the membrane [6]. Adding more anionic lipid does not help protein binding.

Electrostatic interactions bring the *Bt*PI-PLC to its binding-competent orientation and are followed by the short-range protein lipid interactions. Among those, the cation-π interactions between protein tyrosines and choline groups of PC anchor the protein for

catalysis and increase with PC content. This particular balance of electrostatic, hydrophobic and cation-π interactions is optimal for *Bt*PI-PLC to find its substrates, GPI-anchored proteins. These occur in the outer leaflet of the eukaryotic cell plasma membrane, which is rich in PC and sphingomyelin. Such optimized binding behavior contributes to bacterial pathogenicity. Although the detailed mechanism has not been determined, it is thought that release of key GPI-anchored proteins by bacterial secreted PI-PLCs affects the innate immune response of mammalian cells and allows the bacteria to colonize the area.

For most of these Lys or Arg → Ala mutations, the enzyme specific activity towards pure PI vesicles was substantially decreased with removal of one of the cationic residues, even if some of them were fairly distant from the active site. In terms of the binding profiles of mutant proteins compared with WT, Lys38 and Lys44 were found to be particularly important for PC binding. Especially Lys44, which is an interfacial residue, has high contribution for membrane binding, due to its position in the headgroup region where it participates in hydrophobic interaction with the lipid tails and long-lasting hydrogen bond with lipid phosphate group.

Reference

1. Heimburg, T., Marsh, D. (1996) In *Biological membranes: a molecular perspective from computation and experiments*; Merz, K. M., Roux, B., Eds.; Birkhäuser Boston: Boston, p 405.
2. Johnson, J. E., and Cornell, R. B. (1999) Amphitropic proteins: regulation by reversible membrane interactions. *Mol Membr Biol*, *16*, 217-235.
3. Murray, D., Arbuzova, A., Hangyas-Mihalyne, G., Gambhir, A., Ben-Tal, N., Honig, B., and McLaughlin, S. (1999) Electrostatic properties of membrane containing acidic lipids and absorbed basic peptides: theory and experiment. *Biophys J*, *77*, 3176-3188.
4. Luckey, M. *Membrane Structural Biology: With Biochemical and Biophysical Foundations*; Cambridge University Press, 2008.
5. Kim, J. Y., Mosior, M., Chung, L. A., Wu, H., and Mclaughlin, S. (1991) Binding of peptides with basic residues to membranes containing acidic phospholipids. *Biophys J*, *60*, 135.
6. Pu, M., Roberts, M. F. and Gershenson, A. (2009) Fluorescence correlation spectroscopy of phosphatidylinositol-specific phospholipase C monitors the interplay of substrate and activator lipid binding. *Biochemistry, 48*, 6835-6845.
7. Guo, S., Zhang, X., Seaton, B. A., and Roberts, M. F. (2008) Role of helix B residues in interfacial activation of a bacterial phosphatidylinositol-specific phospholipase C. *Biochemistry*, *47*, 4201−4210.
8. Pu, M., Fang, X., Redfield, A. G., Gershenson, A., and Roberts, M. F. (2009) Correlation of vesicle binding and phospholipid dynamics with phospholipase C activity.
9. Johnson, J. E., and Cornell, R. B. (1999) Amphitropic proteins: regulation by reversible membrane interactions. *Mol Membr Biol 16*, 217-235.

Chapter 7

DNF2—a plant protein with homology to bacterial PI-PLC enzymes

7.1 Introduction

A lot of legume family species are able to form symbiotic associations with nitrogen-fixing bacteria, resulting in the development of a new compartment in the plant cell when the bacteria enters the plant cell by endocytosis to form the symbiosome. This specialized organ in the root system is also called the nodule. A model organism for studying legume biology, and more particularly the symbiosis between the plant and nitrogen-fixing bacteria, is *Medicago truncatula*, a plant native to Mediterranean regions (Figure 7-1).

Figure 7-1. Images of (A) the *Medicago truncatula* plant and (B) the root nodules (symbiosomes).

http://www.fao.org/ag/agp/AGPC/doc/gallery/pictures/meditrunc/meditrunc.htm

http://www.fao.org/ag/agp/AGPC/doc/gallery/pictures/meditrunc/meditrunc.htm

The gene *dnf2*, from the plant *Medicago truncatula* (a relative of alfafa with a genome only half the size of the more common plant) is found in the symbiosome and is required for nitrogen fixation [1]. Although sequence alignment of bacterial PI-PLC and plant DNF2 does not show much sequence similarity, a homology model predicted with I-tasser [2] predicted it would adopt a structure similar to a *Bacillus* PI-PLC (PBD: 1PTD) with aligned helix B and interfacial loops (Figure 7-2). Inspection of this homology model identified His residues aligned with those conserved in the active site of the *B.*

cereus PI-PLC. This prompts the question: is DNF2 a PI-PLC enzyme? If so, what is its role in symbiosome function and signaling?

Figure 7-2. Homology model of DNF2. Blue: Bacillus cereus PI-PLC (PDB: 1PTG); Yellow: ITASSER [2] prediction for DNF2; Pink, Phyre [3] prediction for DNF2. Myo-inositol present in the bacterial protein is shown in stick representation.

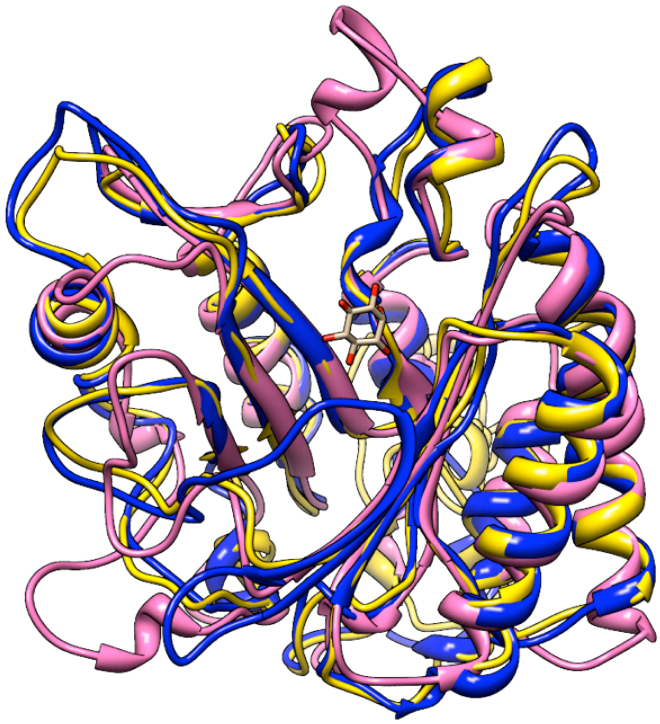

In this study, the wild-type *M. truncatula dnf2* gene was cloned into an intein-tagged overexpression system for further expression and purification. It was found that DNF2 is a plant PI-PLC. Enzymatic activities using a variety of assay systems were measured, and mutations were designed to identify the key residues in the active site. Parallel to this, Onur Oztas and Prof. Dong Wang, our collaborators at the University of Massachusetts, Amherst, showed that DNF2 protein could cause GPI-anchored protein cleavage in plants. These initial results showed that DNF2 is indeed a PI-PLC with

specificity for PI and GPI-anchors but with low enzymatic activity compared to its bacterial counterparts.

7.2 Cloning, expression and purification of DNF2

7.2.1 Signal sequence determination for recombinant protein construct

The original gene plasmid (Figure 7-3) was obtained from Dr. Dong Wang, University of Massachusetts Amherst. The full *dnf2* sequence encodes 334 amino acids. Using online prediction server TargetP (http://www.cbs.dtu.dk/services/TargetP/) [4] and SignalP (http://www.cbs.dtu.dk/services/SignalP/) [5], the first 18 amino acids were determined as signal sequence and therefore not included in any subsequent recombinant cloning. The *dnf2* gene cloned for expression contains 11 Cys residues and has a molecular weight of 36kDa. Similar sized bacterial PI-PLCs have very few Cys residues (zero in *Bt*PI-PLC and two in *L. monocytogenes* PI-PLC). The theoretical pI for the protein, estimated with the ExPASy ProtParam tool, was 8.96. The extinction coefficient (0.1%Abs) is calculated to be 1.491. The calculated instability index of DNF2 is 49.18, which classifies DNF2 as unstable.

Figure 7-3. DNF2 DNA and corresponding amino acid sequences.

```
   1  ATGGAGAATTACCTT CTAATCGCAACTTTG ATTAGTGCAAGTCTT GTATTTGGTTGCTAT
   1   M  E  N  Y  L   L  I  A  T  L   I  S  A  S  L   V  F  G  C  Y

  61  GTACTTGTTCAGATT GGGGAAACATGCTCC CGCGACGTCAATGAC TGTGGTACGGGGCTG
  21   V  L  V  Q  I   G  E  T  C  S   R  D  V  N  D   C  G  T  G  L

 121  CAGTGCCTGGAATGC AACTCACAAAGCCGG TGTACACGAGTCCGA ACTTCAAGTCCTATT
  41   Q  C  L  E  C   N  S  Q  S  R   C  T  R  V  R   T  S  S  P  I

 181  TCAAAAGTGATGGAG CTTCCATTTAACCAT TACTCATGGCTTACA ACTCACAACTCTTAT
  61   S  K  V  M  E   L  P  F  N  H   Y  S  W  L  T   T  H  N  S  Y

 241  GCTTCGAGGGCAGCG AACTTGAGTATAGAC TCTAAAATTTCGTCG GTCATGAACCAGGAA
  81   A  S  R  A  A   N  L  S  I  D   S  K  I  S  S   V  M  N  Q  E

 301  GACTCCATTACAGAT CAGCTGCGTAATGGT GTGAGAGGAATAATG TTAGATATGCATGAT
 101   D  S  I  T  D   Q  L  R  N  G   V  R  G  I  M   L  D  M  H  D

 361  TACTATGGTGACATT TGGTTGTGTCGCGGA CCGTGCACAATATTT ACCGCCTTTCAACCT
 121   Y  Y  G  D  I   W  L  C  R  G   P  C  T  I  F   T  A  F  Q  P

 421  GCTATTAATGTTCTG AGAGAGATCAATACA TTTCTCACACGACAC CGAACTGAGATAGTC
 141   A  I  N  V  L   R  E  I  N  T   F  L  T  R  H   R  T  E  I  V

 481  ACCGTTTTCATCAAG GATCGTGTAACATCA CCAAATGGTGTGAAC AAGGTGTTTAATAAA
 161   T  V  F  I  K   D  R  V  T  S   P  N  G  V  N   K  V  F  N  K

 541  GCTGGTTTGAGGAAA TTCTGGTTTCCGGTA TATAAAATGCCAAAG AATGGTAGTGATTGG
 181   A  G  L  R  K   F  W  F  P  V   Y  K  M  P  K   N  G  S  D  W

 601  CTAACAGTTAAAAAA ATGTTAAGAATGAAT CATAGGTTAATTGTG TTCACTTCAAATGCA
 201   L  T  V  K  K   M  L  R  M  N   H  R  L  I  V   F  T  S  N  A

 661  ACAAAAGAGGCTTCT GAACGCATTGCCTAT GAATGGAACTATGTT GTGGAAAATAAATAT
 221   T  K  E  A  S   E  R  I  A  Y   E  W  N  Y  V   V  E  N  K  Y

 721  GGAAATGATGGAATG GGAAGAGATCATTGT TTACATAGAGCAGAA TCATATCCAATGAAC
 241   G  N  D  G  M   G  R  D  H  C   L  H  R  A  E   S  Y  P  M  N

 781  ACAACAACAAAATCA CTAGTCCTAATGAAC TATTACAGAAATGTC CTAAATTCCAATGAA
 261   T  T  T  K  S   L  V  L  M  N   Y  Y  R  N  V   L  N  S  N  E

 841  GCATGTAAGGATAAC TCATCCCCATTGATT CGAAAGATGCATACT TGCTATAAAGATGCT
 281   A  C  K  D  N   S  S  P  L  I   R  K  M  H  T   C  Y  K  D  A

 901  GGTAACCGATGGCCT AACTACATTGCTGTA GACTTTTACAAGAGA GGTGATGGTGGGGGA
 301   G  N  R  W  P   N  Y  I  A  V   D  F  Y  K  R   G  D  G  G  G

 961  GCTCCAGAAGCATTA GATGTTGCAAATCGA AATTTGTTTGTGTGA
 321   A  P  E  A  L   D  V  A  N  R   N  L  F  V  -
```

7.2.2 Phosphatidylinositol-specific activity

The *dnf2* gene without the nucleic acid sequence coding for the first 18 amino acids was first cloned into a pET-23b vector to be expressed with a C-terminal His-tag. An NdeI site was used for cloning the 5' end of the target gene with a forward primer 5'-gacctggCATATGtgctatgtacttgttcagatt-3' (NdeI site underlined). An XhoI site was used for cloning the 3' end of the target gene with a reverse primer 5'-gactccCTCGAGcacaaacaaatttcgatttgc-3' (XhoI site underlined). The new plasmid was prepared and sequenced as previously described in Chapter 2, section 2.2. It was then transformed and overexpressed in *E. coli* with 100 µg/mL ampicillin. This strain of *E. coli* expressed with an empty expression vector yields no PI-PLC enzymes; cell extracts cannot cleave PI. When the crude cell lysate from cells expressing DNF2 was mixed with PI/PC vesicles, PI was cleaved to cyclic inositol phosphate (cIP). Confirmation of the product was provided by the ^{31}P NMR spectrum (Figure 7-4).

Figure 7-4. ^{31}P NMR spectrum showing DNF2 activity towards PI/PC (2mM: 2mM) vesicles, in 50mM HEPES, pH 7.5.

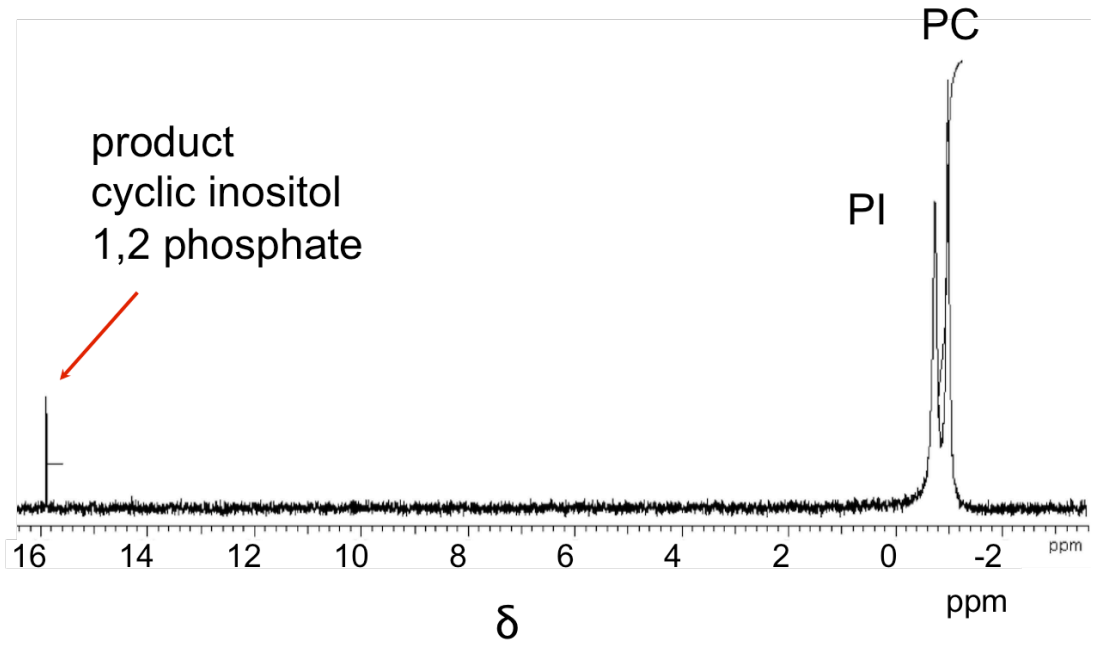

The PI-PLC activity was low, however, most of the expressed protein was found in inclusion bodies, likely caused by the 11 cysteine residues. This precluded purificationof adequate amounts of protein. DNF2 was then cloned into other vectors to try and optimize expression of soluble active protein.

N-terminal His-tagged DNF2 (pET-28a) and GST-tagged DNF2 were generated. These also were found in the inclusion bodies. In contrast to the C-terminal His-tagged DNF2, no PI cleavage was observed with these N-terminal tagged protein, even after prolonged incubations of crude cell extracts with PI/PC vesicles. It should be noted that 6 of the 11 cysteines in the protein are in the N-terminal region (first 33 amino acids), and the N-terminal His tag might have interfered with the subsequent protein folding.

7.2.3 Intein-tagged DNF2 purification

According to the homology model, the first 26 amino acids are unstructured (random coil) and independent of the well-folded core of DNF2. Therefore, the *dnf2* gene encoding amino acids 27-333 was cloned into a pTXB1 vector (IMPACT kit, New England Biolabs), which adds a C-terminal intein fusion tag (28 kDa) to DNF2 (35 kDa). The residue Val334 was not included, since according to the IMPACT protocol, the C-terminal residue has an effect on on-column cleavage efficiency by DTT. A Val C-terminus has a much lower cleavage efficiency compared to Phe333 so the codon for Val334 was not included in the pTXB1 vector. An NdeI site was used for cloning the 5' end of the target gene with a forward primer 5'- gataatCATATGgaaacatgctcccgcgacgtc-3' (NdeI site underlined). A SapI site was used for cloning the 3' end of the target gene with a reverse primer 5'-ggtggttGCTCTTCcgcaaaacaaatttcgatt-3' (SapI site underlined).

Protein was overexpressed in BL21 (DE3) cells and eluted from a chitin column with the purification protocol provided by the manufacturer.

Cells (1 L) were inoculated at 37 °C and DNF2 expression induced by 0.1 mM IPTG when the OD_{600} reached 0.7. The induced cells were grown at 16°C for 20 h and then the suspension was centrifuged. The cell pellet was re-suspended in 40 mL column buffer (20 mM Tris, pH 8.5, 0.5 M NaCl) and sonicated for 10 x 30 s on ice, and centrifuged at 15,000 rpm for 35 min. The supernatant was loaded at 0.5 mL/min onto a 10 mL chitin bead column, which was pre-equilibrated with the same column buffer. After loading, the chitin column was washed with at least 10 volumes column buffer to thoroughly remove the unbound contaminants. The on-column cleavage was initiated by adding 30mL cleavage buffer (20 mM Tris, pH 8.5, 0.5 M NaCl, 50 mM DTT) at 2 mL/min to evenly distribute thiols through the column. Flow through the column was stopped and the column was incubated at room temperature for 20 h. The flow-through was collected and subjected to SDS-PAGE analysis. The SDS-PAGE result showed that the intein tag was not cleaved from the recombinant DNF2. The fusion protein molecular weight was 63 kDa (Figure 7-5). The C-terminal intein tag did not prevent most of the protein from ending up in inclusion bodies. Instead, the stability provided by this additional domain enhanced fusion protein stability and the high specificity for chitin beads made it possible to purify the small amount of soluble DNF2 protein. This recombinant protein was judged pure enough and the amount adequate for initial biochemical characterization of the PI-PLC enzymatic activity of this plant enzyme. Future efforts may be focused on obtaining tag-less DNF2.

Figure 7-5. SDS-PAGE of the purified DNF2-Interin fusion protein fractios.

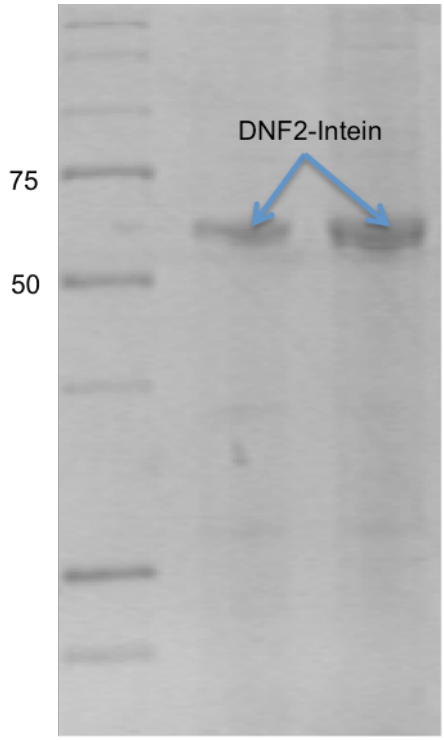

7.3 Secondary structure of the DNF2-intein fusion protein

Both secondary structure and thermal stability was measured from CD spectra of purified DNF2 fusion protein was obtained (Table 6-1). Compared to *Bt*PI-PLC, the fusion protein has a slightly higher stability, T_m= 62 °C, most likely caused by the intein fusion tag. Secondary structure is different because of the contribution of the intein tag.

Table 7-1. Analysis of secondary structure and thermal stability of DNF2-intein compared to *Bt*PI-PLC.

	Secondary Structure (%)				T_m (ºC)
	α-helix	β-sheet	β-turn	random coil	
DNF2-intein	18.0	33.7	16.6	31.6	62
*Bt*PI-PLC	22.2	30.0	17.4	29.9	56.7

7.4 PI-PLC activity assay

The specific activity of purified DNF2 fusion protein was first measured towards PI (8 mM) solubilized in Triton X-100 (25 mM) micelles over a pH range 5.5-8.0. As shown in Figure 7-6A, the highest specific activity was achieved at pH 7.4, with a value of 72 nmol mg^{-1} min^{-1}, much lower than that observed for bacterial PI-PLCs [6].

Many other PI-PLC enzymes exhibit higher activity when non-substrate lipids are added [7,9]. For *Bt*PI-PLC, *Sa*PI-PLC and *Listeria monocytogenes* PI-PLC, cleavage of a monomeric substrate like dihexanoyl-PI (diC_6PI) is enhanced with PC added, although the mechanism of activation is different for each one. As shown in Figure 7-6B, the cleavage of 2 mM diC_6PI, which is monomeric (its critical micelle concentration is ~12-14 mM depending on buffer), is enhanced 2- to 3-fold by the addition of either micellar diC_7PC or long chain PC vesicles. This could be a specific activation effect of the added PC or it could be the result of incorporating some of the PI in aggregates - micelles or vesicles. To determine the cause of the interfacial activation, we checked PC activation of of diC_8PI, which by itself has a lower CMC (~0.5 mM) than the diC_6PI (12-14 mM) (Figure 7-6C). The addition of 2 mM diC_7PC to the diC_8PC micelles had no significant effect on diC_8PI cleavage. The observed activity was comparable to what was observed for 2 mM diC_6PI with 2 mM diC_7PC added (Figure 7-6B). This result suggests the enhanced activity towards diC_6PI with diC_7PC added is the result of providing an interfacial substrate for the enzyme. For DNF2 acting on diC_8PI with the diC_7PC increased, there was a further enhancement in specific activity reminiscent of what was observed for *L. monocytogenes* PI-PLC, where increasing PC content in micelles or

vesicles reduced the formation of nonproductive aggregates of the PI-PLC with anionic lipids [7].

Figure 7-6: Specific activities of DNF2-intein fusion protein. (A) Specific activities toward PI (8 mM)/Triton X-100 (12.5mM) micelles as a function of pH. (B) Specific activities of DNF2 toward pure 2 mM diC_6PI in the absence or presence of 2 mM diC_7PC or 1 mM POPC vesicles. (C) Specific activities of DNF2 toward 2 mM diC_8PI, in the absence or presence of 2 or 4 mM diC_7PC. (D) Specific activities of DNF2 toward PI (8 mM) solubilized in Triton X-100 (12.5 mM) or diC_7PC (32 mM), in the absence or presence of 5 mM EDTA. All these assays were carried out in 50 mM HEPES, pH 7.4, with a protein concentration kept at 20.8 μg/mL.

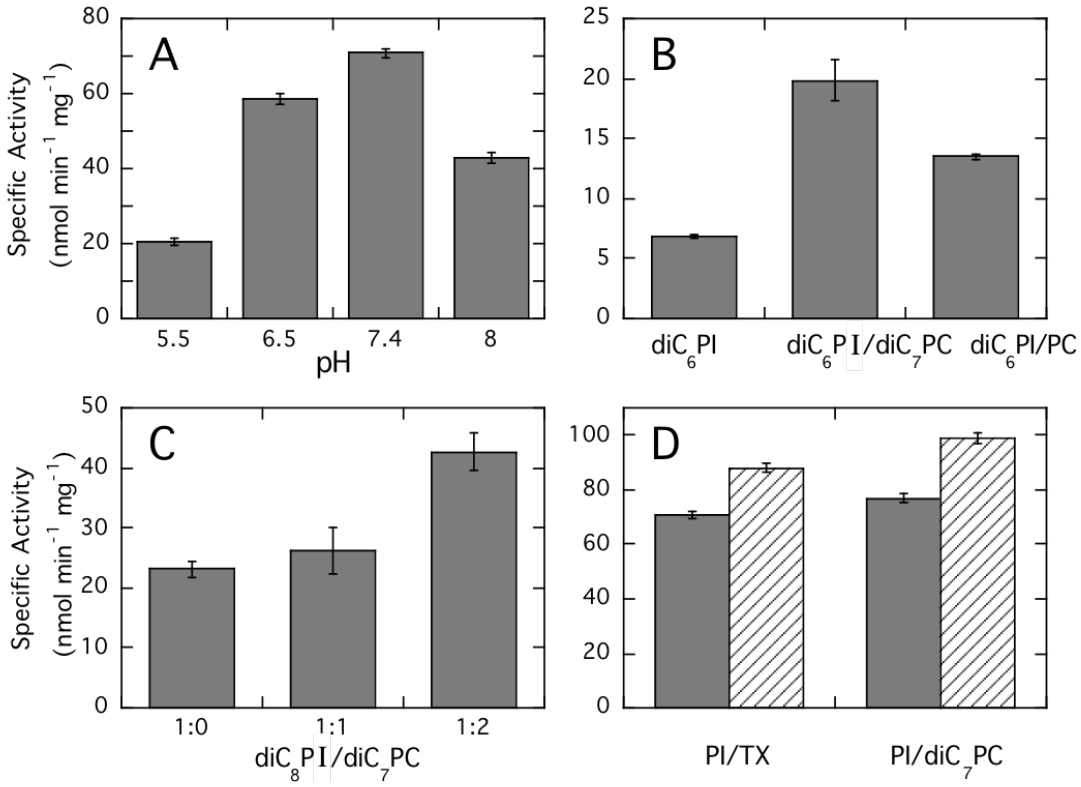

DNF2 incubated with 10 mM EDTA for 2 h shows a small increase in activity (~1.25-fold) compared to non-EDTA treated DNF2 in both PI/TX and PI/diC_7PC assay systems (Figure 7-6D). The lack of a decrease in activity indicates this PI-PLC, unlike mammalian PLC enzymes, is not Ca^{2+}-dependent. The very small increase probably

represents removal of some metal ions that tend to interact with the anionic substrate PI. *B. thuringiensis* PI-PLC activity is also not inhibited by EDTA.

7.5 Histidine mutants

The homology model of DNF2 structure provides a framework for testing suspected active site residues. While much of DNF2 fits well on this framework, there is a switch of the positions of the analogs to His82 (the general acid) and Arg69 (that stabilizes the negative charge of the tetrahedral intermediate) [8]. The low PI-PLC activity detected for DNF2 has the same pH profile and some of the interfacial characteristics of both *Bt*PI-PLC and *Lm*PI-PLC enzymes. As a test to see if this spatial change could account for the low activity of DNF2, His82 and Arg69 were switched in *Bt*PI-PLC. The mutant enzyme H82R/R69H loses all its PI cleavage activity. This confirms that our DNF2 activity, though low, is real and not the result of switching the positions of the His and Arg. This result suggested that perhaps the detailed catalytic mechanism is somewhat different for DNF2 compared to small bacterial PI-PLC enzymes.

The pH profile of the DNF2 reaction suggested one or more His were involved in the mechanism. Also, the BLAST of DNF2 against *Bt*PI-PLC suggested that DNF2 His77 aligns with an active site His in the bacterial PI-PLC. Single mutations to alanine were made to all 8 His residues in DNF2, and specific activity toward PI/TX was measured with wildtype DNF2 as a control. Surprisingly, all the single His mutants retained the ability to cleave PI activity, although H70A, H77A and H155A only showed ~1/3 of the wildtype activity. Mutation of a single histidine residue does not inactivate the PI-PLC activity of DNF2 (as seen for the bacterial enzymes), but rather modestly reduces it.

However, there is another way to look at these results. DNF2 activity is measured in nmol min^{-1} mg^{-1}; the bacterial PI-PLC activities are typically 1000-fold or more higher. Knocking out the active site His residues (or the Arg that stabilizes the tetrahedral intermediate) in the bacterial PI-PLCs reduces the PI cleavage activity by a factor of 10^3-10^4. From the homology model, it appears that the analogues to the bacterial general acid and the key residue that stabilizes the tetrahedral intermediate have been swapped. This would certainly lead to a much lower activity where removal of key His might have only minor effects by comparison.

This leads to a very interesting conundrum: if DNF2 is a PI-PLC but with very low activity what is its function in cells? Is its enzymatic activity required or is there a factor in the symbiosome that can enhance PI or GPI-anchor cleavage?

7.6 DNF2 PI-PLC activity is in extracts from symbiosomes?

To understand how DNF2 functions in the symbiosome, Onur Oztas (University of Massachusetts, Amherst) incubated the WT and *dnf2* knockdown mutant symbiosomes with GPI-anchored proteins. The anti-CRD antibody can recognize the cIP epitope and was used for the western blot shown in Figure 7-7A. The three bands correspond to three epitopes of the GPI-cleaved products [10]. DNF2 is clearly required for the cleavage of GPI-anchored proteins in the symbiosome as monitored by the loss of bands in the extract from the knockdown mutant. Prior to immune detection with anti-CRD antibody, the SDS-PAGE was subjected to Ponseau S stain for visualization of the total protein without affecting the following anti-CRD detection (Figure 7-7B). Total protein and its distribution appeared the same for WT and *dnf2* knockdown cell extracts. The results of the anti-CRD blot strongly suggest that DNF2 is not only a PI-PLC as shown in model

studies with the reocbinant enzyme, but also functions as a GPI-PLC in the plant symbiosome.

Figure 7-6. GPI cleavage by DNF2 wildtype and mutant. (A) Western blot using anti-CRD for cIP recognizing; (B) SDS- PAGE stained with Ponseau S.

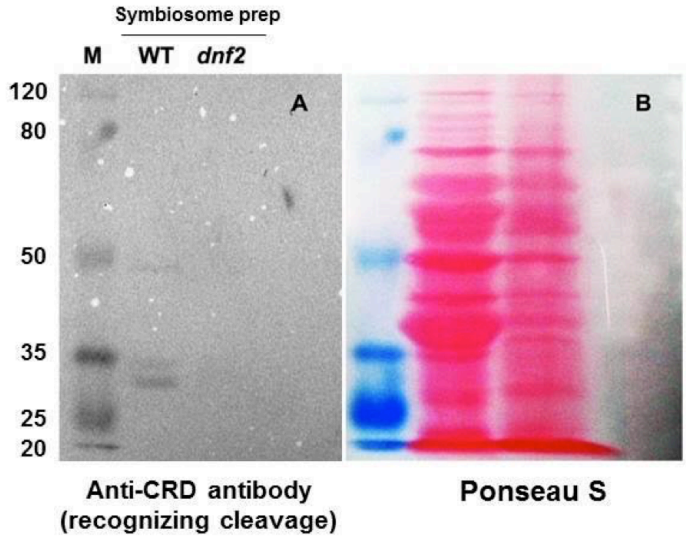

7.7 Conclusion

In this study, we have shown that DNF2 is a novel plant PI-PLC with a key role in symbiosome biology. The activity for the recombinant protein in model assay systems is low. This might suggest this protein generated in situ is subjected to post modification in some way [11] to enhance activity or that it is activated by a partner protein when secreted into the symbiosome [12]. GPI-anchored protein cleavage also confirms that DNF2 is required for GPI-anchored protein cleavage in symbiosome. However, many questions still need to be addressed. First and foremost is to find a better expression system that generates DNF2 without the intein. Perhaps this can be accomplished by extending the C-terminus with a flexible spacer that allows DTT-induced cleavage after purification. If such protein can be generated, attempts to repeat kinetics with protein that

has no C-terminal fusion tag and perhaps even attempts at crystallization should be considered.

Reference

1. 1.Starker, C. G., Parra-Colmenares, A. L., Smith, L., Mitra R. M., and Long, S. R. (2006) Nitrogen fixation mutants of Medicago truncatula fail to support plant and bacterial symbiotic gene expression. *Plant Physiology, 140*, 671-680.
2. Yang, J., Yan, R., Roy, A., Xu, D., Poisson, J., and Zhang, Y. (2015) The I-TASSER suite: protein structure and function prediction. *Nature Methods, 12*, 7-8.
3. Kelley, L. A., Mezulis, S., Yates, C. M., Wass, M. N., and Sternberg, M. (2015) The Phyre web portal for protein modeling, prediction and analysis. *Nature Protocols, 10*, 845-858.
4. Emanuelsson, O., Nielsen, H., Brunak, S., and Heijne, G. (2000) Predicting subcellular localization of proteins based on their N-terminal amino acid sequence. *J. Mol. Biol., 300*, 1005-1016.
5. Peterson, T. H., Brunak, S., Heijne, G., and Nielsen, H. (2011) SignalP 4.0: discriminating signal peptides from transmembrane regions. *Nature Methods, 8*, 785-786.
6. Zhou, C., Wu, Y., and Roberts, M. F. (1997) Activation of phosphatidylinositol-specific phospholipase C toward inositol 1,2-(cyclic)-phosphate. *Biochemistry, 36*, 347-355.
7. Chen, W., Goldfine, H., Ananthanarayanan, B., Cho, W., and Roberts, M. F. (2009) Listeria monocytogenes phosphatidylinositol-specific phospholipase C: kinetic activation and homing in on different interfaces. *Biochemistry, 48,* 3578-3592.
8. Heinz, D. W., Ryan, M., Bullock, T. L., and Griffith, O. H. (1995) Crystal structure of the phosphatidylinositol-specific phospholipase C from Bacillus cereus in complex with myo-inositol. *The EMBO Journal, 14*, 3855-3863.
9. Volwerk, J. J., Filthuth, E., Griffith, O. H., and Jain, M. K. (1994) Phosphatidylinositol-specific phospholipase C from Bacillus cereus at the lipid-water interface: interfacial binding, catalysis, and activation. *Biochemistry, 32*, 8836-8841.
10. Muller, A., Kloppei, C., Smith-Valentine, M., Houten, J. V., and Simon, M. (2012) Selective and programmed cleavage of GPI-anchored proteins from the surface membrane by phospholipase C. *Biomembranes, 1818*, 117-124.
11. Berrabah, F., Ratet, P., and Gourion, B. (2015) Multiple steps control immunity during the intracellular accommodation of rhizobia. *J. Exp. Bot., 66*, 1977-1985.
12. Berrabah, F., Bourcy, M., Cayrel, A., Eschstruth, A., Mondy, S., Ratet, P., and Gourion, B. (2014) Growth conditions determine the DNF2 requirement for symbiosis. *PLoS ONE 9(3):* e91866. Doi: 10.1371/journal.pone.0091866.

Chapter 8

Future Direction

GPI-anchored protein cleavage, is the release of particular proteins associated with bacterial virulence?

SaPI-PLC as well as *Bacillus* PI-PLC target GPI-anchored proteins on the outer leaflet of eukaryotic cells. While μM concentrations of commercial preparations of *B. cereus* PI-PLC are used to non-specifically cleave GPI-anchored proteins off the surface of mammalian cells, PI-PLC activity and specificity towards GPI-anchored proteins at the lower, physiologically relevant concentrations and shorter time scales are unclear. Shorter time scales are particularly relevant for escape from phagocytosis, a process in which bacterial PI-PLC activity has been implicated. In the phagosome, the membrane facing a target bacterium comes from the outer leaflet of the plasma membrane and is likely to display GPI-anchored proteins. PI-PLC mediated cleavage of GPI-anchored proteins will generate DAG, weakening this membrane. Is there also a role for cleavage of specific GPI-anchored proteins in hindering or arresting phagocytosis? To investigate this question, we will determine the identities of released proteins and whether the members of this population change over time.

a. GPI-anchored protein release by SaPI-PLC

Neutrophils are the first host defense cells to reach infection sites. We will therefore use these cells as well as erythrocytes to investigate the identities of released GPI-anchored proteins. Whole blood, obtained commercially, will be fractionated into individual cell types using an autoMACS Pro Separator (Miltenyi Biotec) available in the laboratory of Dr. Ken Williams (Boston College). Up to 20 ml of cells can be fractionated in this instrument and the low temperature keeps neutrophils from being

activated. Aliquots of each desired cell type will be assessed for purity by flow cytometry using the B.C. Biology Department's flow cytometry center.

We will start out with the more abundant erythrocytes. Initially two samples, one with 1 nM and the other with 1 mM *Sa*PI-PLC will be incubated at 37° C, and aliquots removed as a function of time, centrifuged to remove the cell pellet. The supernatant will be collected and precipitated with ammonium sulfate. Once this is centrifuged, the resulting pellet will be resuspended in phosphate buffered saline (PBS) and the ammonium sulfate will be removed using a desalting column. SDS-PAGE (and silver staining) will then be used to determine if any proteins were released into solution. The two extremes in enzyme concentration should give us a handle on picking the right concentration of *Sa*PI-PLC so that GPI-anchored proteins are released over a 1 h time scale.

From this point, we will follow the procedure used in the Roberts lab when working with protein extracts from RAW cells. In brief, the proteins in the supernatant are unfolded in 6 M urea, reduced with DTT, heated to denature the proteins, then reacted with iodoacetamide to prevent disulfide formation. Protein samples are then digested with trypsin. After removal of the protease, the peptides need to be desalted and dried for analysis by LC-MS/MS analysis.

A parallel incubation of cells with the inactive *Bt*PI-PLC variant H32A will serve as a negative control. As a positive control, at least for the erythrocytes, ghosts will be formed, then mixed with Triton X-100 to solubilize membrane components including the GPI-linkages in detergent mixed micelles. Proteins in the micelles should be more accessible to *Sa*PI-PLC and thus more easily released with mM protein. This should also

provide us with a normalization factor for how much of a given GPI-anchored protein is released by the enzyme and is critical in looking for particularly susceptible proteins.

Since there is no data on the time course for protein release, these experiments should provide an interesting view into whether *Bt*PI-PLC targets specific GPI-anchored proteins. An absence of specificity would indicate that DAG production is the primary reason that *Bt*PI-PLC increases bacterial virulence.

b. GPI-anchored protein release by SaPI-PLC

These experiments will use the same techniques described in section a above. *Bacillus* species and *S. aureus* occupy different environmental niches, for example *S. aureus* colonizes skin and while *B. anthracis* can also attack skin cells, some the most lethal infections result from inhalation of anthrax spores. In parallel with this environmental difference, PI-PLCs from these bacteria have very different lipid binding specificities with *Bacillus* PI-PLC binding specifically to PC. We therefore expect that, at the very least, *Bt*PI-PLC and *Sa*PI-PLC will have different efficiencies for GPI-anchored protein cleavage. In addition, if there is cleavage specificity for GPI-anchored proteins, the different lipid specificities for these two related enzymes are likely to result in different target populations.

The results of these mass-spectrometry based proteomics experiments will reveal whether the increased virulence associated with PI-PLC expression by Gram-positive bacterial pathogens arises simply from the generation of DAG in host cell membranes or if specific cleavage of GPI-anchored proteins is also important.

Can we identify cation-π interactions in other amphitropic proteins?

*Bt*PI-PLC has been used as a model system for characterization of cation-π interactions between amphitropic proteins and membranes. Prof. Nathalie Reuter and her coworkers have screened the OPM (Orientation of Proteins in/on membranes) database for protein structures that have Tyr within 10 Å of the hydrocarbon boundary. They found a lot of proteins fit the criteria. This might suggest that cation-π interactions are a general mechanism for membrane binding of amphitropic proteins.

To test this hypothesis, we can choose one of two of proteins that fit the search criteria. For example, we can choose bovine seminal plasma PCD-9 (PDB: 1H8P), which has phosphorylcholine co-crystallized in the structure indicating that this protein is involved in cation-π interactions with PC head groups. To confirm this, we can replace Tyr22 (which is around the choline binding site) with a Y-F_2. By measuring the binding affinity for membrane of the wild type and mutant we will be able to assess how the cation-π interactions affect the protein affinity for membrane. Furthermore, we can also co-crystalize the mutant protein with phosphorylcholine to have a detailed structure analysis.